AD-A170 317 A THEORETICAL FRAMEWORK FOR EXAMINING GEOGRAPHICAL VARIABILITY IN THE MIC. (U) ILLINOIS STATE WATER SURVEY DIV URBANA D B JOHNSON JUN 86 AFOSR-TR-86-0484 1/2

UNCLASSIFIED AFOSR-82-0079 F/G 4/2 NL

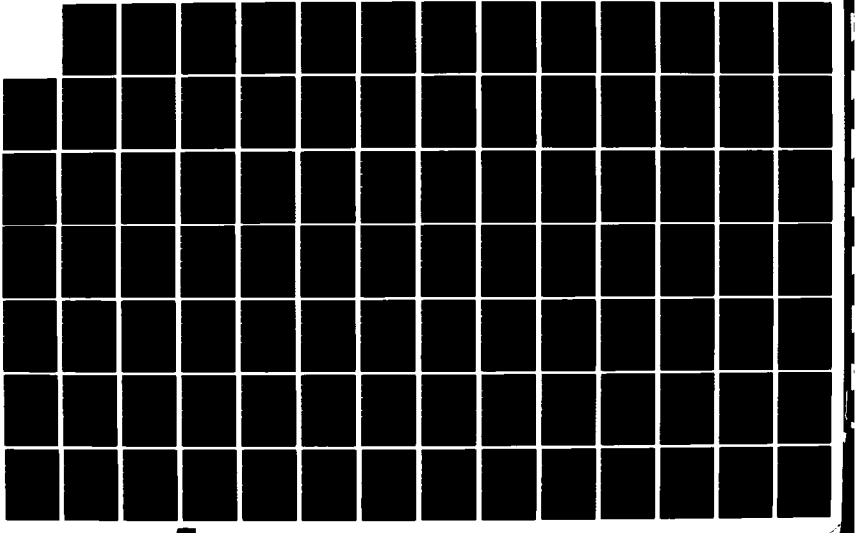

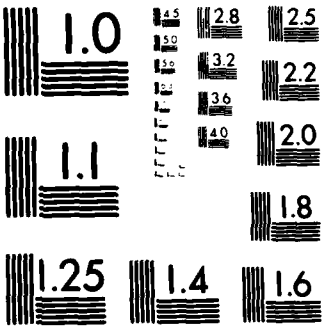

State Water Survey Division
CLIMATE AND METEOROLOGY SECTION
AT THE
UNIVERSITY OF ILLINOIS

ENR
Illinois Department of
Energy and Natural Resources

SWS Contract Report 391

FINAL REPORT

A THEORETICAL FRAMEWORK FOR EXAMINING GEOGRAPHICAL VARIABILITY IN THE MICROPHYSICAL MECHANISMS OF PRECIPITATION DEVELOPMENT

GRANT NUMBER AFOSR 82-0079

Principal Investigator: David B. Johnson

June 1986

AD-A170317

REPORT DOCUMENTATION PAGE

1a. REPORT SECURITY CLASSIFICATION: Unclassified	1b. RESTRICTIVE MARKINGS
2a. SECURITY CLASSIFICATION AUTHORITY	3. DISTRIBUTION / AVAILABILITY OF REPORT: Approved for public release distrubution unlimited
2b. DECLASSIFICATION / DOWNGRADING SCHEDULE	
4. PERFORMING ORGANIZATION REPORT NUMBER(S)	5. MONITORING ORGANIZATION REPORT NUMBER(S): AFOSR-TR- 86-0484
6a. NAME OF PERFORMING ORGANIZATION: University of Illinois; 6b. OFFICE SYMBOL (If applicable)	7a. NAME OF MONITORING ORGANIZATION: AFOSR/NC
6c. ADDRESS (City, State, and ZIP Code): Climate & Meteorology Section, Urbana, IL 61820	7b. ADDRESS (City, State, and ZIP Code): Bldg 410, Bolling AFB, DC20332-6448
8a. NAME OF FUNDING / SPONSORING ORGANIZATION: AFOSF; 8b. OFFICE SYMBOL (If applicable): NC	9. PROCUREMENT INSTRUMENT IDENTIFICATION NUMBER: AFOSR-82-0013
8c. ADDRESS (City, State, and ZIP Code): Bldg 410, Bolling AFB, DC 20332-6448	10. SOURCE OF FUNDING NUMBERS: PROGRAM ELEMENT NO. 61102F; PROJECT NO. 2310; TASK NO. A2; WORK UNIT ACCESSION NO

11. TITLE (Include Security Classification)
(U) A Theoretical Framework for Examining Geographical Variability in the Microphysical Mechanisms of Precipitation Development

12. PERSONAL AUTHOR(S)
David B. Johnson

13a. TYPE OF REPORT	13b. TIME COVERED	14. DATE OF REPORT (Year, Month, Day)	15. PAGE COUNT
Final	FROM 1/15/82 TO 1/14/85	June 1986	100

16. SUPPLEMENTARY NOTATION

17. COSATI CODES			18. SUBJECT TERMS (Continue on reverse if necessary and identify by block number)
FIELD	GROUP	SUB-GROUP	Microphysical, Parameters, Geographical, Climatological, Precipitation, Snowflake

19. ABSTRACT (Continue on reverse if necessary and identify by block number)

The overall goal of this study was to identify and evaluate the environmental or microphysical parameters that control the efficiency of the various mechanisms of precipitation development. Such evaluations can then be used as the basis for studying, or even predicting the effect of geographical or climatological differences between regions on the microphysical mechanisms of precipitation development. This study included work on warm rain initiation and development, ice multiplication, snowflake aggregation, and the growth of graupel by collection of supercooled water droplets. During the first year of the study, work concentrated on the warm-cloud studies and began on the investigation of snowflake aggregation. With the extension of the study into a third year, additional investigations were made on snowflake aggregation and preliminary investigations were begun to extend these studies into mixed-phase (riming) precipitation. The studies of riming and graupel development were quite successful and indicated that the studies of warm rain initiation and development could be extended to include mixed-phase precipitation

20. DISTRIBUTION / AVAILABILITY OF ABSTRACT: ☒ UNCLASSIFIED/UNLIMITED ☐ SAME AS RPT ☐ DTIC USERS	21. ABSTRACT SECURITY CLASSIFICATION: Unclassified
22a. NAME OF RESPONSIBLE INDIVIDUAL: Dr. Francis J. Wodarczyk	22b. TELEPHONE (Include Area Code): 202-767-4960; 22c. OFFICE SYMBOL: NC

DD FORM 1473, 84 MAR — 83 APR edition may be used until exhausted. All other editions are obsolete.

SECURITY CLASSIFICATION OF THIS PAGE
Unclassified

19. Abstract (cont)
development. In general, the study identified a number of key parameters that control the microphysical development of precipitation. The two primary parameters that need to be measured on a climatological basis are cloud base temperature and cloud droplet concentration. Other key parameters include the degree of entrainment and stability of the environment.

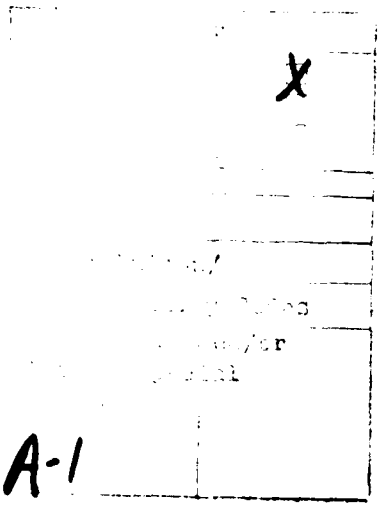

A THEORETICAL FRAMEWORK FOR EXAMINING GEOGRAPHICAL VARIABILITY IN THE MICROPHYSICAL MECHANISMS OF PRECIPITATION DEVELOPMENT

INTRODUCTION

This Final Report covers all work performed under grant number AFOSR-82-0079, covering the period 15 January 1982-14 January 1985. The overall goal of this study was to identify and evaluate the environmental or microphysical parameters that control the efficiency of the various mechanisms of precipitation development. Such evaluations can then be used as the basis for studying, or even predicting, the effect of geographical or climatological differences between regions on the microphysical mechanisms of precipitation development.

This study includes work on warm rain initiation and development, ice multiplication, snowflake aggregation, and the growth of graupel by collection of supersooled water droplets. During the first year of the study, work concentrated on the warm-cloud studies and on ice multiplication. During the second year, work continued on the warm-cloud studies and began on the investigation of snowflake aggregation. With the extension of the study into a third year, additional investigations were made on showflake aggregation and preliminary investigations were begun to extend these studies into mixed-phase (riming) precipitation. The studies of riming and graupel development were quite successful and indicated that the studies of warm rain initiation and development could be extended to include mixed-phase precipitation development. These background studies have been summarized in a article being submitted for publication, which is presented in the appendix. Other articles resulting from this study are under preparation

and should be completed in the near future.

In general, the study identifies a number of key parameters that control the microphysical development of precipitation. The two primary parameters that need to be measured on a climatological basis are cloud base temperature and cloud droplet concentration. With a knowledge of these parameters it is possible to estimate the liquid water content and mean droplet diameter as functions of the depth of a cloud. This in turn permits an estimate of the likelyhood of warm rain development, ice multiplication, and ice crystal concentration in the cloud (see Hobbs and Rangno, 1985: Journal of the Atmospheric Sciences, 42, 2523-2549.). Combined with satellite observed cloud tops, a climatological knowledge of cloud base temperature and droplet concentration would go a long way toward predicting the type of particle development likely in widely different geographical areas. Other key parameters include the degree of entrainment and stability of the environment. Entrainment is still difficult to predict in any quantitative way, but may not be as variable geographically as some of the other parameters. Studies of stability are currently possible using the large world-wide data base of sounding data currently available. Cloud base temperature and droplet concentration data, on the other hand, are still rare for most parts of the world.

CONTENTS

BACKGROUND STUDIES

From the very onset of these studies it has been clear that cloud base temperature is a uniquely important parameter for assessing geographical variability in the microphysical mechanisms of precipitation development. It has significance in areas ranging from the overall water budget and precipitation efficiency to the actual details of the cloud microstructure and its evolution. If entrainment is neglected, for example, then the consensationally produced liquid water contents at any height above cloud base are uniquely defined by the temperature and pressure at cloud base. The build-up of condensed water with height, of course, is the basic driving force behind precipitation development. Estimates of these adiabatic water contents are shown in Figure 1 (after Ludlam, 1950). In this presentation, the cloud base pressures have been varied in parallel with the cloud base temperatures in order to produce a single graph having applicability to a wide variety of summertime convective clouds. The water content profiles, however, are not very sensitive to variations in cloud base pressure. This means that a single figure of this type can be used to estimate water contents for many different sets of meteorological conditions.

In a sense, Figure 1 represents the maximum liquid water content that would be expected in the absence of a precipitation-related accumulation zone. The <u>average</u> water contents that are observed in convective clouds, however, are typically much lower than the adiabatic values illustrated in Figure 1. Warner (1970), for example, summarized a number of observations of the ratio of the observed mean liquid water content at a given height to the corresponding adiabatic value. Although there is considerable variation

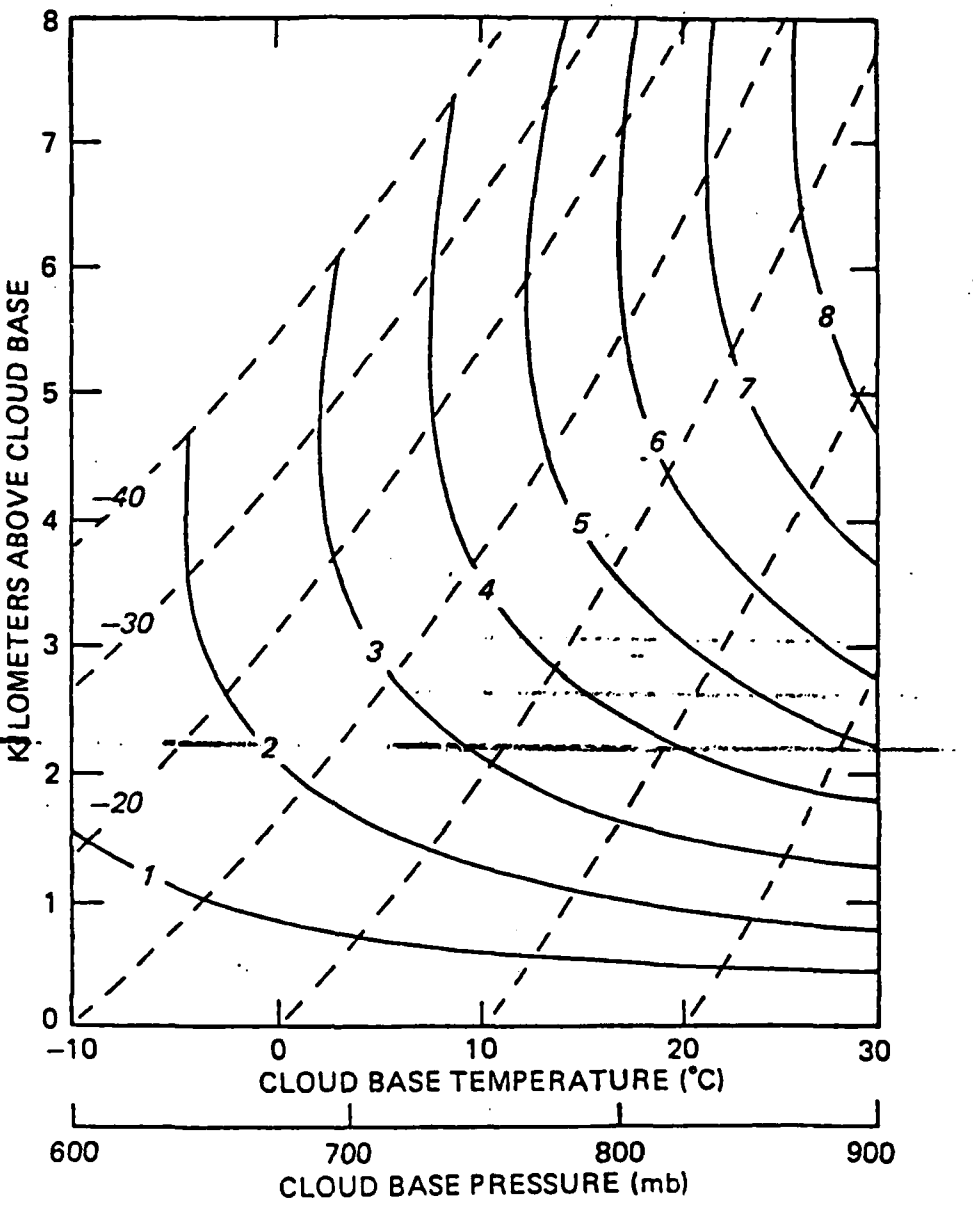

Figure 1. Adiabatic liquid water contents for cumuliform clouds. Saturation with respect to liquid water is assumed throughout with the isopleths labeled in g m^{-3}. The dashed lines indicate the corresponding temperatures within the clouds.

in the observations there is a consistent trend with the ratio decreasing with increasing height above cloud base. This decrease can be approximated by an empirical relation

$$F = 0.2 + \frac{0.16}{H + .20} \quad , \tag{1}$$

where H is the height above cloud base in km and

$$\overline{L} = F\, L_a \quad , \tag{2}$$

where $\overline{L}$ and L_a are the mean liquid water content and adiabatic liquid water contents respectively. Figure 2 illustrates the effect of applying (1) to the water contents shown in Figure 1 to produce an estimate of the expected mean water contents as a function of height above cloud base.

Although cloud base temperature has been frequently ignored in summarizing project results, I was able to compile some data on base temperatures of summertime convective clouds in the United States and Canada. Figure 3a shows the observed distributions of cloud base temperatures for Florida and Hawaii, while 3b shows the distributions for the Midwest and the Great Plains. The Florida data was obtained during the FACE-2 experiment in 1978, 1979, and 1980 and includes data from 48 different operational days. Hawaiian data were obtained from Professor Takahashi at the Cloud Physics Observatory in Hilo and represent observations taken over 32 different days. The Midwest data was combined from three different projects to give data for 72 days. The Great Plains data was similarly combined from the NHRE, HIPLEX, and CCOPE projects to give data for 123 different days. Recently, similar data was obtained from Dr. Schemenauer at the Atmospheric Environment Service (Canada) for two additional Canadian sites (Fig. 3c).

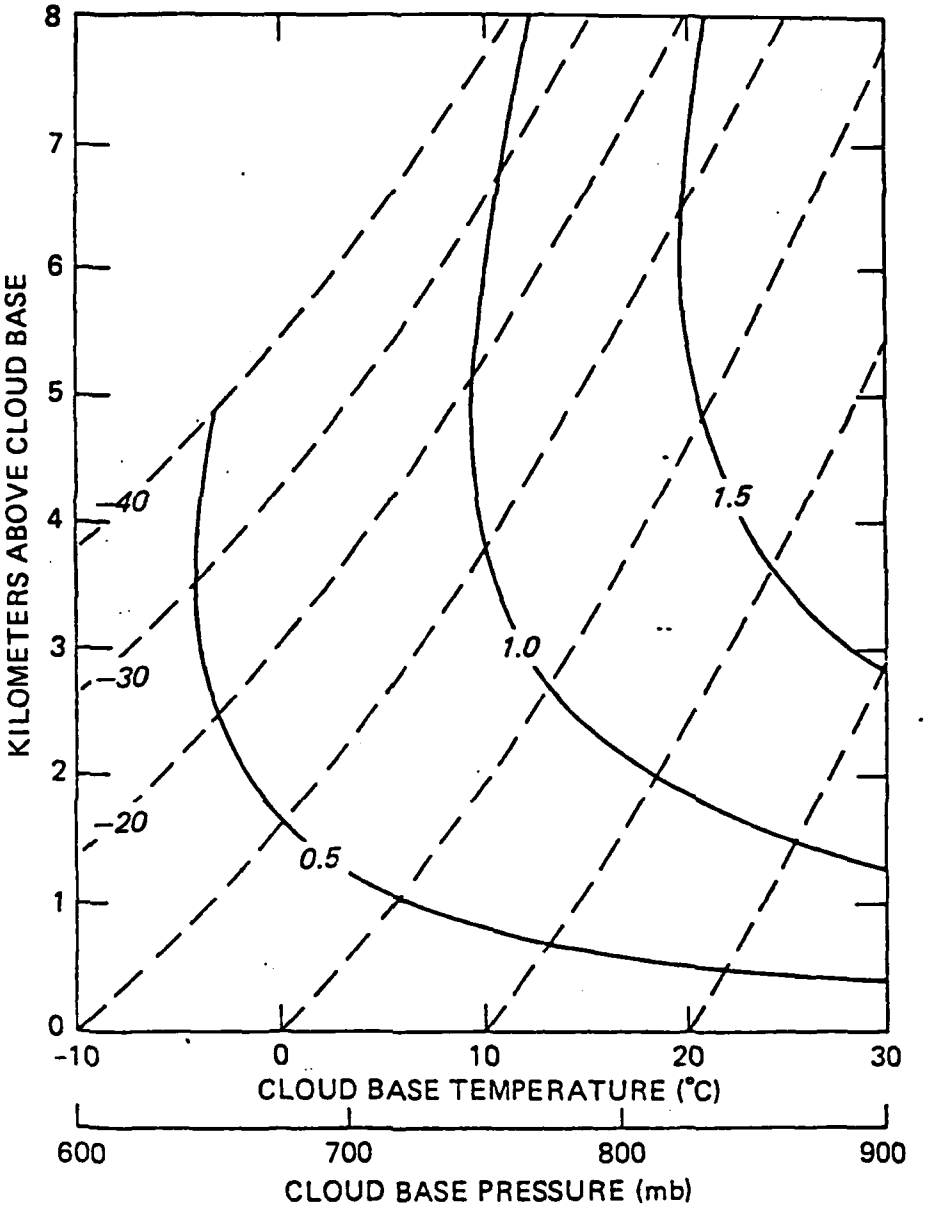

Figure 2. Average liquid water contents for cumuliform clouds. Saturation with respect to liquid water is assumed throughout with the isopleths labeled in g m^{-3}. The dashed lines indicate the corresponding temperatures within the clouds.

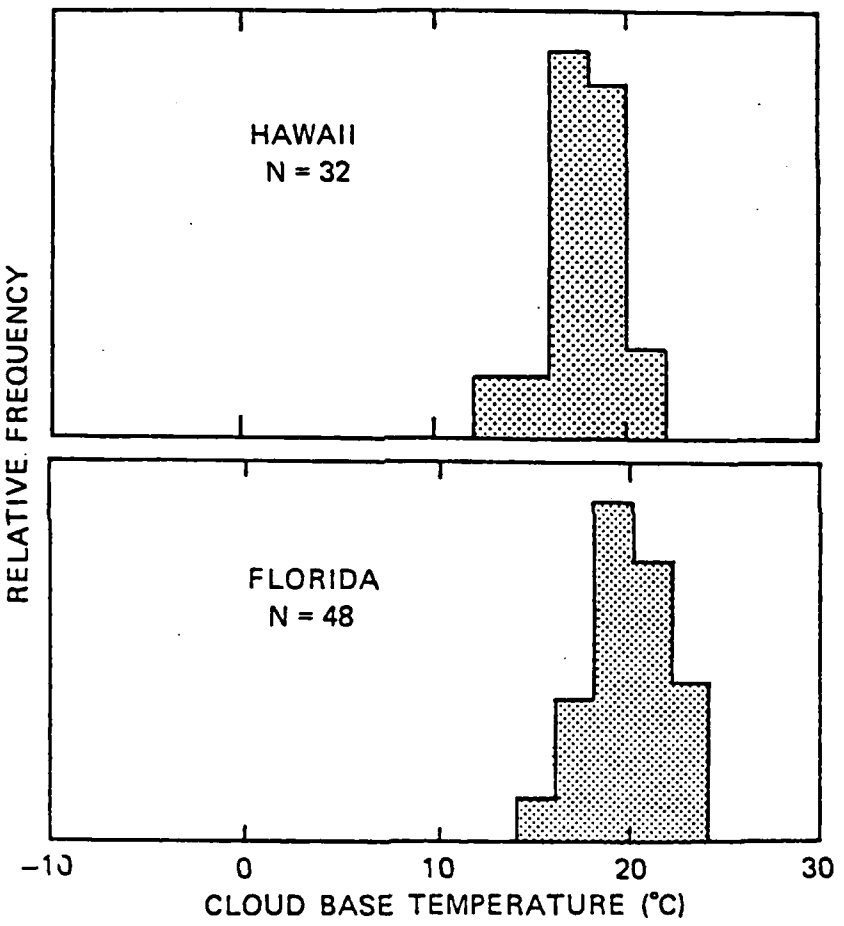

Figure 3a. Observed distributions of cloud base temperature for summertime convective clouds in Hawaii and Florida.

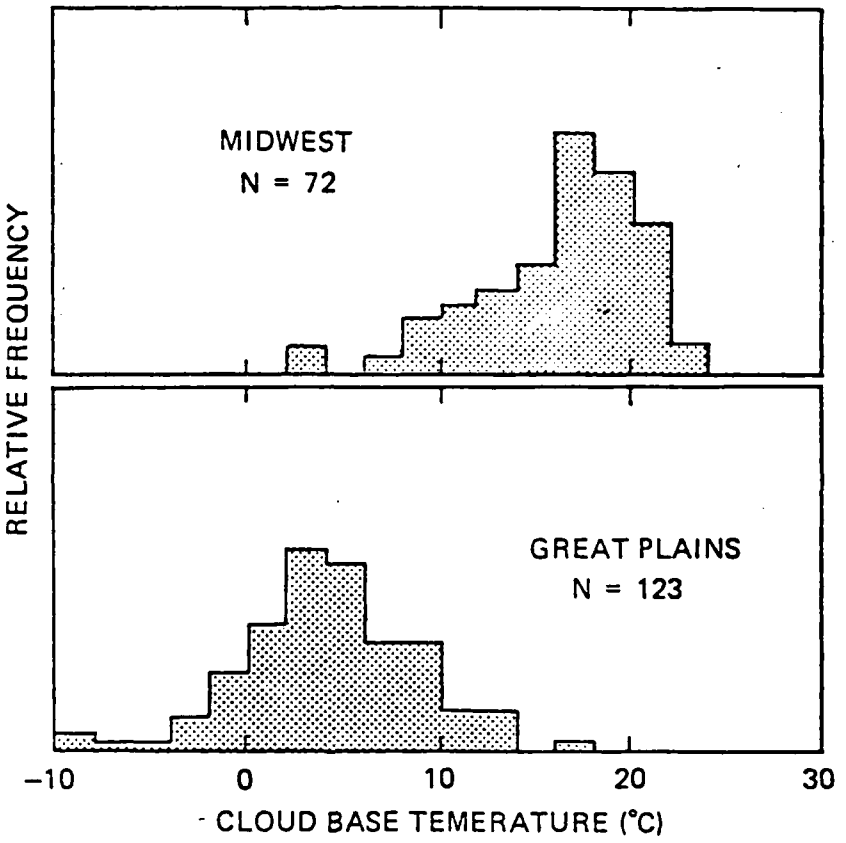

Figure 3b. Observed distributions of cloud base temperature for summertime convective clouds in the Great Plains and the Midwest.

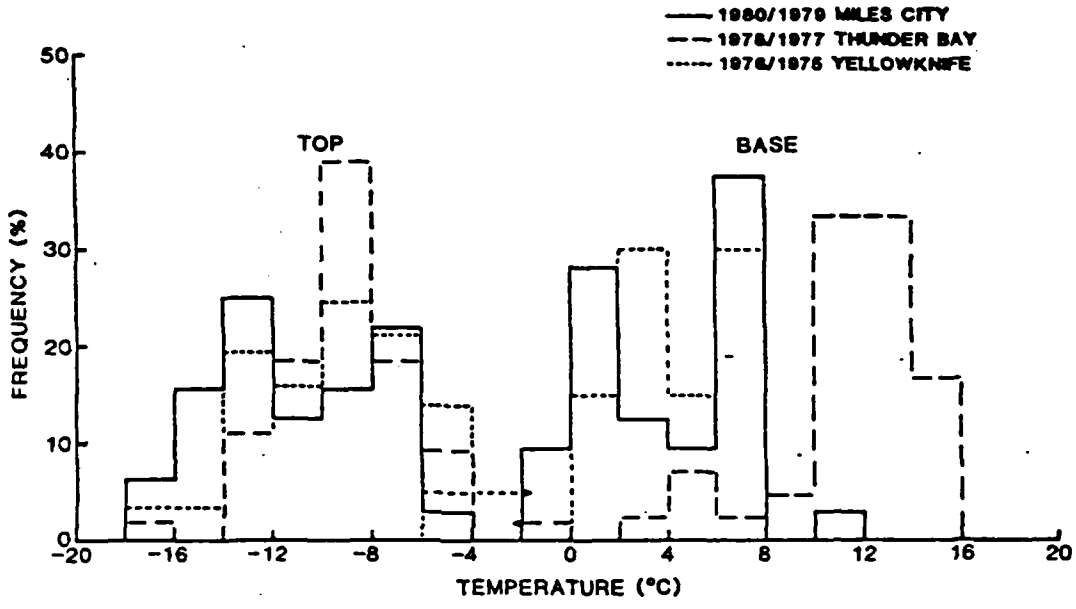

Figure 3c. Observed distributions of cloud base temperature for summertime convective clouds in Montana (Miles City) and two Canadian sites (Thunder Bay and Yellowknife).

These distributions are rather interesting in that they highlight the wide variety of cloud base temperatures expected in summertime convective clouds. Perhaps the most interesting feature of this data is how moist Midwest clouds can be, often having temperatures in the same range as found in Florida or Hawaii. Cloud base temperatures in the Great Plains, on the other hand, are significantly colder than those in the other two regions with little overlap between the observed distributions. Studies of clouds in the Great Plains are thus not likely to be relevant to clouds over much of Central and Eastern areas of the United States.

WARM RAIN INITIATION

In earlier studies (e.g., Johnson, 1978; 1980) it was suggested that a quantitative threshold could be defined that would signal the onset of effective coalescence growth. This concept was the direct result of a limited number of tests, with the threshold that was ultimately suggested ($\frac{1}{M}\frac{dM}{dt} > 4 \times 10^{-3}$ sec^{-1}) growing directly out of a graphical examination of drop growth as a function of time. In the current studies, this concept was re-examined and tested over a wide range of conditions. In these studies, possible thresholds were redefined in terms of the mass doubling time of the growing drop. Two different thresholds were examined - mass doubling in 3 minutes and mass doubling in 5 minutes. The mass doubling time (MDT) is a more appealing way of expressing the coalescence threshold since it can be relatively easily interpreted in terms of significant drop growth over cloud lifetimes. Since large cloud droplets beginning their growth to raindrops will have to double in mass approximately ten times before reaching raindrop proportions, these possible thresholds effectively

restrict the description of growth as "effective" to those situations in which coalescence rain could be produced in the 30-50 min lifetime of a convective cloud.

Figures 4-11 illustrate the growth of large drops in a variety of situations. In each case, drop growth is modeled in a constant updraft framework in which continued condensation results in a steady build up in water content as the parcel is lifted. In a separate series of runs drop growth was computed in clouds having a constant liquid water content and negligible updraft (1 cm s^{-1}). In effect, the former runs correspond to growth in a convective cloud, while the latter runs simulate stratiform clouds.

The model used for these calculations is essentially the continuous collection parcel model discussed in Johnson (1982). For use in this study, however, the model was modified ot include an adjustment in the calculated terminal velocities of cloud droplets and raindrops to account for changes in air density as the parcel rises. In addition, the model was modified to permit drop growth by condensation to be arbitrarily restricted to any fraction of the expected growth in an adiabatic parcel. If desired, the condensational growth can also be controlled to yield water contents that follow the empirically derived mean water contents specified by equation (1).

In the convective cases (Figs. 4-11) the basic pattern is one of slow initial growth followed at some point by a sudden spurt of growth. This overall pattern and the seeming suddenness of the transition from slow growth to fast growth were the original features which suggested that it might be possible to define the transition from one growth regime to

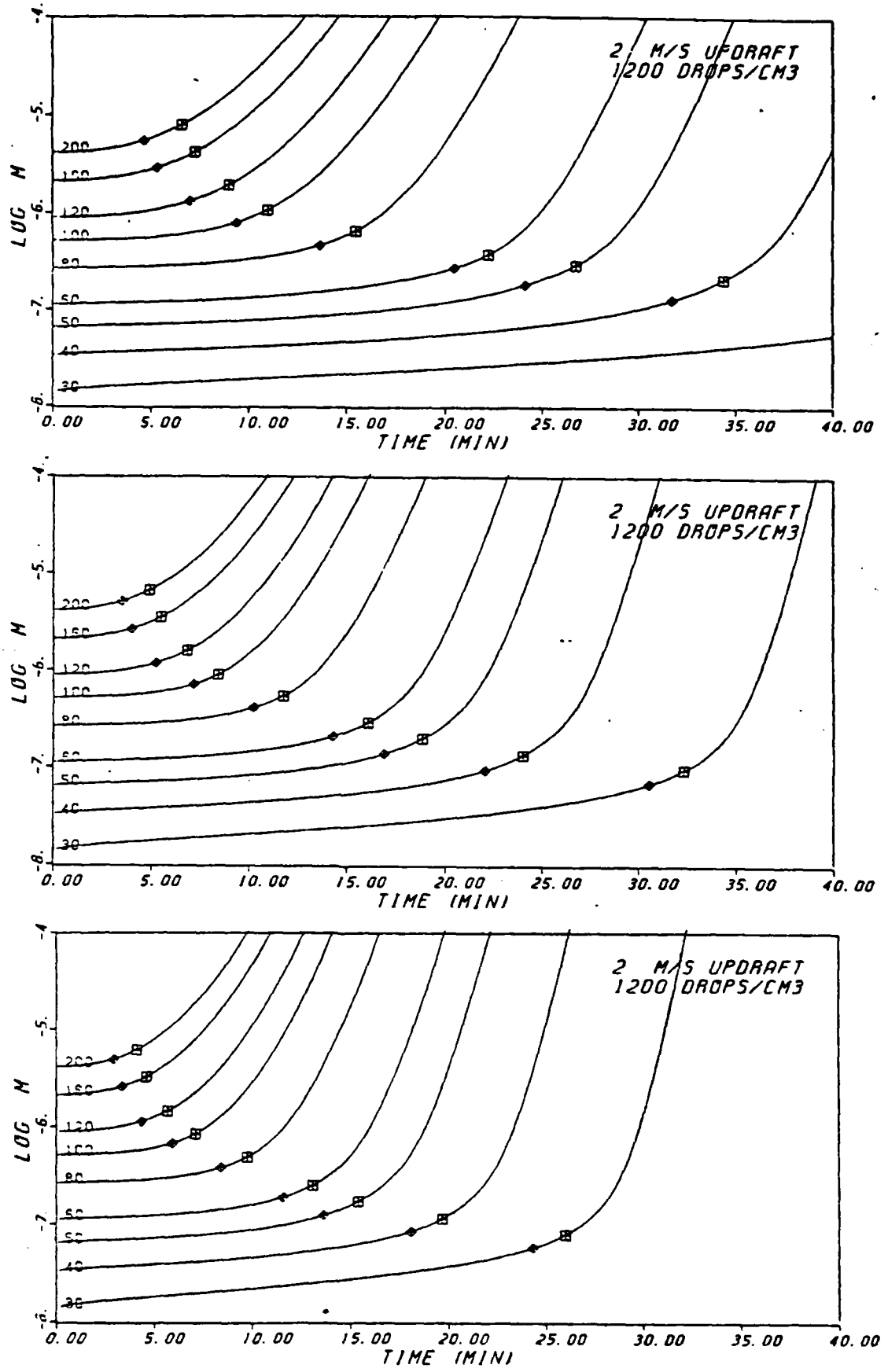

Figure 4. Growth of large drops (30-200 μm initial diameter) in a simple cloud model. The upper plot assumed a cloud base temperature of 0°C. The middle plot assumed a 10°C base temperature and the bottom plot assumed a base temperature of 20°C. Each case involved adiabatic water contents.

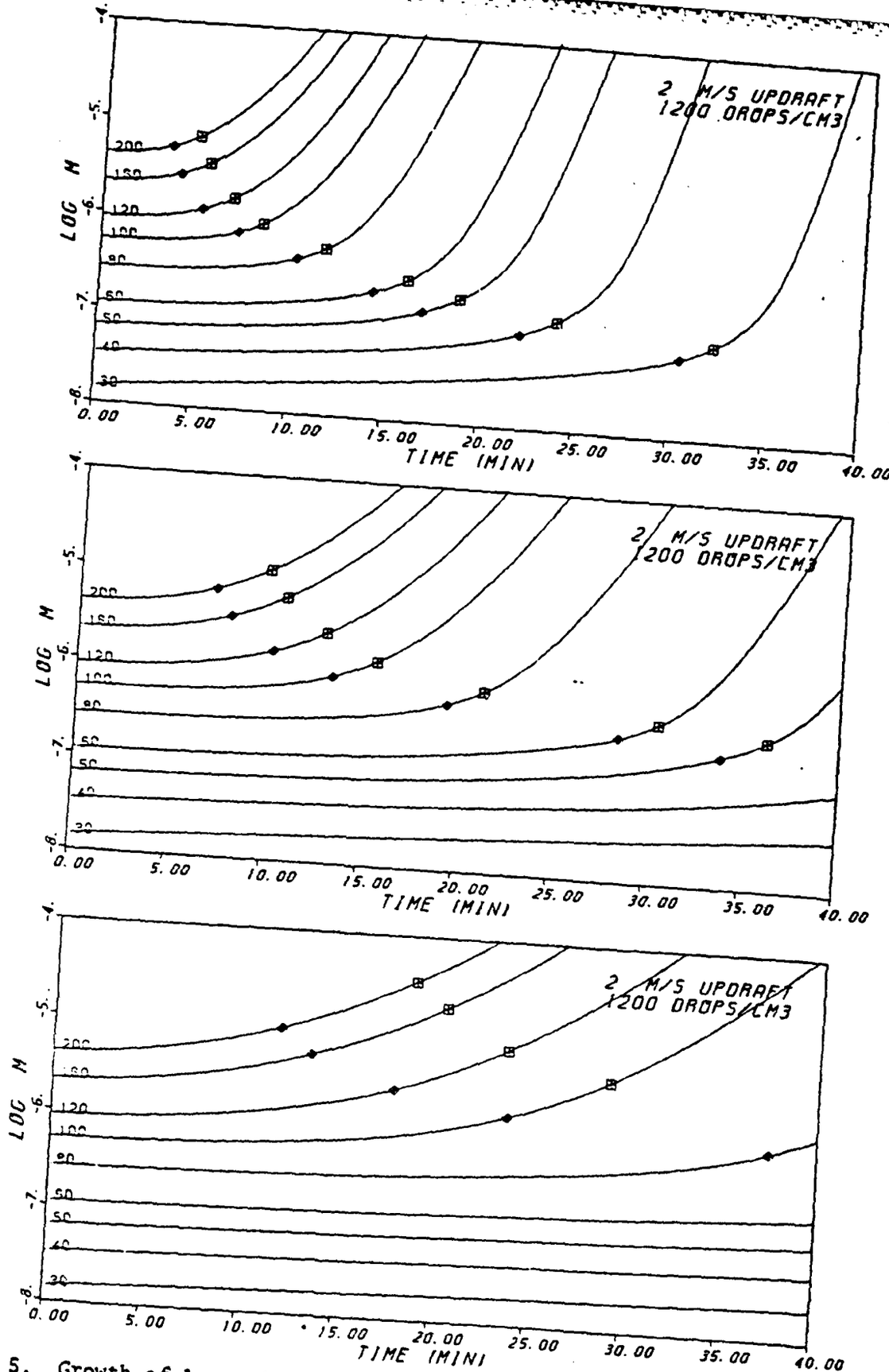

Figure 5. Growth of large drops (30-200 μm initial diameter) in a simple cloud model. The upper plot assumed adiabatic water contents, the middle plot assumed water contents that were half of the adiabatic values, and the bottom plot assumed a height dependent fraction of the adiabatic water content that corresponds to Figure 2. In each case, the cloud base temperature was assumed to be 10°C.

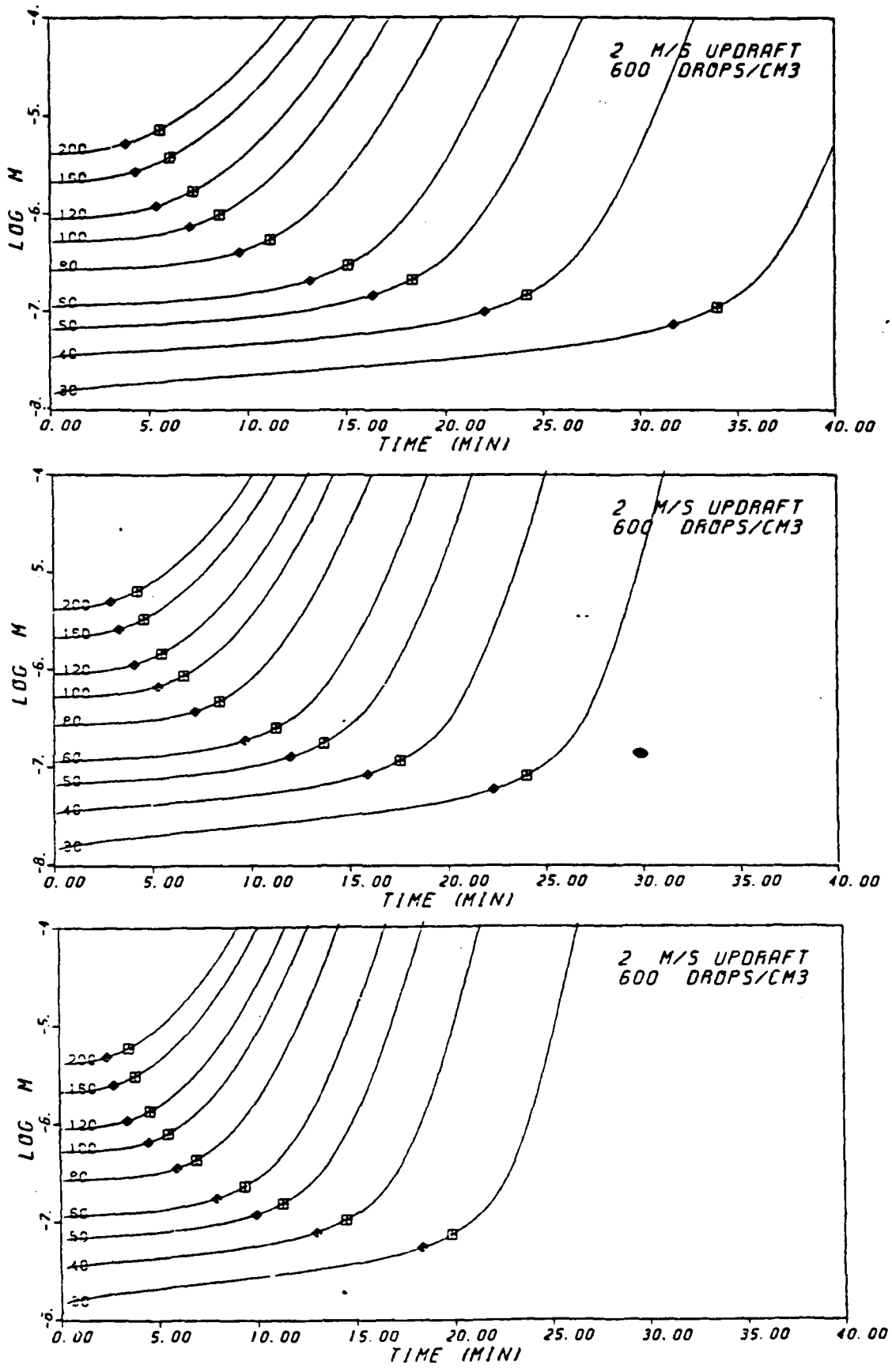

Figure 6. Growth of large drops (30-200 μm initial diameter) in a simple cloud model. The upper plot assumed a cloud base temperature of 0°C. The middle plot assumed a 10°C base temperature and the bottom plot assumed a base temperature of 20°C. Each case involved adiabatic water contents.

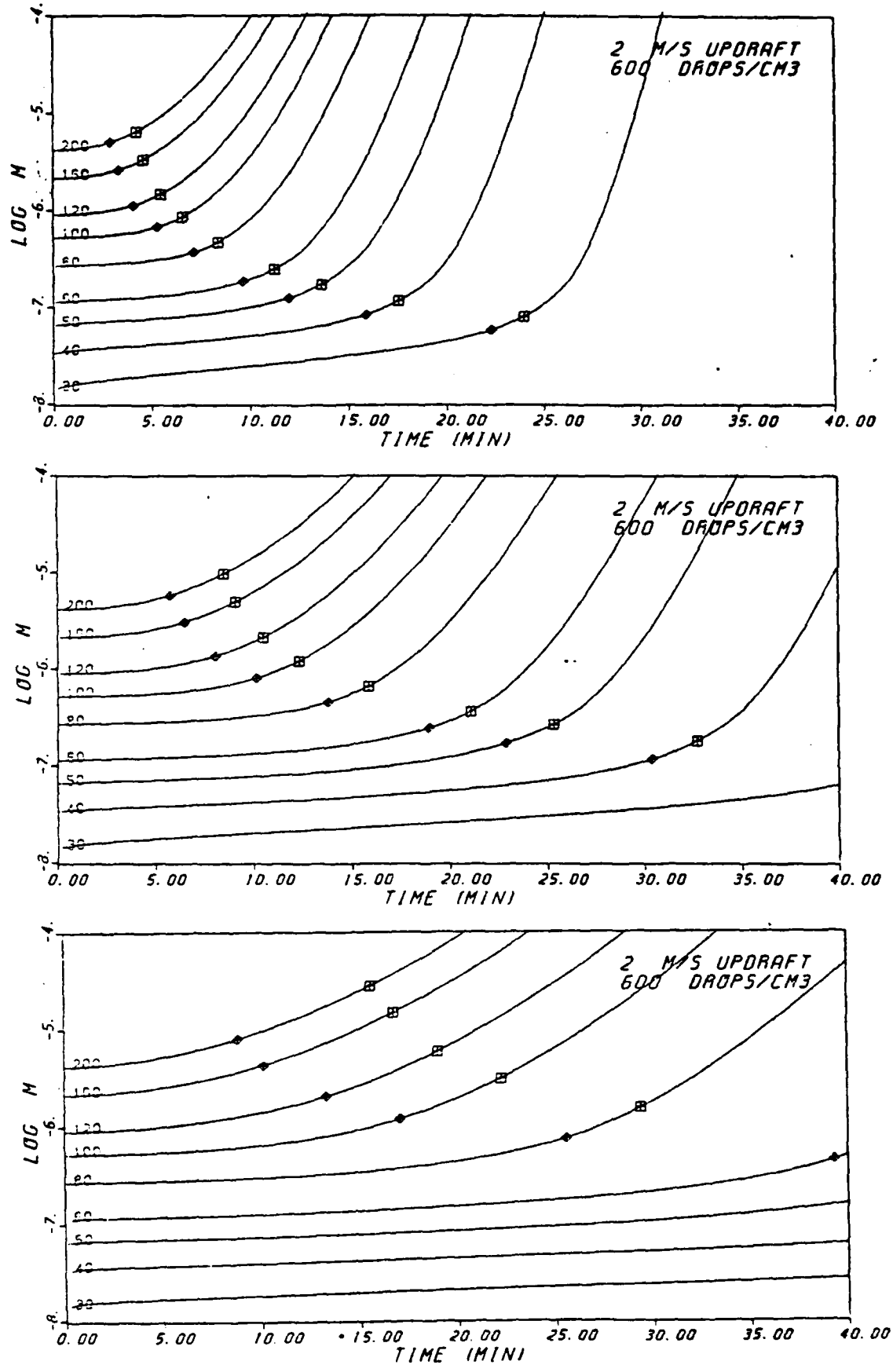

Figure 7. Growth of large drops (30-200 μm initial diameter) in a simple cloud model. The upper plot assumed adiabatic water contents, the middle plot assumed water contents that were half of the adiabatic values, and the bottom plot assumed a height dependent fraction of the adiabatic water content that corresponds to Figure 2. In each case, the cloud base temperature was assumed to be 10°C.

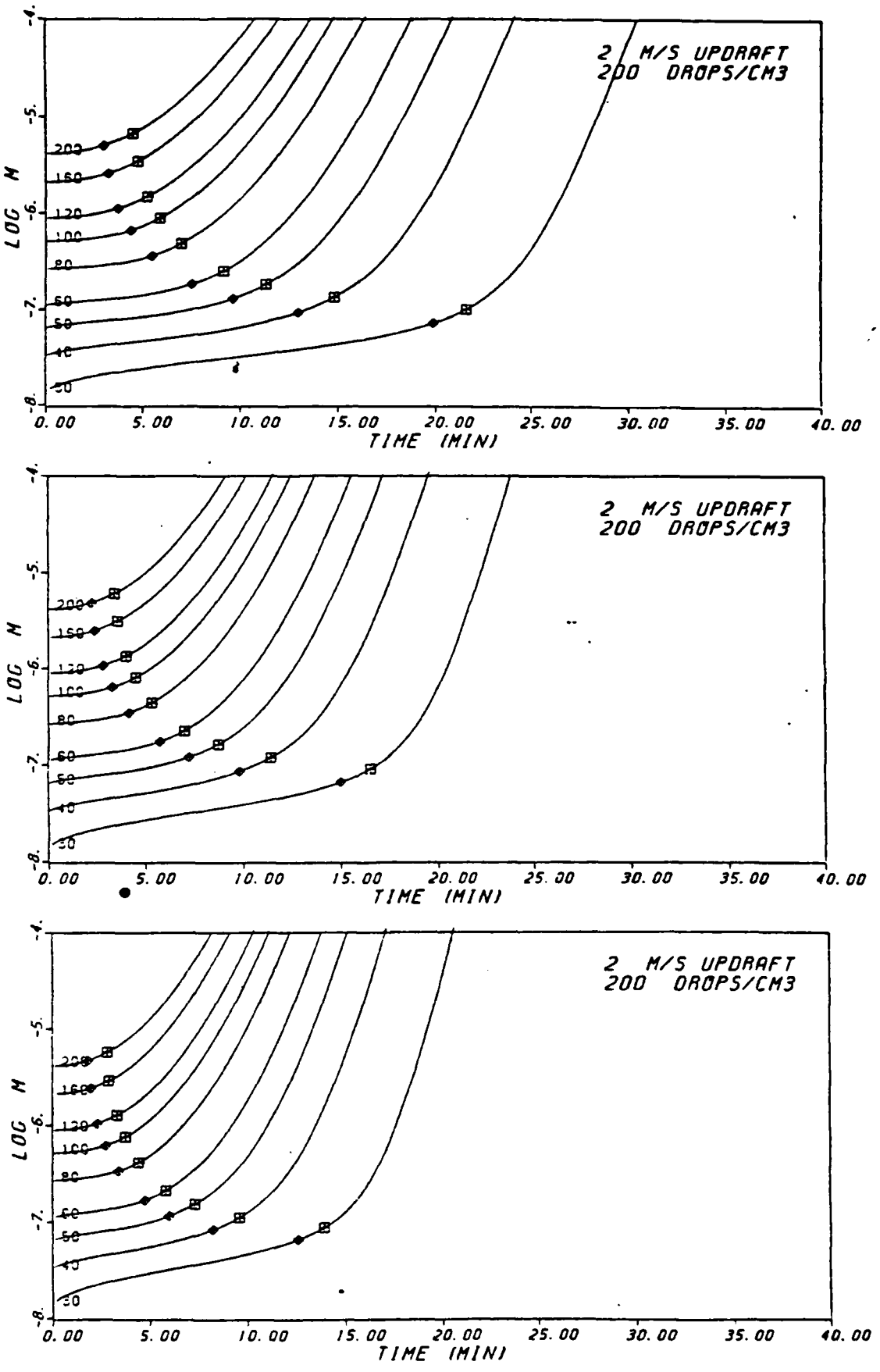

Figure 8. Growth of large drops (30-200 μm initial diameter) in a simple cloud model. The upper plot assumed a cloud base temperature of 0°C. The middle plot assumed a 10°C base temperature and the bottom plot assumed a base temperature of 20°C. Each case involved adiabatic water contents.

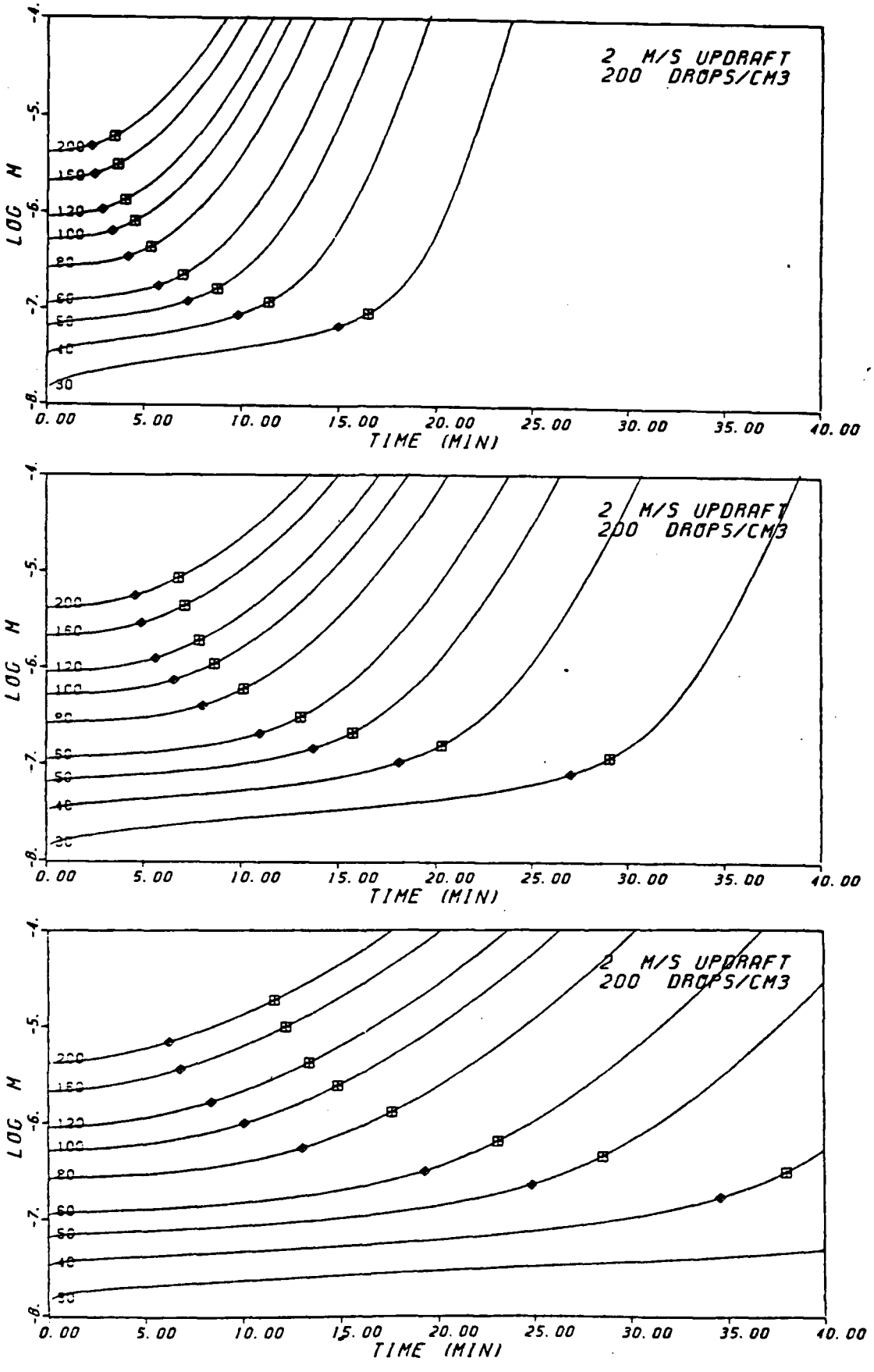

Figure 9. Growth of large drops (30-200 μm initial diameter) in a simple cloud model. The upper plot assumed adiabatic water contents, the middle plot assumed water contents that were half of the adiabatic values, and the bottom plot assumed a height dependent fraction of the adiabatic water content that corresponds to Figure 2. In each case, the cloud base temperature was assumed to be 10°C.

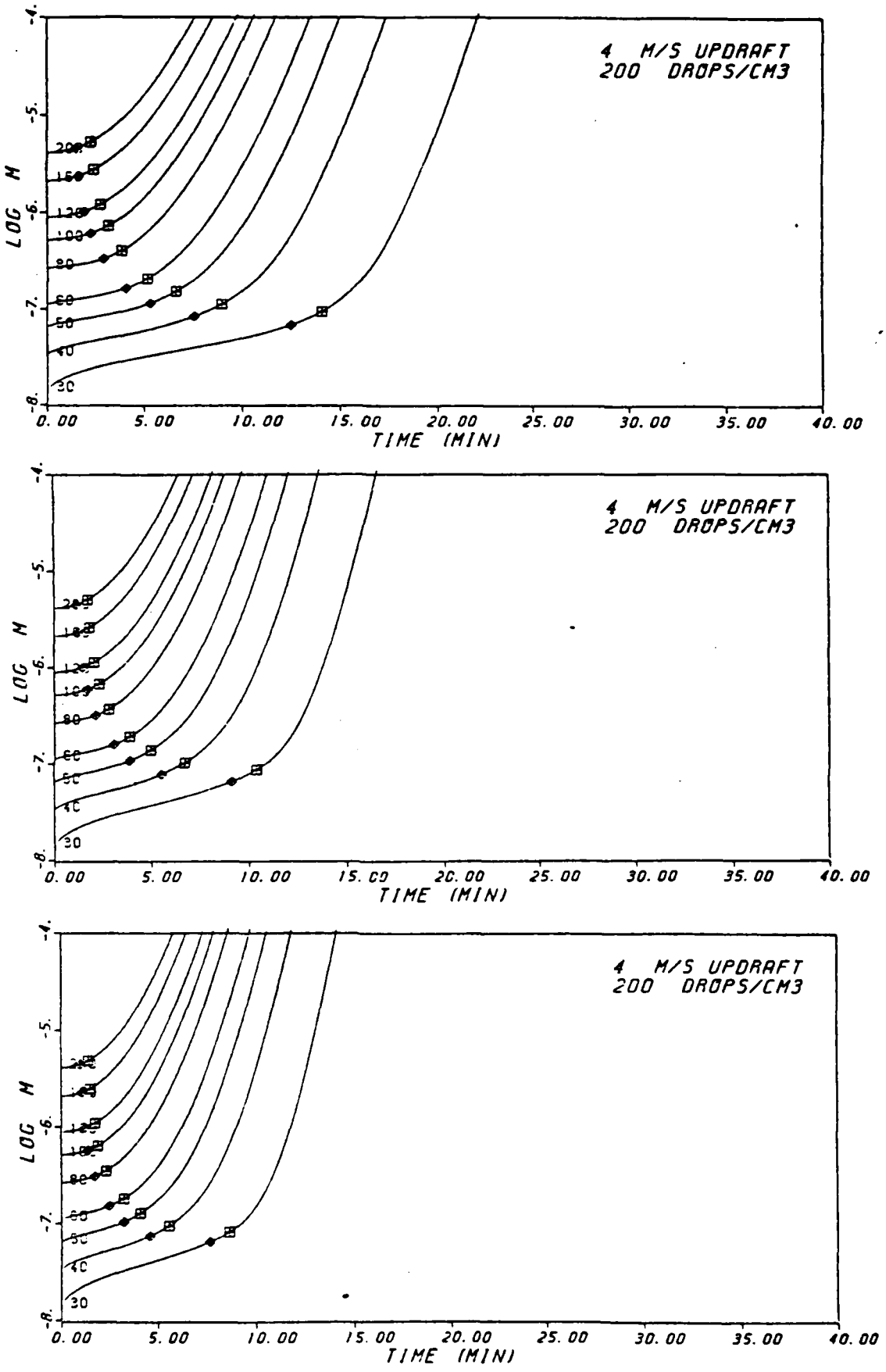

Figure 10. Growth of large drops (30-200 μm initial diameter) in a simple cloud model. The upper plot assumed a cloud base temperature of 0°C. The middle plot assumed a 10°C base temperature and the bottom plot assumed a base temperature of 20°C. Each case involved adiabatic water contents.

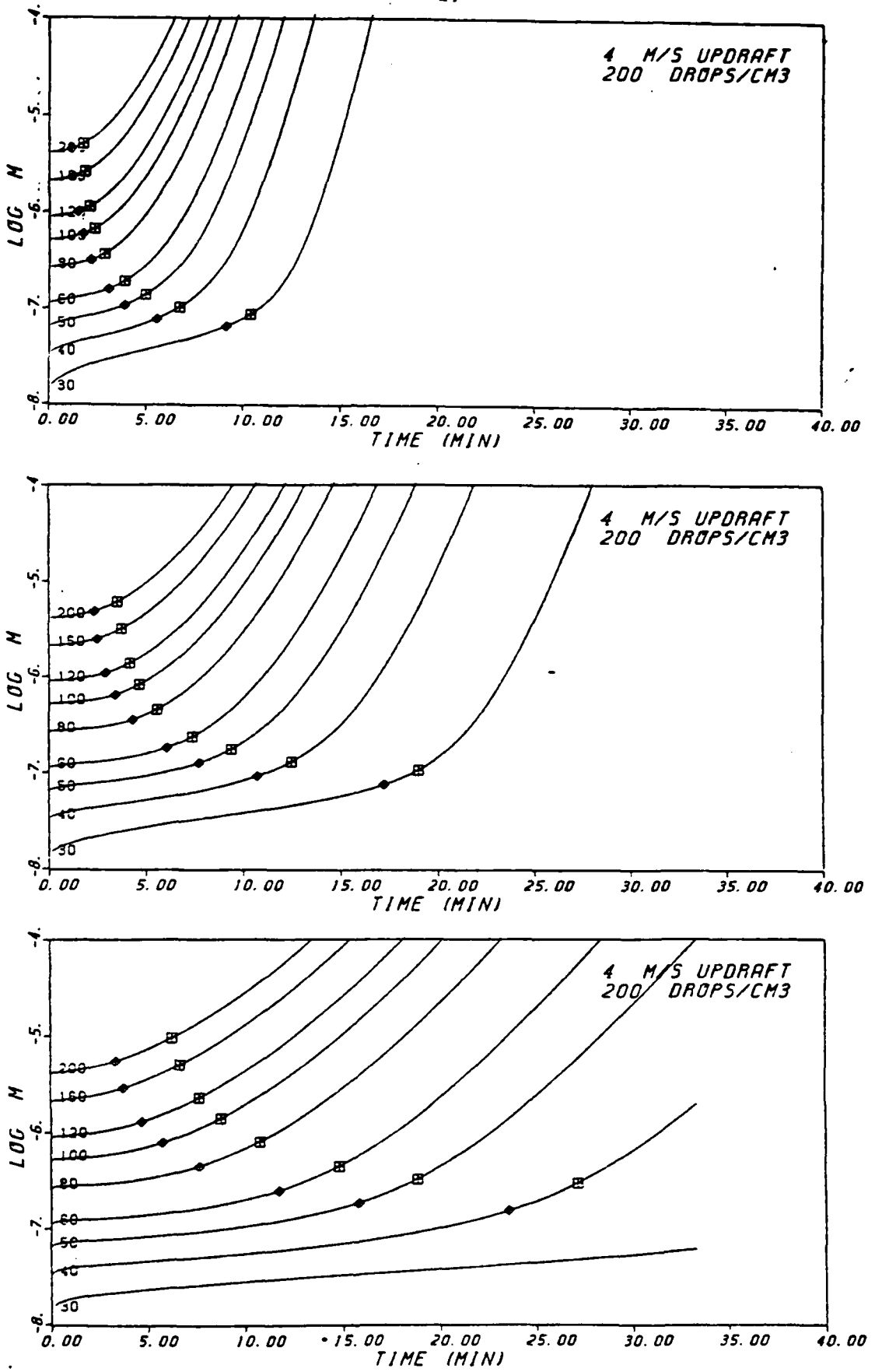

Figure 11. Growth of large drops (30-200 μm initial diameter) in a simple cloud model. The upper plot assumed adiabatic water contents, the middle plot assumed water contents that were half of the adiabatic values, and the bottom plot assumed a height dependent fraction of the adiabatic water content that corresponds to Figure 2. In each case, the cloud base temperature was assumed to be 10°C.

the other in terms of a "coalescence threshold." The symbols superimposed on each growth curve indicate the points at which the coalescence growth alone is adequate to make a MDT of 5 minutes (left-most symbol) or 3 minutes (right-most symbol). Either of these possible thresholds is capable of partitioning the growth curves into a slow initial growth regime and a rapid growth regime that quickly produces drops of raindrop dimensions. Of these two possible thresholds, the 3-min doubling is a rather conservative measure of the onset of rapid growth while the 5-min doubling is a rather optimistic estimate of the transition point. In most cases, however, the transition from slow to rapid growth is so fast that these two alternatives for defining a threshold value are not very far apart. This is particularly true in the cases for which drop growth is relatively rapid. For this reason, the most sensitive comparisons of the two possible thresholds are those runs in which the evolution of raindrops is relatively slow - i.e., those runs which have the coolest cloud base temperatures, highest total drop concentrations, weakest updrafts, or most entrainment.

The stratiform runs examined drop growth in situations in which the weak updrafts present do not force the cloud development by the continual buildup in condensed liquid water, but rather have liquid water contents that are effectively constant with time. In these cases the onset of effective coalescence growth was less dramatic and the critical parameter for raindrop or drizzle production seemed to be the overall time available for growth to continue. Although the coalescence threshold (MDT of 3 or 5 minutes) didn't signify any marked change in the stratiform growth curves, it still serves as a rough indicator of the relative speed of drop growth.

To be useful in the context of interpreting cloud structure and evolution, the coalescence threshold (MDT of 3-5 minutes) must be re-expressed in terms that directly relate to cloud thickness or degree of development. Figures 12 and 13 are a start in this direction, identifying those drops that will grow at or above the 3 (Fig. 12) or 5 (Fig. 13) minute MDT threshold for liquid water contents between 0 and 3 grams per cubic meter. In each Figure, plots have been generated for each of six different total droplet concentrations (N = 50, 100, 200, 400, 800, and 1200 cm^{-3}). It is clear that there are minimum liquid water contents (and minimum drop diameters) for effective coalescence growth. If the shaded region of each plot were strictly rectangular, it would be possible to identify specific minimum water contents and drop diameters for effective coalescence growth. Since the lower-left-hand corner of the shaded region is curved, however, there is a degree of uncertainty in assigning any single minimum value of liquid water content as marking the transition to effective coalescence growth. One identifiable critical water content is the lowest value for which any size drop can meet the threshold criteria of a 3 or 5 minute MDT. In general, however, drops meeting this criteria will have to already be approaching millimeter dimensions. The more crucial question is when drops in the vicinity of 50 μm diameter are capable of starting effective coalescence growth since these drops may be numerous enough to have significant impact on subsequent cloud development (Johnson, 1982). This means that some compromise must be invoked between the minimum water content that can support effective coalescence for any sized drop and selection of a water content that permits the smallest diameter (and hence the most

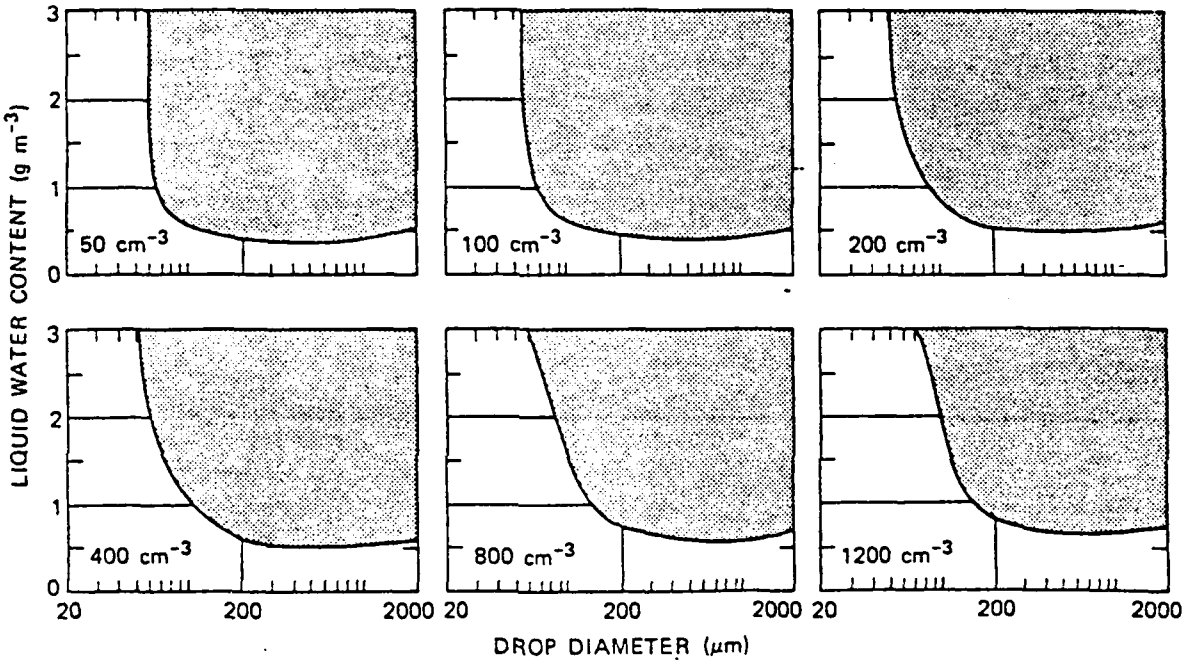

Figure 12. Plots identifying the liquid water contents (shaded region) which are capable of supporting effective coalescence growth (MDT = 3 minutes) as a function of the diameter of the growing drop.

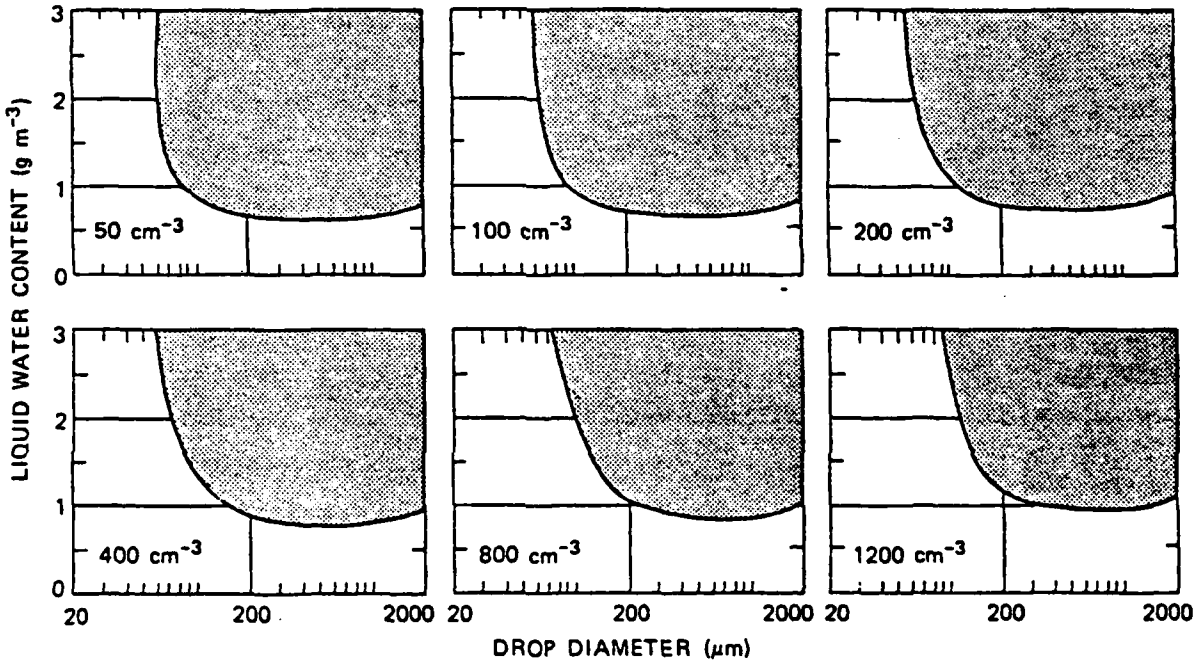

Figure 13. Plots identifying the liquid water contents (shaded region) which are capable of supporting effective coalescence growth (MDT = 5 minutes) as a function of the diameter of the growing drop.

numerous) drops possible to grow effectively. Close examination of the plots included in Figures 12 and 13 (as well as other plots not shown) led to a simple relation that may be adequate to specify a rough estimate of the minimum water content that could support effective coalescence growth as a function of the total droplet concentration:

$$L_{min} = 0.6 + 0.01\ N^{0.5}\ , \qquad (3)$$

where L_{min} is the minimum liquid water content in g m^{-3} and N is the total droplet concentration in cm^{-3}. This particular relation corresponds rather well to both the minimum value of water content that can ever meet a MDT threshold of 5 minutes and (simultaneously) allow relatively small large drops to exceed a MDT threshold of 3 minutes.

A similar, but independent, estimate of the minimum radius of large drop capable of effective coalescence growth led to the relation

$$\log_{10} R_{min} = 1.5 + 0.006\ N^{0.5} \qquad (4)$$

where, as before, N is the total droplet concentration in cm^{-3} and R_{min} is the minimum large drop radius in microns.

Figure 14 repeats several of the growth curves for individual large drops that were previously discussed, but with additional shading to identify the region of the plot which (3) and (4) identify as being capable of supporting effective coalescence growth. While the correspondence with the individual growth curves is not perfect, it is apparent that these suggested relations can be useful tools in quantifying the start of effective coalescence growth.

Another way of looking at this same threshold is illustrated in Figure 15. This figure is a copy of Figure 2, but with an overlay identifying

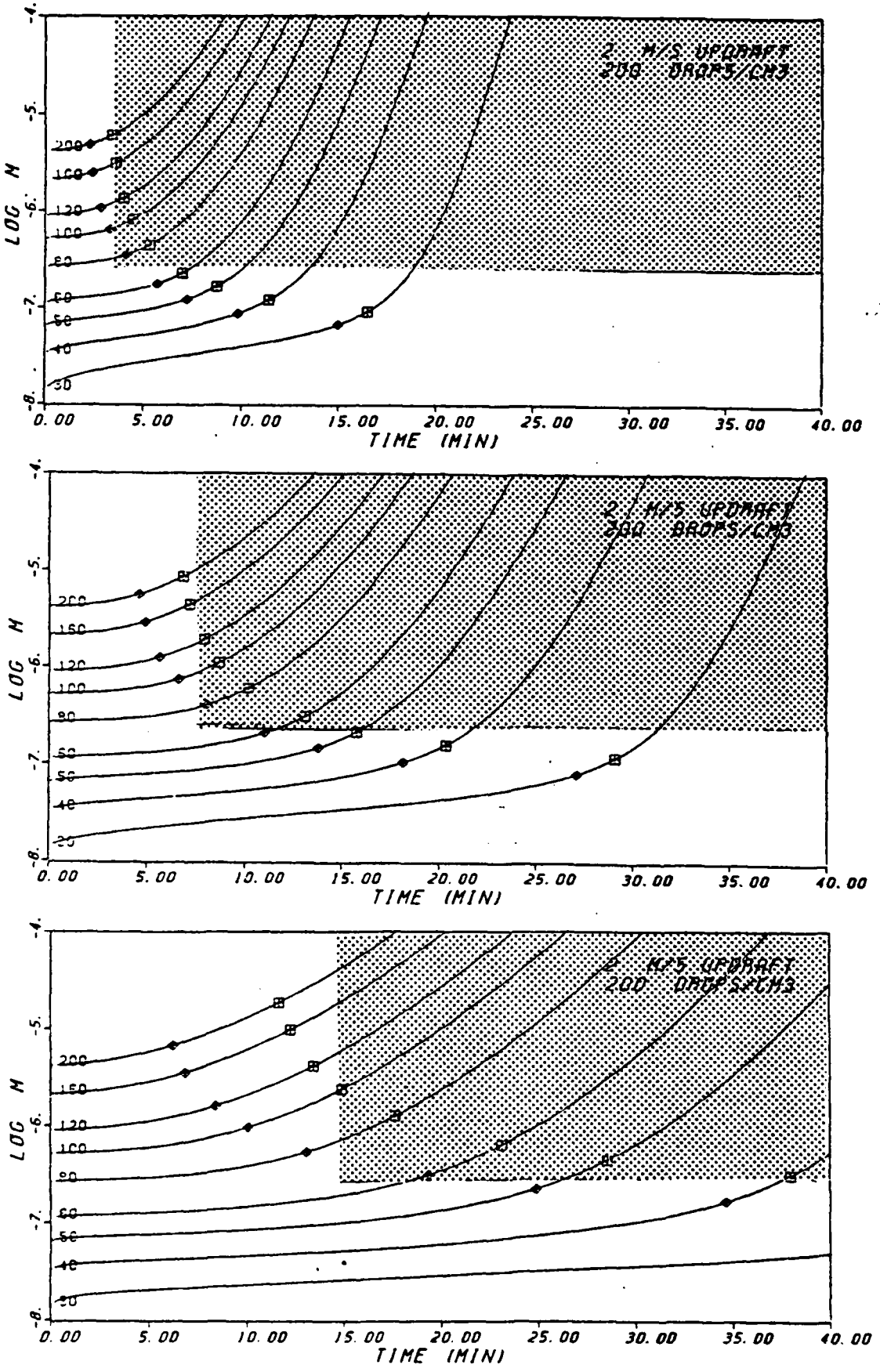

Figure 14. Growth of large drops (30-200 μm initial diameter) in a simple cloud model. The shaded area indicates the region of the graph which might be expected to support effective coalescence growth.

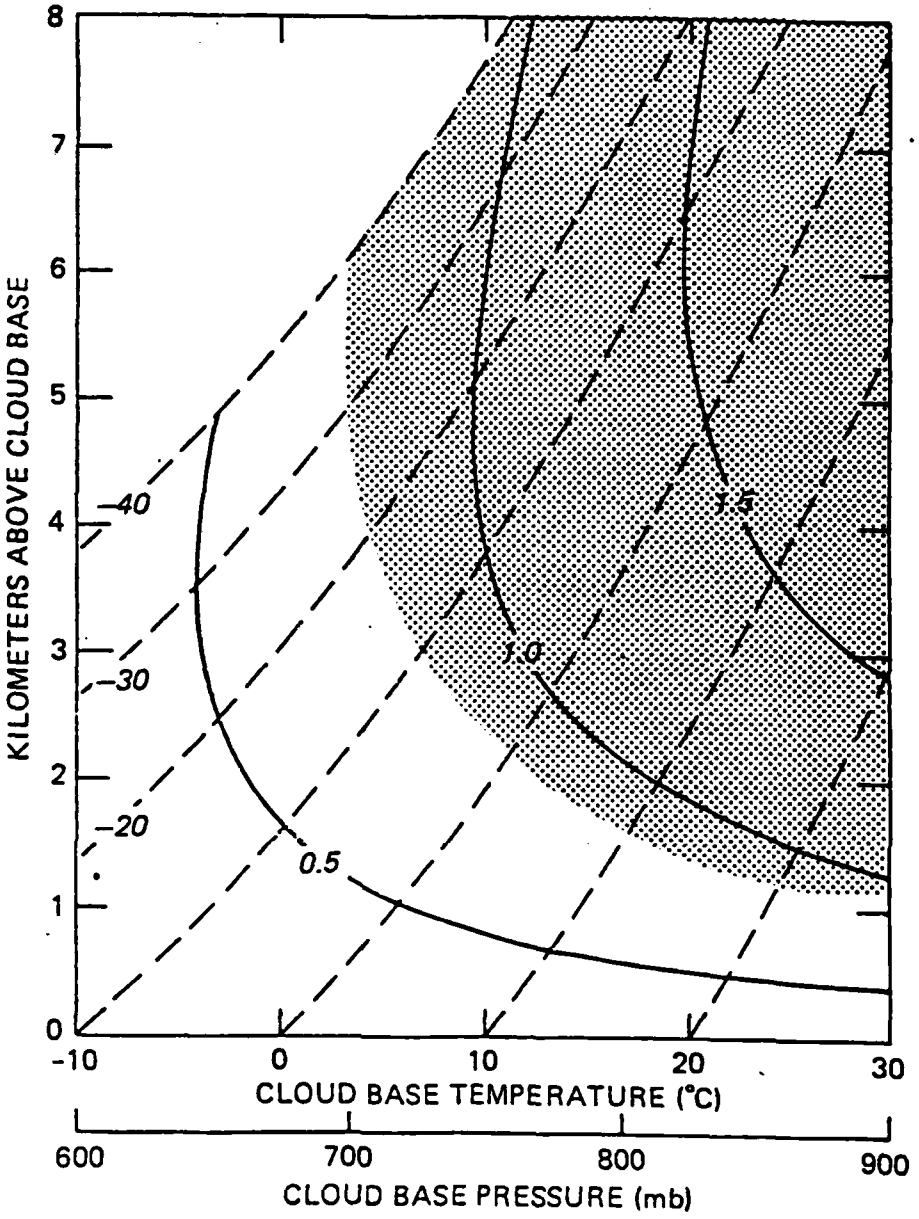

Figure 15. Mean liquid water contents for cumuliform clouds superimposed with shading to indicate the regions which might be expected to support effective coalescence growth.

the region of effective coalescence growth as defined by (3) for a cloud base droplet concentration of 600 cm^{-3}. This figure suggest a major difference between clouds with base temperatures substantially below 10°C and those with base temperatures substantially above 10°C. In either case, effective coalescence can begin within an adiabatic core within a kilometer or so of cloud base. In the warm based clouds, however, effective coalescence growth can still occur even in regions that have average water contents. On the other hand, in cold-based clouds average water contents would not be adequate to support effective coalescence growth.

TIME AND LOCATION OF WARM RAIN DEVELOPMENT

Following the study of coalescence onset, additional studies were performed to identify the time and location of precipitation formation as a function of the cloud base temperature, updraft velocity, total droplet concentration, and degree of entrainment. These studies made up the bulk of the first year effort of this study. Ihe initial studies of this type all used the same continuous collection parcel model employed in the studies of the growth of individual particles (Figs. 4-11).

Table 1 shows some of the results of these studies - presenting the height (m) at which the radars reflectivity factor first exceeds 10 dBZ. This is a commonly used measure of precipitation onset and corresponds to the first development of significant concentrations of raindrops. In all cases in which the parcel exceeded 8 km altitude or fell below -40°C before reaching 10 dBZ, the height entry is replaced with a full field of asterisks. Tables 2 and 3 present similar data, but in these tables sub-adiabatic water

TABLE 1

RADIAT = 1.0

10 DBZ ECHO HEIGHTS

UPDRAFT VELOCITY, M/S (# CONCENTRATION, CM-3)	CLOUD BASE TEMPERATURE -10	-5	0	5	10	15	20	25	30
16.0 (50.)	******	******	******	******	6038.	5499.	5100.	4811.	4588.
16.0 (200.)	******	******	******	******	6134.	5553.	5170.	4899.	4698.
16.0 (600.)	******	******	******	******	6110.	5520.	5132.	4858.	4654.
16.0 (1200.)	******	******	******	******	6350.	5688.	5263.	4969.	4754.
14.0 (50.)	******	******	******	6348.	5567.	5067.	4721.	4468.	4275.
14.0 (200.)	******	******	******	6433.	5617.	5115.	4778.	4536.	4355.
14.0 (600.)	******	******	******	6427.	5603.	5093.	4750.	4505.	4321.
14.0 (1200.)	******	******	******	******	5832.	5260.	4883.	4618.	4421.
12.0 (50.)	******	******	******	5680.	5041.	4619.	4323.	4103.	3935.
12.0 (200.)	******	******	******	5771.	5094.	4665.	4370.	4156.	3994.
12.0 (600.)	******	******	******	5774.	5089.	4653.	4352.	4135.	3971.
12.0 (1200.)	******	******	******	6094.	5307.	4818.	4487.	4250.	4073.
10.0 (50.)	******	******	******	5016.	4499.	4149.	3899.	3711.	3567.
10.0 (200.)	******	******	******	5112.	4559.	4195.	3941.	3754.	3612.
10.0 (600.)	******	******	******	5125.	4562.	4192.	3933.	3743.	3598.
10.0 (1200.)	******	******	******	5410.	4768.	4354.	4069.	3860.	3703.
8.0 (50.)	******	******	4964.	4341.	3932.	3648.	3441.	3294.	3163.
8.0 (200.)	******	******	5131.	4442.	4001.	3699.	3483.	3323.	3200.
8.0 (600.)	******	******	5198.	4466.	4011.	3704.	3484.	3320.	3195.
8.0 (1200.)	******	******	******	4716.	4203.	3861.	3618.	3439.	3302.
6.0 (50.)	******	******	4095.	3637.	3324.	3100.	2935.	2808.	2710.
6.0 (200.)	******	******	4248.	3741.	3400.	3160.	2984.	2850.	2747.
6.0 (600.)	******	******	4327.	3780.	3422.	3173.	2992.	2856.	2750.
6.0 (1200.)	******	******	4591.	3989.	3595.	3321.	3122.	2973.	2858.
4.0 (50.)	******	3653.	3186.	2869.	2644.	2479.	2354.	2258.	2183.
4.0 (200.)	******	3848.	3323.	2972.	2725.	2546.	2412.	2308.	2228.
4.0 (600.)	******	4004.	3412.	3028.	2764.	2573.	2431.	2323.	2239.
4.0 (1200.)	******	4241.	3604.	3190.	2905.	2701.	2548.	2432.	2340.
3.0 (50.)	3601.	3054.	2692.	2439.	2257.	2122.	2018.	1938.	1875.
3.0 (200.)	******	3225.	2818.	2539.	2339.	2191.	2079.	1992.	1924.
3.0 (600.)	******	3370.	2913.	2604.	2387.	2228.	2108.	2015.	1943.
3.0 (1200.)	******	3549.	3065.	2738.	2507.	2338.	2211.	2113.	2036.
2.0 (50.)	2793.	2407.	2143.	1954.	1815.	1710.	1630.	1567.	1517.
2.0 (200.)	2995.	2554.	2257.	2047.	1894.	1780.	1692.	1623.	1569.
2.0 (600.)	3173.	2682.	2352.	2120.	1952.	1826.	1730.	1656.	1598.
2.0 (1200.)	3328.	2807.	2462.	2220.	2045.	1914.	1814.	1736.	1674.
1.0 (50.)	1882.	1648.	1481.	1358.	1266.	1195.	1141.	1098.	1063.
1.0 (200.)	2033.	1765.	1576.	1438.	1336.	1258.	1198.	1150.	1113.
1.0 (600.)	2143.	1858.	1655.	1506.	1395.	1311.	1245.	1193.	1152.
1.0 (1200.)	2246.	1937.	1723.	1558.	1452.	1365.	1298.	1244.	1202.
.5 (50.)	1301.	1152.	1042.	958.	895.	845.	807.	776.	752.
.5 (200.)	1423.	1249.	1122.	1027.	956.	900.	857.	823.	796.
.5 (600.)	1488.	1308.	1176.	1077.	1002.	944.	898.	862.	833.
.5 (1200.)	1591.	1375.	1229.	1122.	1042.	981.	933.	896.	866.

TABLE 2

ADIBAT = .5

10 DBZ ECHO HEIGHTS

UPDRAFT VELOCITY, M/S (# CONCENTRATION, CM-3)	CLOUD BASE TEMPERATURE -10	-5	0	5	10	15	20	25	30
16.0 (50.)	******	******	******	******	******	******	******	7460.	7077.
16.0 (200.)	******	******	******	******	******	******	******	7518.	7130.
16.0 (600.)	******	******	******	******	******	******	******	7509.	7112.
16.0 (1200.)	******	******	******	******	******	******	******	7811.	7368.
14.0 (50.)	******	******	******	******	******	******	7324.	6850.	6518.
14.0 (200.)	******	******	******	******	******	******	7413.	6917.	6576.
14.0 (600.)	******	******	******	******	******	******	7426.	6920.	6571.
14.0 (1200.)	******	******	******	******	******	******	7789.	7213.	6824.
12.0 (50.)	******	******	******	******	******	7217.	6620.	6222.	5939.
12.0 (200.)	******	******	******	******	******	7372.	6723.	6301.	6004.
12.0 (600.)	******	******	******	******	******	7411.	6745.	6314.	6010.
12.0 (1200.)	******	******	******	******	******	7860.	7085.	6597.	6259.
10.0 (50.)	******	******	******	******	7129.	6376.	5899.	5570.	5330.
10.0 (200.)	******	******	******	******	7383.	6538.	6016.	5662.	5407.
10.0 (600.)	******	******	******	******	7496.	6591.	6048.	5684.	5423.
10.0 (1200.)	******	******	******	******	******	6983.	6363.	5954.	5664.
8.0 (50.)	******	******	******	******	6087.	5523.	5147.	4881.	4683.
8.0 (200.)	******	******	******	******	6321.	5688.	5276.	4986.	4773.
8.0 (600.)	******	******	******	******	6444.	5758.	5321.	5019.	4798.
8.0 (1200.)	******	******	******	******	6863.	6093.	5606.	5271.	5027.
6.0 (50.)	******	******	******	5677.	5043.	4631.	4344.	4135.	3977.
6.0 (200.)	******	******	******	5981.	5257.	4796.	4480.	4251.	4079.
6.0 (600.)	******	******	******	6210.	5390.	4885.	4544.	4300.	4118.
6.0 (1200.)	******	******	******	******	5713.	5157.	4787.	4524.	4326.
4.0 (50.)	******	******	4993.	4355.	3941.	3656.	3450.	3296.	3177.
4.0 (200.)	******	******	5345.	4601.	4132.	3814.	3586.	3417.	3287.
4.0 (600.)	******	******	******	4806.	4275.	3921.	3672.	3488.	3347.
4.0 (1200.)	******	******	******	5072.	4504.	4126.	3861.	3665.	3516.
3.0 (50.)	******	******	4137.	3660.	3339.	3112.	2945.	2818.	2720.
3.0 (200.)	******	******	4430.	3878.	3515.	3261.	3076.	2937.	2828.
3.0 (600.)	******	******	4693.	4067.	3659.	3376.	3172.	3018.	2900.
3.0 (1200.)	******	******	4939.	4268.	3838.	3542.	3327.	3167.	3042.
2.0 (50.)	******	3750.	3240.	2903.	2668.	2497.	2369.	2271.	2194.
2.0 (200.)	******	4083.	3479.	3092.	2826.	2634.	2492.	2383.	2298.
2.0 (600.)	******	4346.	3682.	3253.	2960.	2749.	2592.	2473.	2379.
2.0 (1200.)	******	4584.	3856.	3398.	3089.	2870.	2708.	2584.	2488.
1.0 (50.)	2909.	2492.	2206.	2003.	1853.	1741.	1656.	1589.	1536.
1.0 (200.)	3245.	2731.	2392.	2155.	1984.	1858.	1762.	1687.	1628.
1.0 (600.)	3414.	2871.	2515.	2266.	2085.	1951.	1848.	1768.	1705.
1.0 (1200.)	3710.	3051.	2641.	2367.	2173.	2030.	1922.	1839.	1773.
.5 (50.)	1957.	1711.	1535.	1405.	1306.	1231.	1173.	1127.	1090.
.5 (200.)	2196.	1898.	1687.	1533.	1419.	1332.	1265.	1212.	1170.
.5 (600.)	2299.	1981.	1760.	1600.	1482.	1393.	1324.	1269.	1226.
.5 (1200.)	2522.	2139.	1880.	1695.	1561.	1461.	1384.	1325.	1278.

TABLE 3

ADIBAT = -1.0

10 DBZ ECHO HEIGHTS

UPDRAFT VELOCITY, M/S (# CONCENTRATION, CM-3)	CLOUD BASE TEMPERATURE -10	-5	0	5	10	15	20	25	30
16.0 (50.)	******	******	******	******	******	******	******	******	******
16.0 (200.)	******	******	******	******	******	******	******	******	******
16.0 (600.)	******	******	******	******	******	******	******	******	******
16.0 (1200.)	******	******	******	******	******	******	******	******	******
14.0 (50.)	******	******	******	******	******	******	******	******	******
14.0 (200.)	******	******	******	******	******	******	******	******	******
14.0 (600.)	******	******	******	******	******	******	******	******	******
14.0 (1200.)	******	******	******	******	******	******	******	******	******
12.0 (50.)	******	******	******	******	******	******	******	******	******
12.0 (200.)	******	******	******	******	******	******	******	******	******
12.0 (600.)	******	******	******	******	******	******	******	******	******
12.0 (1200.)	******	******	******	******	******	******	******	******	******
10.0 (50.)	******	******	******	******	******	******	******	******	******
10.0 (200.)	******	******	******	******	******	******	******	******	******
10.0 (600.)	******	******	******	******	******	******	******	******	******
10.0 (1200.)	******	******	******	******	******	******	******	******	******
8.0 (50.)	******	******	******	******	******	******	******	7674.	7248.
8.0 (200.)	******	******	******	******	******	******	******	******	7597.
8.0 (600.)	******	******	******	******	******	******	******	******	7807.
8.0 (1200.)	******	******	******	******	******	******	******	******	******
6.0 (50.)	******	******	******	******	******	7400.	6721.	6278.	5965.
6.0 (200.)	******	******	******	******	******	7954.	7145.	6636.	6282.
6.0 (600.)	******	******	******	******	******	******	7487.	6903.	6506.
6.0 (1200.)	******	******	******	******	******	******	7964.	7327.	6898.
4.0 (50.)	******	******	******	******	6160.	5513.	5093.	4798.	4581.
4.0 (200.)	******	******	******	******	6709.	5929.	5439.	5102.	4855.
4.0 (600.)	******	******	******	******	7217.	6301.	5741.	5360.	5083.
4.0 (1200.)	******	******	******	******	7675.	6658.	6052.	5648.	5358.
3.0 (50.)	******	******	******	5761.	5011.	4542.	4222.	3991.	3817.
3.0 (200.)	******	******	******	6390.	5455.	4897.	4527.	4263.	4066.
3.0 (600.)	******	******	******	******	5843.	5211.	4795.	4501.	4283.
3.0 (1200.)	******	******	******	******	6177.	5484.	5038.	4727.	4498.
2.0 (50.)	******	******	5034.	4291.	3820.	3499.	3269.	3099.	2968.
2.0 (200.)	******	******	******	4753.	4175.	3795.	3528.	3332.	3183.
2.0 (600.)	******	******	******	5076.	4448.	4036.	3746.	3533.	3371.
2.0 (1200.)	******	******	******	5423.	4697.	4242.	3929.	3703.	3532.
1.0 (50.)	******	3615.	3069.	2709.	2456.	2273.	2136.	2030.	1948.
1.0 (200.)	******	4206.	3490.	3033.	2723.	2502.	2339.	2215.	2118.
1.0 (600.)	******	4478.	3685.	3200.	2874.	2643.	2473.	2344.	2243.
1.0 (1200.)	******	******	4077.	3470.	3078.	2809.	2615.	2471.	2359.
.5 (50.)	2694.	2250.	1954.	1747.	1597.	1485.	1399.	1333.	1280.
.5 (200.)	3171.	2609.	2240.	1985.	1802.	1665.	1561.	1480.	1416.
.5 (600.)	3485.	2792.	2367.	2088.	1892.	1748.	1640.	1556.	1491.
.5 (1200.)	******	3168.	2648.	2308.	2072.	1901.	1773.	1674.	1598.

contents were employed (half of adiabatic in Table 2 and a variable fraction of adiabatic corresponding to equation (1) in Table 3). One of the most interesting results of this study is the relative insensitivity of the time and location of precipitation onset to total droplet concentration.

The first echo heights can be redefined in terms of the additional time (or height) required to reach the 10 dBZ echo intensity after passing the threshold water content defined by (3). These "adjusted" heights are presented in Tables 4, 5, and 6 for the same three bulk entrainment rates invoked in generating Tables 1-3. Adjustments of this sort to allow for the initial "incubation" period of a cloud in which coalescence growth is either absent or ineffective may ultimately simplify predictions of the time and location of precipitation onset and reduce some of the variability introduced by differing updraft velocities or entrainment rates.

The parcel model used for these studies is an attractive tool for investigations of this sort. It is relatively inexpensive to run and produces a rather precise estimate of the height of precipitation development. These are both valuable attributes when performing a large set of runs for intercomparison. While intercomparisons between runs are relatively reliable with this model, the absolute accuracy of the locations of precipitation onset is suspect since the model neglects differential sedimentation of the falling drops. This problem can be addressed by using a "trajectory" model that allows explicit consideration of the relative motion of the growing raindrops. When incorporated into an appropriate framework (see Johnson, 1982), this sort of model can produce time-height cross-sections of radar reflectivity that behave very much like observed radar "first echoes" (e.g., Battan, 1953). Figure 16 shows one such cross-section calculated with an improved version

TABLE 4

ADIBAT = 1.0
ECHO HEIGHTS ADJUSTED FOR THRES2

10 DBZ ECHO HEIGHTS

UPDRAFT VELOCITY, M/S (# CONCENTRATION, CM-3)	CLOUD BASE TEMPERATURE -10	-5	0	5	10	15	20	25	30
16.0 (50.)	******	******	******	******	5708.	5159.	4790.	4531.	4328.
16.0 (200.)	******	******	******	******	5714.	5173.	4830.	4589.	4408.
16.0 (600.)	******	******	******	******	5630.	5090.	4742.	4498.	4324.
16.0 (1200.)	******	******	******	******	5810.	5208.	4833.	4569.	4384.
14.0 (50.)	******	******	******	5908.	5187.	4727.	4411.	4188.	4015.
14.0 (200.)	******	******	******	5943.	5197.	4735.	4438.	4226.	4065.
14.0 (600.)	******	******	******	5867.	5123.	4663.	4360.	4145.	3991.
14.0 (1200.)	******	******	******	******	5292.	4780.	4453.	4218.	4051.
12.0 (50.)	******	******	******	5240.	4661.	4279.	4013.	3823.	3675.
12.0 (200.)	******	******	******	5281.	4674.	4285.	4030.	3846.	3704.
12.0 (600.)	******	******	******	5214.	4609.	4223.	3962.	3775.	3641.
12.0 (1200.)	******	******	******	5464.	4767.	4338.	4057.	3850.	3703.
10.0 (50.)	******	******	******	4576.	4119.	3809.	3589.	3431.	3307.
10.0 (200.)	******	******	******	4622.	4139.	3815.	3601.	3444.	3322.
10.0 (600.)	******	******	******	4565.	4082.	3762.	3543.	3383.	3268.
10.0 (1200.)	******	******	******	4780.	4228.	3874.	3639.	3460.	3333.
8.0 (50.)	******	******	4434.	3901.	3552.	3308.	3131.	3004.	2903.
8.0 (200.)	******	******	4551.	3952.	3581.	3319.	3143.	3013.	2910.
8.0 (600.)	******	******	4528.	3906.	3531.	3274.	3094.	2960.	2865.
8.0 (1200.)	******	******	******	4086.	3663.	3381.	3188.	3039.	2932.
6.0 (50.)	******	******	3565.	3197.	2944.	2760.	2625.	2528.	2450.
6.0 (200.)	******	******	3668.	3251.	2980.	2780.	2644.	2540.	2457.
6.0 (600.)	******	******	3657.	3220.	2942.	2743.	2602.	2496.	2420.
6.0 (1200.)	******	******	3831.	3359.	3055.	2841.	2692.	2573.	2488.
4.0 (50.)	******	3003.	2656.	2429.	2264.	2139.	2044.	1978.	1923.
4.0 (200.)	******	3118.	2743.	2482.	2305.	2166.	2072.	1998.	1938.
4.0 (600.)	******	3164.	2742.	2468.	2284.	2143.	2041.	1963.	1909.
4.0 (1200.)	******	3281.	2844.	2560.	2365.	2221.	2118.	2032.	1970.
3.0 (50.)	2751.	2404.	2162.	1999.	1877.	1782.	1709.	1658.	1615.
3.0 (200.)	******	2495.	2238.	2049.	1919.	1811.	1739.	1682.	1634.
3.0 (600.)	******	2530.	2243.	2044.	1907.	1798.	1718.	1655.	1613.
3.0 (1200.)	******	2589.	2305.	2108.	1967.	1858.	1781.	1713.	1666.
2.0 (50.)	1943.	1757.	1613.	1514.	1435.	1370.	1320.	1287.	1257.
2.0 (200.)	2035.	1824.	1677.	1557.	1474.	1400.	1352.	1313.	1279.
2.0 (600.)	2043.	1842.	1682.	1560.	1472.	1396.	1340.	1296.	1268.
2.0 (1200.)	2028.	1847.	1702.	1590.	1505.	1434.	1384.	1336.	1304.
1.0 (50.)	1032.	998.	951.	918.	886.	855.	831.	818.	803.
1.0 (200.)	1073.	1035.	996.	948.	916.	878.	858.	840.	823.
1.0 (600.)	1013.	1018.	985.	946.	915.	881.	855.	833.	822.
1.0 (1200.)	946.	977.	963.	938.	912.	885.	866.	844.	832.
.5 (50.)	451.	502.	512.	518.	515.	505.	497.	496.	492.
.5 (200.)	463.	519.	542.	537.	536.	520.	517.	513.	506.
.5 (600.)	358.	468.	506.	517.	522.	514.	508.	502.	503.
.5 (1200.)	281.	415.	469.	492.	502.	501.	503.	496.	496.

TABLE 5

ADIBAT = .5
ECHO HEIGHTS ADJUSTED FOR THRES2

10 DBZ ECHO HEIGHTS

UPDRAFT VELOCITY, M/S (# CONCENTRATION, CM-3)	CLOUD BASE TEMPERATURE -10	-5	0	5	10	15	20	25	30
16.0 (50.)	******	******	******	******	******	******	******	6880.	6547.
16.0 (200.)	******	******	******	******	******	******	******	6878.	6540.
16.0 (600.)	******	******	******	******	******	******	******	6779.	6432.
16.0 (1200.)	******	******	******	******	******	******	******	6991.	6608.
14.0 (50.)	******	******	******	******	******	******	6694.	6270.	5988.
14.0 (200.)	******	******	******	******	******	******	6713.	6277.	5986.
14.0 (600.)	******	******	******	******	******	******	6626.	6190.	5891.
14.0 (1200.)	******	******	******	******	******	******	6889.	6393.	6064.
12.0 (50.)	******	******	******	******	******	6517.	5990.	5642.	5409.
12.0 (200.)	******	******	******	******	******	6592.	6023.	5661.	5414.
12.0 (600.)	******	******	******	******	******	6511.	5945.	5584.	5330.
12.0 (1200.)	******	******	******	******	******	6850.	6185.	5777.	5499.
10.0 (50.)	******	******	******	******	6329.	5676.	5269.	4990.	4800.
10.0 (200.)	******	******	******	******	6493.	5758.	5316.	5022.	4817.
10.0 (600.)	******	******	******	******	6466.	5691.	5248.	4954.	4743.
10.0 (1200.)	******	******	******	******	******	5973.	5463.	5134.	4904.
8.0 (50.)	******	******	******	******	5287.	4823.	4517.	4301.	4153.
8.0 (200.)	******	******	******	******	5431.	4908.	4576.	4346.	4183.
8.0 (600.)	******	******	******	******	5414.	4858.	4521.	4289.	4118.
8.0 (1200.)	******	******	******	******	5693.	5083.	4706.	4451.	4267.
6.0 (50.)	******	******	******	4737.	4243.	3931.	3714.	3555.	3447.
6.0 (200.)	******	******	******	4921.	4367.	4016.	3780.	3611.	3489.
6.0 (600.)	******	******	******	4990.	4360.	3985.	3744.	3570.	3438.
6.0 (1200.)	******	******	******	******	4543.	4147.	3887.	3704.	3566.
4.0 (50.)	******	******	3833.	3415.	3141.	2956.	2820.	2716.	2647.
4.0 (200.)	******	******	4035.	3541.	3242.	3034.	2886.	2777.	2697.
4.0 (600.)	******	******	******	3586.	3245.	3021.	2872.	2758.	2667.
4.0 (1200.)	******	******	******	3672.	3334.	3116.	2961.	2845.	2756.
3.0 (50.)	******	******	2977.	2720.	2539.	2412.	2315.	2238.	2190.
3.0 (200.)	******	******	3120.	2818.	2625.	2481.	2376.	2297.	2238.
3.0 (600.)	******	******	3153.	2847.	2629.	2476.	2372.	2288.	2220.
3.0 (1200.)	******	******	3159.	2868.	2668.	2532.	2427.	2347.	2282.
2.0 (50.)	******	2210.	2080.	1963.	1868.	1797.	1739.	1691.	1664.
2.0 (200.)	******	2313.	2169.	2032.	1936.	1854.	1792.	1743.	1708.
2.0 (600.)	******	2176.	2142.	2033.	1930.	1849.	1792.	1743.	1699.
2.0 (1200.)	******	1904.	2076.	1998.	1919.	1860.	1808.	1764.	1728.
1.0 (50.)	379.	952.	1046.	1063.	1053.	1041.	1026.	1009.	1006.
1.0 (200.)	******	961.	1082.	1095.	1094.	1078.	1062.	1047.	1038.
1.0 (600.)	******	701.	975.	1046.	1055.	1051.	1048.	1038.	1025.
1.0 (1200.)	******	371.	861.	967.	1003.	1020.	1022.	1019.	1013.
.5 (50.)	******	171.	375.	465.	506.	531.	543.	547.	560.
.5 (200.)	******	128.	377.	473.	529.	552.	565.	572.	580.
.5 (600.)	******	******	220.	380.	452.	493.	524.	539.	546.
.5 (1200.)	******	******	100.	295.	391.	451.	484.	505.	518.

TABLE 6

ADIRAT = -1.0
ECHO HEIGHTS ADJUSTED FOR THRES2

10 DBZ ECHO HEIGHTS

UPDRAFT VELOCITY, M/S (# CONCENTRATION, CM-3)	CLOUD BASE TEMPERATURE -10	-5	0	5	10	15	20	25	30
16.0 (50.)	******	******	******	******	******	******	******	******	******
16.0 (200.)	******	******	******	******	******	******	******	******	******
16.0 (600.)	******	******	******	******	******	******	******	******	******
16.0 (1200.)	******	******	******	******	******	******	******	******	******
14.0 (50.)	******	******	******	******	******	******	******	******	******
14.0 (200.)	******	******	******	******	******	******	******	******	******
14.0 (600.)	******	******	******	******	******	******	******	******	******
14.0 (1200.)	******	******	******	******	******	******	******	******	******
12.0 (50.)	******	******	******	******	******	******	******	******	******
12.0 (200.)	******	******	******	******	******	******	******	******	******
12.0 (600.)	******	******	******	******	******	******	******	******	******
12.0 (1200.)	******	******	******	******	******	******	******	******	******
10.0 (50.)	******	******	******	******	******	******	******	******	******
10.0 (200.)	******	******	******	******	******	******	******	******	******
10.0 (600.)	******	******	******	******	******	******	******	******	******
10.0 (1200.)	******	******	******	******	******	******	******	******	******
8.0 (50.)	******	******	******	******	******	******	******	6824.	6498.
8.0 (200.)	******	******	******	******	******	******	******	******	6717.
8.0 (600.)	******	******	******	******	******	******	******	******	6707.
8.0 (1200.)	******	******	******	******	******	******	******	******	******
6.0 (50.)	******	******	******	******	******	6210.	5731.	5428.	5215.
6.0 (200.)	******	******	******	******	******	6544.	5975.	5636.	5402.
6.0 (600.)	******	******	******	******	******	******	6037.	5663.	5406.
6.0 (1200.)	******	******	******	******	******	******	6214.	5827.	5578.
4.0 (50.)	******	******	******	******	4660.	4323.	4103.	3948.	3831.
4.0 (200.)	******	******	******	******	4909.	4519.	4269.	4102.	3975.
4.0 (600.)	******	******	******	******	4917.	4541.	4291.	4120.	3983.
4.0 (1200.)	******	******	******	******	4785.	4508.	4302.	4148.	4038.
3.0 (50.)	******	******	******	3681.	3511.	3352.	3232.	3141.	3067.
3.0 (200.)	******	******	******	3790.	3655.	3487.	3357.	3263.	3186.
3.0 (600.)	******	******	******	******	3543.	3451.	3345.	3261.	3183.
3.0 (1200.)	******	******	******	******	3287.	3334.	3288.	3227.	3178.
2.0 (50.)	******	******	******	2211.	2320.	2309.	2279.	2249.	2218.
2.0 (200.)	******	******	******	2153.	2375.	2385.	2358.	2332.	2303.
2.0 (600.)	******	******	******	1166.	2148.	2276.	2296.	2293.	2271.
2.0 (1200.)	******	******	******	******	1807.	2092.	2179.	2203.	2212.
1.0 (50.)	******	******	******	629.	956.	1083.	1146.	1180.	1198.
1.0 (200.)	******	******	******	433.	923.	1092.	1169.	1215.	1238.
1.0 (600.)	******	******	******	******	574.	883.	1023.	1104.	1143.
1.0 (1200.)	******	******	******	******	188.	659.	865.	971.	1039.
.5 (50.)	******	******	******	******	97.	295.	409.	483.	530.
.5 (200.)	******	******	******	******	2.	255.	391.	480.	536.
.5 (600.)	******	******	******	******	******	******	190.	316.	391.
.5 (1200.)	******	******	******	******	******	******	23.	174.	278.

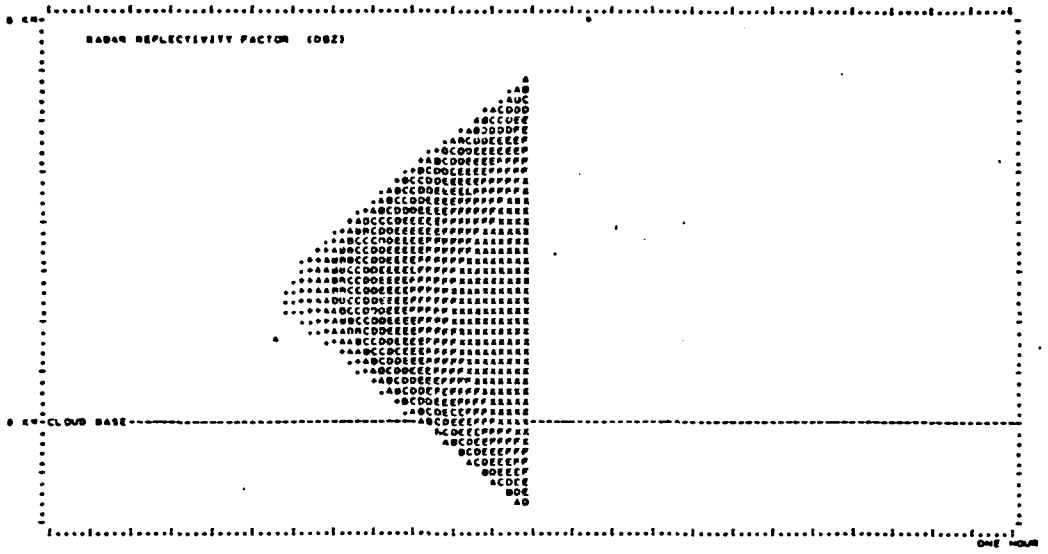

REFLECTIVITY FACTOR CODE (DBZ)

: > -10	B > +5	E > +20	
A > -5	C > +10	F > +30	
A > 0	D > +15	X > +40	

**SEDIMENTATION RUN, 6 M/SEC, 101 LOG SPACED CATEGORIES

600.0 CLOUD DROPLETS PER CM3
10.0 C CLOUD BASE TEMPERATURE
825.0 MB CLOUD BASE PRESSURE
400.0 CM/SEC [illegible]DRAFT VELOCITY

ADJUSTMENT FACTOR = 1.000E+00

90.6 ADIABATIC WATER CONTENTS

3 MIN FIRST ECHO (5 DBZ)

	TEMP(C)	HEIGHT(KM)
CLOUD TOP	.1	6.8
ECHO TOP	6.2	2.7
ECHO BASE	12.0	1.7
		1.0 KM THICK

30 SECOND DATA

3.2	3.4	3.6	3.8	4.0	4.0	
2.6	2.8	1.8	1.8	1.4	1.2	

3 MIN FIRST ECHO (10 DBZ)

	TEMP(C)	HEIGHT(KM)
CLOUD TOP	-1.1	4.7
ECHO TOP	3.8	3.7
ECHO BASE	13.8	1.6
		2.2 KM THICK

30 SECOND DATA

3.0	3.6	3.6	4.0	4.0	4.2
2.2	2.0	1.6	1.4	1.2	1.0

Figure 16. Time-height reflectivity cross-section from "trajectory" model of precipitation initiation.

of the "trajectory" model. Rather than producing a single estimate of the height at which the radar reflectivity reaches detectable limits, this sort of model actually predicts the base and top heights of the echo as a function of time. By scanning over the calculated cross-sections, it is then possible to estimate the average heights of the echo top and base expected in an observational study.

The current version of this model has been improved to include the velocity adjustments for changing air densities and variable entrainment algorithms already introduced into the parcel model. In addition, in order to improve the resolution of the calculated cross-sections, it has been necessary to increase the number of drop categories used in the computations by a factor of four over that used in the parcel calculations (to 101 categories). The extension of the warm rain studies to include results from the trajectory model comprised the major portion of the year two efforts of this study.

A full set of runs of this model have been completed, almost a thousand in all, covering a wide range of updraft velocities, cloud base temperatures (and pressures), droplet concentrations, and degrees of entrainment. Table 7 shows the temperature of the predicted first echo for an adiabatic updraft (°C). Temperatures for both the top and the base of the 10 dBZ 3-minute first echo are shown. [The "three-minute first echo" is just the average top and base of the echo which has reached a 10 dBZ threshold, followed over three minutes of development.] At the upper left hand side of the table, no data are given since the model never developed a 10 dBZ echo. At the lower left, one run is also indeterminant since no echo was formed within one hour, and calculations were

TABLE 7

ADIBAT = 1.0

10 DBZ FIRST ECHO TEMPERATURE (TOP/BASE)

UPDRAFT VELOCITY, M/S (# CONCENTRATION, CM-3)	CLOUD BASE TEMPERATURE -5	0	5	10	15	20	25	30
16.0 (50.)	***/***	***/***	-44/-30	-36/-17	-23/ -8	-11/ 1	0/ 8	7/ 16
16.0 (200.)	***/***	***/***	-43/-30	-33/-17	-20/ -8	-8/ 1	0/ 9	9/ 16
16.0 (600.)	***/***	***/***	-44/-32	-36/-18	-20/ -8	-8/ 1	0/ 8	9/ 15
16.0 (1200.)	***/***	***/***	-42/-34	-35/-20	-23/ -9	-11/ 0	0/ 8	7/ 15
14.0 (50.)	***/***	-40/-38	-40/-25	-28/-14	-17/ -5	-6/ 3	2/ 11	11/ 17
14.0 (200.)	***/***	-40/-39	-41/-24	-29/-13	-17/ -4	-6/ 4	3/ 11	10/ 17
14.0 (600.)	***/***	***/***	-40/-27	-28/-15	-17/ -6	-6/ 3	1/ 10	10/ 17
14.0 (1200.)	***/***	***/***	-40/-29	-31/-16	-16/ -7	-8/ 3	2/ 10	11/ 16
12.0 (50.)	***/***	-39/-30	-36/-19	-24/-10	-13/ -2	-3/ 6	4/ 12	12/ 18
12.0 (200.)	***/***	-40/-32	-34/-20	-24/-10	-14/ -1	-3/ 6	5/ 12	12/ 19
12.0 (600.)	***/***	-39/-33	-36/-21	-24/-11	-13/ -2	-3/ 5	6/ 12	12/ 19
12.0 (1200.)	***/***	-39/-35	-37/-23	-26/-12	-12/ -3	-3/ 4	4/ 12	12/ 18
10.0 (50.)	-38/-31	-40/-23	-31/-14	-18/ -6	-9/ 1	0/ 8	8/ 14	14/ 21
10.0 (200.)	-38/-33	-40/-23	-31/-14	-19/ -6	-9/ 2	0/ 8	8/ 15	14/ 21
10.0 (600.)	-36/-35	-39/-26	-30/-16	-18/ -7	-9/ 1	0/ 8	8/ 14	14/ 21
10.0 (1200.)	***/***	-39/-28	-31/-17	-20/ -8	-11/ 0	-2/ 7	7/ 14	15/ 20
8.0 (50.)	-40/-27	-35/-20	-25/-10	-14/ -2	-5/ 4	3/ 11	10/ 17	16/ 23
8.0 (200.)	-38/-28	-36/-17	-25/ -9	-14/ -2	-4/ 4	4/ 10	10/ 17	17/ 22
8.0 (600.)	-38/-29	-37/-19	-24/-12	-13/ -4	-5/ 4	3/ 10	10/ 16	16/ 22
8.0 (1200.)	-38/-31	-36/-21	-27/-12	-14/ -4	-7/ 3	1/ 10	9/ 16	16/ 22
6.0 (50.)	-37/-22	-28/-14	-17/ -7	-8/ 0	-1/ 7	6/ 13	13/ 19	19/ 25
6.0 (200.)	-38/-21	-27/-14	-17/ -7	-8/ 0	-1/ 7	6/ 13	13/ 19	20/ 24
6.0 (600.)	-37/-20	-29/-14	-20/ -6	-9/ 0	-2/ 7	6/ 12	12/ 19	19/ 25
6.0 (1200.)	-37/-20	-30/-14	-19/ -7	-11/ 1	-3/ 7	6/ 12	13/ 18	18/ 24
4.0 (50.)	-29/-13	-20/ -7	-12/ -1	-4/ 4	3/ 10	10/ 15	16/ 21	21/ 27
4.0 (200.)	-29/-13	-21/ -7	-12/ -2	-5/ 4	3/ 10	10/ 15	16/ 21	22/ 27
4.0 (600.)	-30/-12	-23/ -7	-14/ -1	-5/ 3	2/ 10	9/ 16	16/ 20	22/ 26
4.0 (1200.)	-28/-11	-20/ -7	-14/ -1	-6/ 5	2/ 10	9/ 15	15/ 21	21/ 26
3.0 (50.)	-23/ -9	-16/ -3	-8/ 1	-1/ 6	6/ 12	11/ 17	17/ 23	23/ 28
3.0 (200.)	-22/-11	-16/ -4	-9/ 1	-1/ 6	5/ 12	11/ 17	17/ 22	23/ 28
3.0 (600.)	-25/ -9	-17/ -4	-10/ 1	-2/ 6	4/ 12	10/ 17	16/ 22	23/ 27
3.0 (1200.)	-22/ -8	-15/ -4	-10/ 2	-3/ 6	3/ 13	10/ 18	16/ 23	22/ 28
2.0 (50.)	-17/ -7	-10/ -1	-3/ 3	2/ 9	8/ 14	14/ 19	20/ 24	25/ 29
2.0 (200.)	-17/ -7	-10/ -2	-4/ 3	2/ 8	8/ 14	14/ 19	19/ 24	25/ 29
2.0 (600.)	-18/ -7	-12/ -2	-6/ 3	1/ 7	7/ 13	13/ 19	19/ 24	25/ 29
2.0 (1200.)	-17/ -6	-11/ -1	-5/ 3	0/ 9	7/ 14	13/ 19	19/ 24	24/ 29
1.0 (50.)	-10/ -4	-4/ 0	1/ 5	6/ 10	12/ 15	17/ 20	22/ 25	27/ 30
1.0 (200.)	-12/ -4	-6/ 0	0/ 5	6/ 10	11/ 15	17/ 20	22/ 25	27/ 30
1.0 (600.)	-13/ -5	-6/ 0	-1/ 5	5/ 10	10/ 15	16/ 21	21/ 25	27/ 30
1.0 (1200.)	***/***	-6/ 0	-2/ 6	4/ 10	10/ 15	15/ 20	21/ 25	26/ 30

terminated. In addition to looking at the temperature of the first echoes, the height of the echoes was investigated. Table 8 shows the same results as Table 7, but now presents the echo heights in terms of height above cloud base (km). In this presentation, the effect of cloud base temperature on echo height is weakened considerably as compared to the parcel model previously employed. The water contents within the cloud are lower when the cloud base temperatures are reduced and the echo takes longer to form, but the actual position of the echo that eventually does form is not dramatically different. For example, for the case of a 8 m/sec updraft (600 droplets cm^{-3}) the parcel model predicted that you might produce a 10 dBZ first echo by 3.2 km above cloud base for a 30°C cloud base temperature and by 4.0 km above cloud base for a 10°C base temperature. With the trajectory model, the base of the echo for the 30°C cloud base temperature would be at 2.1 km and top of the echo at 3.9 km. For a 10°C cloud base temperature, the echo base would be at 2.6 km and the top at 4.3 km. In this particular example the sensitivity to variations in cloud base temperature is essentially cut in half.

Table 9 shows the effect of reducing the liquid water contents to half their adiabatic values. As would be expected. the reduction in liquid water content results in higher first echoes, but the effect is not as dramatic as was predicted with the parcel model. Table 10 shows the effect of further reducing the water contents. In this case, they have been reduced to a function of height above cloud base specified by (1). As discussed above (see Background Section), this expression gives an estimate of the mean water content expected in a convective cloud. As expected, echoes are higher still and the conditions for which the model fails to predict echo formation are enlarged.

TABLE 8

10 DBZ FIRST ECHO HEIGHT (TOP/BASE)

ADIBAT = 1.0

UPDRAFT VELOCITY, M/S (# CONCENTRATION, CM-3)	CLOUD BASE TEMPERATURE -5	0	5	10	15	20	25	30
16.0 (50.)	***/***	***/***	7.0/5.4	7.3/4.8	7.0/4.6	6.5/4.4	6.1/4.2	6.1/4.0
16.0 (200.)	***/***	***/***	6.9/5.4	6.8/4.8	6.5/4.6	6.1/4.2	6.2/4.0	5.7/4.0
16.0 (600.)	***/***	***/***	6.9/5.6	7.2/5.0	6.5/4.6	6.1/4.4	6.2/4.2	5.7/4.0
16.0 (1200.)	***/***	***/***	6.8/5.8	7.1/5.2	7.0/4.8	6.6/4.6	6.2/4.4	6.2/4.2
14.0 (50.)	***/***	5.5/5.3	6.6/4.7	6.3/4.3	6.0/4.1	5.7/3.9	5.7/3.6	5.3/3.7
14.0 (200.)	***/***	5.5/5.4	6.7/4.7	6.4/4.2	6.1/4.0	5.7/3.8	5.3/3.6	5.4/3.6
14.0 (600.)	***/***	***/***	6.5/5.0	6.3/4.4	6.0/4.2	5.7/4.0	5.8/3.8	5.4/3.6
14.0 (1200.)	***/***	***/***	6.6/5.2	6.7/4.6	6.0/4.4	6.1/4.0	5.7/3.8	5.3/3.8
12.0 (50.)	***/***	5.4/4.4	6.1/4.0	5.8/3.8	5.5/3.5	5.2/3.4	5.2/3.2	4.9/3.2
12.0 (200.)	***/***	5.6/4.6	5.9/4.1	5.8/3.7	5.6/3.4	5.2/3.3	4.9/3.2	4.9/3.0
12.0 (600.)	***/***	5.4/4.7	6.1/4.2	5.7/3.8	5.5/3.6	5.2/3.4	4.8/3.4	4.9/3.2
12.0 (1200.)	***/***	5.4/5.0	6.2/4.5	6.0/4.0	5.4/3.8	5.1/3.6	5.2/3.4	4.9/3.4
10.0 (50.)	4.4/3.6	5.5/3.5	5.5/3.2	5.0/3.1	4.8/2.9	4.5/2.8	4.2/2.7	4.3/2.6
10.0 (200.)	4.4/3.9	5.5/3.5	5.5/3.3	5.1/3.1	4.8/2.9	4.6/2.8	4.3/2.7	4.4/2.6
10.0 (600.)	4.2/4.0	5.4/3.9	5.4/3.5	4.9/3.2	4.8/3.0	4.5/2.9	4.3/2.8	4.3/2.7
10.0 (1200.)	***/***	5.4/4.1	5.5/3.7	5.2/3.4	5.1/3.2	4.8/3.0	4.5/2.9	4.3/2.8
8.0 (50.)	4.6/3.1	4.9/3.0	4.7/2.6	4.4/2.4	4.2/2.3	4.0/2.2	3.8/2.2	3.9/2.0
8.0 (200.)	4.4/3.2	5.1/2.7	4.7/2.5	4.4/2.4	4.0/2.4	3.8/2.3	3.8/2.1	3.6/2.1
8.0 (600.)	4.4/3.3	5.1/2.9	4.6/2.9	4.3/2.6	4.2/2.4	4.0/2.3	3.8/2.2	3.9/2.1
8.0 (1200.)	4.4/3.5	5.1/3.2	5.0/2.9	4.4/2.8	4.4/2.5	4.2/2.4	4.0/2.3	3.8/2.3
6.0 (50.)	4.3/2.5	4.1/2.2	3.7/2.1	3.4/2.0	3.3/1.8	3.3/1.7	3.1/1.7	3.1/1.5
6.0 (200.)	4.4/2.4	4.0/2.3	3.7/2.1	3.5/2.0	3.4/1.7	3.3/1.7	3.1/1.6	2.9/1.7
6.0 (600.)	4.3/2.2	4.3/2.2	4.0/1.9	3.6/1.9	3.5/1.7	3.2/1.8	3.3/1.6	3.1/1.6
6.0 (1200.)	4.2/2.3	4.3/2.2	4.0/2.1	3.9/1.9	3.7/1.8	3.3/1.9	3.2/1.8	3.3/1.6
4.0 (50.)	3.3/1.2	3.1/1.2	3.0/1.1	2.7/1.3	2.6/1.0	2.4/1.2	2.3/1.2	2.4/0.9
4.0 (200.)	3.3/1.3	3.3/1.2	2.9/1.4	2.8/1.1	2.6/1.1	2.4/1.2	2.4/1.2	2.3/1.2
4.0 (600.)	3.4/1.1	3.4/1.1	3.3/1.1	2.9/1.4	2.7/1.2	2.7/1.1	2.5/1.2	2.4/1.2
4.0 (1200.)	3.2/1.0	3.1/1.2	3.2/1.1	3.1/1.0	2.8/1.1	2.7/1.2	2.7/1.1	2.6/1.1
3.0 (50.)	2.6/0.6	2.5/0.6	2.4/0.7	2.2/0.8	2.1/0.7	2.1/0.7	2.1/0.6	2.0/0.6
3.0 (200.)	2.5/0.9	2.5/0.7	2.5/0.7	2.3/0.7	2.2/0.7	2.1/0.7	2.1/0.7	2.1/0.7
3.0 (600.)	2.8/0.6	2.7/0.7	2.6/0.7	2.4/0.9	2.4/0.7	2.3/0.7	2.3/0.7	2.1/0.8
3.0 (1200.)	2.5/0.4	2.5/0.7	2.6/0.6	2.5/0.7	2.6/0.5	2.5/0.5	2.4/0.6	2.4/0.5
2.0 (50.)	1.7/0.3	1.7/0.2	1.5/0.3	1.5/0.3	1.5/0.2	1.5/0.2	1.4/0.3	1.4/0.3
2.0 (200.)	1.8/0.3	1.7/0.3	1.7/0.3	1.6/0.4	1.6/0.3	1.6/0.2	1.5/0.3	1.5/0.3
2.0 (600.)	1.9/0.3	1.9/0.4	1.9/0.4	1.7/0.5	1.7/0.4	1.7/0.3	1.7/0.3	1.6/0.4
2.0 (1200.)	1.8/0.2	1.9/0.2	1.9/0.3	1.9/0.3	1.8/0.3	1.7/0.4	1.7/0.4	1.8/0.2
1.0 (50.)	0.8/-.2	0.8/-.1	0.8/-.1	0.8/0.0	0.8/0.0	0.8/-.1	0.8/0.0	0.8/0.0
1.0 (200.)	1.0/-.1	1.0/-.1	0.9/0.0	0.9/0.0	0.8/0.0	0.9/0.0	0.8/0.0	0.8/0.0
1.0 (600.)	1.2/0.0	1.1/0.0	1.1/0.0	1.0/0.1	1.1/0.1	1.1/-.1	1.0/0.0	0.9/0.0
1.0 (1200.)	***/***	1.0/0.0	1.3/-.2	1.3/0.0	1.2/0.0	1.2/0.0	1.2/0.0	1.2/0.0

TABLE 9

10 DBZ FIRST ECHO HEIGHT (TOP/BASE)

ADIBAT = 0.5

UPDRAFT VELOCITY, M/S (# CONCENTRATION, CM-3)	CLOUD BASE TEMPERATURE -5	0	5	10	15	20	25	30
16.0 (50.)	***/***	***/***	***/***	7.7/7.4	9.1/6.8	8.9/6.3	8.7/6.0	8.2/5.8
16.0 (200.)	***/***	***/***	***/***	7.8/7.4	8.9/6.7	8.5/6.3	8.2/6.0	7.8/5.9
16.0 (600.)	***/***	***/***	***/***	***/***	9.0/7.0	8.9/6.6	8.6/6.2	8.3/6.0
16.0 (1200.)	***/***	***/***	***/***	***/***	9.0/7.4	9.2/6.8	8.5/6.4	8.1/6.2
14.0 (50.)	***/***	***/***	***/***	7.8/6.6	8.3/6.0	8.2/5.6	7.9/5.4	7.6/5.2
14.0 (200.)	***/***	***/***	***/***	7.8/6.5	8.4/5.9	7.8/5.7	7.5/5.3	7.2/5.2
14.0 (600.)	***/***	***/***	***/***	7.7/6.8	8.6/6.2	8.1/5.8	7.9/5.6	7.6/5.4
14.0 (1200.)	***/***	***/***	***/***	7.7/7.3	8.7/6.6	8.4/6.2	7.7/5.8	7.4/5.6
12.0 (50.)	***/***	***/***	6.4/5.6	7.7/5.5	7.4/5.2	7.4/4.8	7.0/4.5	6.8/4.5
12.0 (200.)	***/***	***/***	6.4/5.8	7.6/5.5	7.5/5.1	7.0/4.9	6.8/4.7	6.4/4.5
12.0 (600.)	***/***	***/***	6.2/6.1	7.6/5.8	7.7/5.3	7.2/5.0	7.0/4.8	6.8/4.6
12.0 (1200.)	***/***	***/***	***/***	7.6/6.1	7.8/5.7	7.4/5.3	7.4/5.1	7.0/5.0
10.0 (50.)	***/***	4.4/3.9	6.4/5.0	7.0/4.6	6.7/4.2	6.3/4.0	6.1/3.9	5.8/3.8
10.0 (200.)	***/***	***/***	6.4/4.8	7.0/4.6	6.7/4.2	6.3/4.1	6.1/3.9	5.9/3.7
10.0 (600.)	***/***	***/***	6.4/5.2	7.2/4.6	6.9/4.4	6.5/4.2	6.0/4.1	5.7/4.0
10.0 (1200.)	***/***	***/***	6.4/5.5	7.1/5.2	6.9/4.7	6.6/4.4	6.1/4.4	6.0/4.2
8.0 (50.)	***/***	5.0/3.7	6.1/4.1	6.2/3.4	5.7/3.4	5.3/3.4	5.2/3.2	5.0/3.1
8.0 (200.)	***/***	5.0/3.8	6.2/3.9	6.1/3.6	5.7/3.5	5.3/3.4	5.2/3.2	5.0/3.1
8.0 (600.)	***/***	4.6/3.9	6.1/4.2	6.0/4.0	5.8/3.7	5.5/3.5	5.4/3.3	5.2/3.2
8.0 (1200.)	***/***	4.2/3.7	6.3/4.2	6.1/4.1	6.0/3.8	5.8/3.5	5.4/3.5	5.3/3.4
6.0 (50.)	2.8/1.9	5.1/3.0	5.3/2.9	4.9/2.8	4.5/2.8	4.5/2.5	4.2/2.6	4.1/2.4
6.0 (200.)	2.8/2.1	5.1/2.9	5.4/2.9	5.1/2.7	4.8/2.6	4.6/2.6	4.2/2.6	4.1/2.5
6.0 (600.)	1.8/1.4	5.0/2.6	5.4/2.9	5.2/2.8	5.0/2.6	4.5/2.8	4.6/2.5	4.5/2.3
6.0 (1200.)	***/***	4.7/2.6	5.3/2.8	5.0/3.2	5.0/2.7	4.7/2.7	4.4/2.7	4.4/2.5
4.0 (50.)	3.5/1.8	4.0/1.6	3.9/1.5	3.8/1.5	3.4/1.8	3.4/1.7	3.4/1.5	3.2/1.6
4.0 (200.)	3.4/1.3	3.9/1.8	3.8/1.9	3.9/1.6	3.4/1.8	3.5/1.6	3.3/1.7	3.3/1.6
4.0 (600.)	2.7/1.1	3.9/1.3	4.0/1.6	4.1/1.4	3.9/1.5	3.7/1.6	3.7/1.5	3.5/1.6
4.0 (1200.)	2.6/0.9	3.5/1.4	3.8/1.4	3.5/1.7	3.9/1.4	3.8/1.4	3.5/1.6	3.4/1.6
3.0 (50.)	3.2/0.8	3.0/1.1	3.0/0.9	2.8/1.1	2.8/1.0	2.8/0.9	2.7/0.9	2.6/1.0
3.0 (200.)	3.1/0.8	3.1/1.0	3.0/1.2	2.9/1.1	3.0/1.0	2.8/1.1	2.8/1.0	2.7/1.1
3.0 (600.)	2.6/0.5	3.1/0.6	3.2/1.0	3.3/0.9	3.1/1.1	3.1/1.0	2.8/1.2	2.9/1.2
3.0 (1200.)	2.3/0.5	2.5/0.7	2.7/0.8	2.8/1.0	3.0/0.9	3.1/0.8	3.0/0.9	3.0/0.9
2.0 (50.)	2.2/0.2	2.2/0.3	2.0/0.6	2.0/0.4	1.9/0.5	1.9/0.4	1.8/0.5	1.9/0.4
2.0 (200.)	2.2/0.3	2.2/0.5	2.2/0.5	2.0/0.6	2.1/0.5	2.0/0.6	2.0/0.5	2.0/0.5
2.0 (600.)	1.7/0.2	2.0/0.3	2.2/0.5	2.4/0.5	2.3/0.6	2.3/0.5	2.1/0.7	2.2/0.6
2.0 (1200.)	***/***	2.0/0.2	2.0/0.5	2.2/0.3	2.1/0.5	2.0/0.6	2.1/0.5	2.1/0.5
1.0 (50.)	***/***	***/***	0.9/-.2	0.9/0.0	0.9/0.0	0.9/0.0	0.9/-.1	0.9/-.1
1.0 (200.)	***/***	***/***	1.2/0.0	1.2/0.0	1.2/0.0	1.1/0.1	1.1/0.2	1.1/0.0
1.0 (600.)	***/***	***/***	***/***	***/***	1.4/0.2	1.4/0.0	1.3/0.1	1.2/0.2
1.0 (1200.)	***/***	***/***	***/***	***/***	***/***	***/***	1.3/0.1	1.3/0.0

TABLE 10

10 DBZ FIRST ECHO HEIGHT (TOP/BASE).

ADIBAT = -1.0

UPDRAFT VELOCITY, M/S (# CONCENTRATION, CM-3)	CLOUD BASE TEMPERATURE -5	0	5	10	15	20	25	30
16.0 (50.)	***/***	***/***	***/***	***/***	***/***	***/9.7	***/9.2	***/8.7
16.0 (200.)	***/***	***/***	***/***	***/***	***/***	***/9.8	***/9.3	***/8.7
16.0 (600.)	***/***	***/***	***/***	***/***	***/***	***/10.	***/9.7	***/9.2
16.0 (1200.)	***/***	***/***	***/***	***/***	***/***	***/***	***/***	***/9.8
14.0 (50.)	***/***	***/***	***/***	***/***	8.6/8.3	***/8.6	***/7.9	***/7.9
14.0 (200.)	***/***	***/***	***/***	***/***	***/***	***/8.4	***/8.2	***/7.7
14.0 (600.)	***/***	***/***	***/***	***/***	***/***	***/9.0	***/8.5	***/8.2
14.0 (1200.)	***/***	***/***	***/***	***/***	***/***	***/9.6	***/9.1	***/8.6
12.0 (50.)	***/***	***/***	***/***	***/***	8.8/7.1	***/7.1	***/7.0	***/6.7
12.0 (200.)	***/***	***/***	***/***	***/***	8.8/7.2	***/7.2	***/6.8	***/6.8
12.0 (600.)	***/***	***/***	***/***	***/***	8.6/8.0	***/7.5	***/7.1	***/7.0
12.0 (1200.)	***/***	***/***	***/***	***/***	***/***	***/8.1	***/7.6	***/7.4
10.0 (50.)	***/***	***/***	***/***	6.8/5.6	8.8/5.7	9.0/5.7	8.6/5.5	8.2/5.4
10.0 (200.)	***/***	***/***	***/***	6.8/6.0	8.8/5.9	9.2/5.6	8.4/5.7	8.2/5.5
10.0 (600.)	***/***	***/***	***/***	***/***	8.4/6.5	8.9/6.2	9.1/5.8	8.5/5.8
10.0 (1200.)	***/***	***/***	***/***	***/***	8.6/6.8	9.1/6.5	9.0/6.2	8.6/6.1
8.0 (50.)	***/***	***/***	4.4/3.7	7.1/4.7	8.0/4.6	7.4/4.8	6.9/4.8	7.0/4.2
8.0 (200.)	***/***	***/***	4.0/3.6	7.0/4.6	7.9/4.8	7.4/4.7	7.1/4.6	6.9/4.5
8.0 (600.)	***/***	***/***	***/***	6.8/4.8	7.6/5.1	7.9/4.7	7.5/4.8	7.0/4.7
8.0 (1200.)	***/***	***/***	***/***	6.6/5.2	7.9/5.0	7.8/4.9	7.7/4.8	7.4/4.7
6.0 (50.)	***/***	1.0/0.4	5.4/2.9	6.4/3.3	6.0/3.7	5.8/3.6	5.9/3.3	5.4/3.5
6.0 (200.)	***/***	0.2/-.1	5.0/2.6	6.4/3.1	6.5/3.2	6.2/3.4	6.0/3.3	5.8/3.1
6.0 (600.)	***/***	***/***	4.2/2.6	5.8/3.2	6.2/3.2	6.4/3.1	6.3/3.3	6.0/3.3
6.0 (1200.)	***/***	***/***	4.0/2.5	5.6/3.2	5.9/3.3	6.1/3.1	6.1/3.2	6.0/3.2
4.0 (50.)	***/***	3.3/1.1	4.1/1.9	4.4/1.9	4.3/1.8	4.2/1.8	4.1/1.7	4.1/1.6
4.0 (200.)	***/***	2.6/0.7	4.4/1.3	4.4/1.9	4.5/1.9	4.2/2.0	4.2/1.8	4.1/2.0
4.0 (600.)	***/***	1.8/0.7	3.5/1.0	4.0/1.3	4.1/1.7	4.5/1.5	4.4/1.6	4.5/1.6
4.0 (1200.)	***/***	***/***	3.3/1.2	3.6/1.4	3.8/1.6	3.7/1.8	4.0/1.7	4.0/1.6
3.0 (50.)	***/***	2.7/0.5	3.1/0.8	3.3/0.8	3.3/1.0	3.3/0.9	3.1/1.1	3.2/0.9
3.0 (200.)	***/***	2.4/0.4	3.2/0.7	3.4/1.1	3.2/1.2	3.3/1.1	3.2/1.1	3.1/1.2
3.0 (600.)	***/***	***/***	2.3/0.3	2.7/0.6	3.1/0.7	3.3/0.7	3.2/0.8	3.2/1.1
3.0 (1200.)	***/***	***/***	2.2/0.6	2.5/0.6	3.0/0.5	3.1/0.6	3.0/0.7	3.0/0.7
2.0 (50.)	***/***	1.4/0.1	2.0/0.0	2.1/0.1	2.2/0.3	2.0/0.3	2.0/0.3	2.0/0.2
2.0 (200.)	***/***	***/***	1.7/0.3	2.0/0.3	2.0/0.5	2.2/0.3	2.1/0.4	2.1/0.5
2.0 (600.)	***/***	***/***	***/***	1.7/0.1	2.0/0.0	1.9/0.3	2.1/0.3	2.2/0.1
2.0 (1200.)	***/***	***/***	***/***	***/***	1.8/0.2	2.0/0.3	1.9/0.2	1.9/0.2
1.0 (50.)	***/***	***/***	***/***	***/***	***/***	***/***	0.6/-.1	0.7/-.3
1.0 (200.)	***/***	***/***	***/***	***/***	***/***	***/***	***/***	1.0/-.2
1.0 (600.)	***/***	***/***	***/***	***/***	***/***	***/***	***/***	***/***
1.0 (1200.)	***/***	***/***	***/***	***/***	***/***	***/***	***/***	***/***

One of the surprising results that was discovered in this analysis was the potential for growth of large liquid drops in relatively cold-based convective clouds. Such clouds are typical of the High Plains (Colorado, Montana, etc.). Although precipitation formation in these clouds is primarily an ice or mixed-phase process, large liquid drops have been observed in these clouds. Since it was thought to be impossible for such drops to grow directly by coalescence, these observations were interpreted as evidence for recycling of ice or graupel that fall below the 0° isotherm, melt, and are then carried back into the updraft. The current model results, on the other hand, suggest that direct growth of liquid drops is not only possible, but likely.

Figure 17 illustrates some of the large drop trajectories in the case of a 5 m/sec updraft and a 5°C cloud base temperature. Figure 18 shows, for this run, the evolution of the expected size distribution of liquid drops that would be found at the -5°C and -10°C levels of the cloud. The small drops are the first to arrive at a given level, with the larger drops lagging behind. Eventually the concentration of large drops builds up, as can also be seen in Figure 19 which shows the concentrations (m^{-3}) of half millimeter (left hand figure) and millimeter (right hand figure) diameter drops. Even at higher updraft velocities it is possible to grow large liquid drops during the primary ascent. Figure 20, for example, shows the possible concentration of millimeter drops (top figures) and half millimeter drops (bottom figures) for updrafts of 10 m/sec (left hand figures), 15 m/sec (middle figures), and 20 m/sec (right hand figures). In each case, the initial concentration of large droplets that grow to raindrop dimensions was based on aerosol observations that were made over the High Plains during the HIPLEX project.

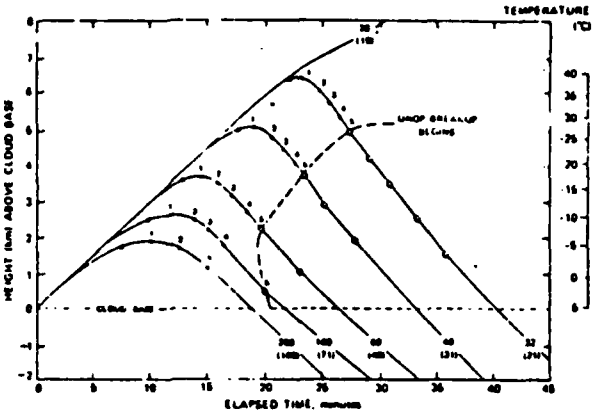

Figure 17. Sample trajectories illustrating the trajectory model.

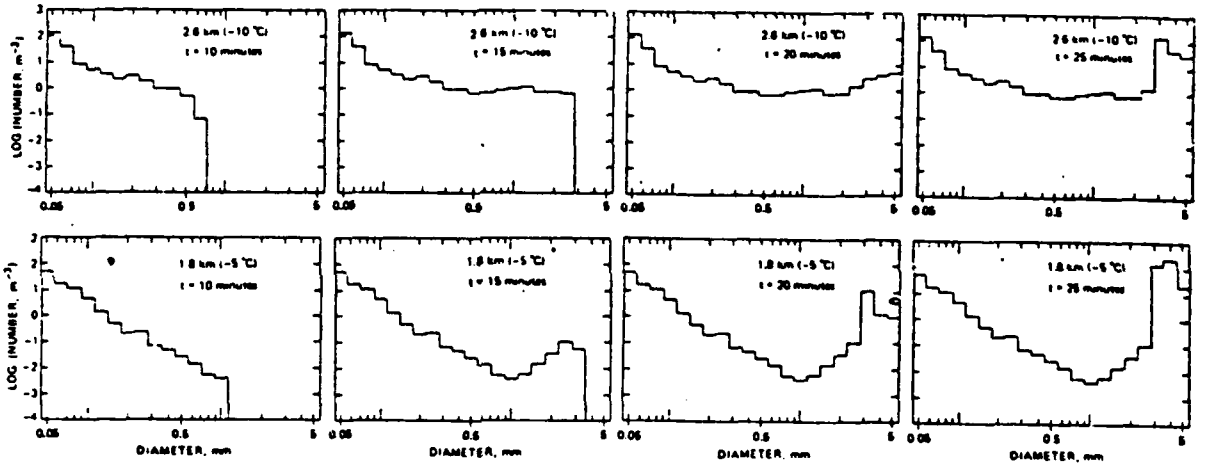

Figure 18. Evolution of the drop-size distribution as a function of time and height above cloud base.

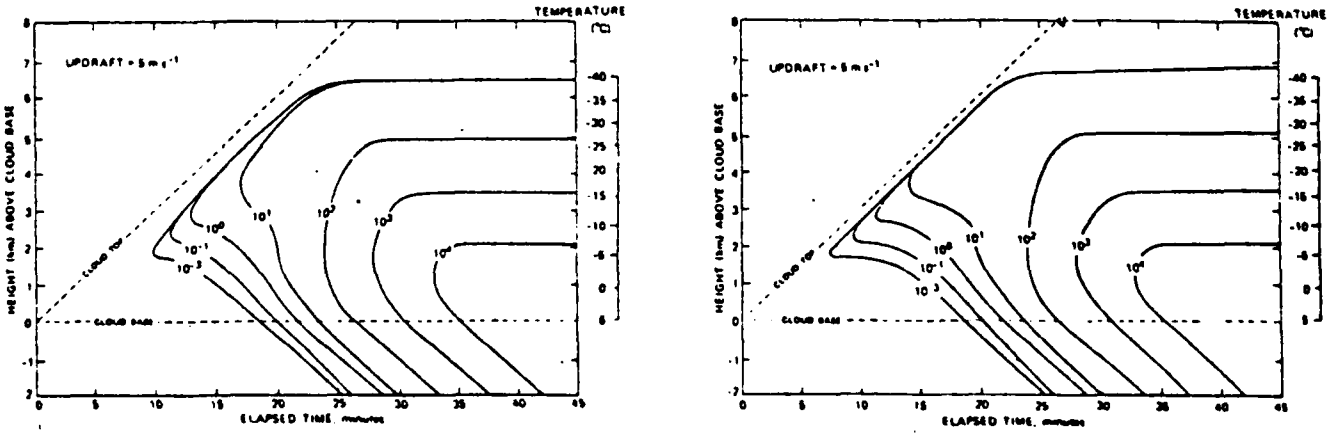

Figure 19. Concentration (m^{-3}) of half millimeter (left figure) and millimeter (right figure) diameter drops.

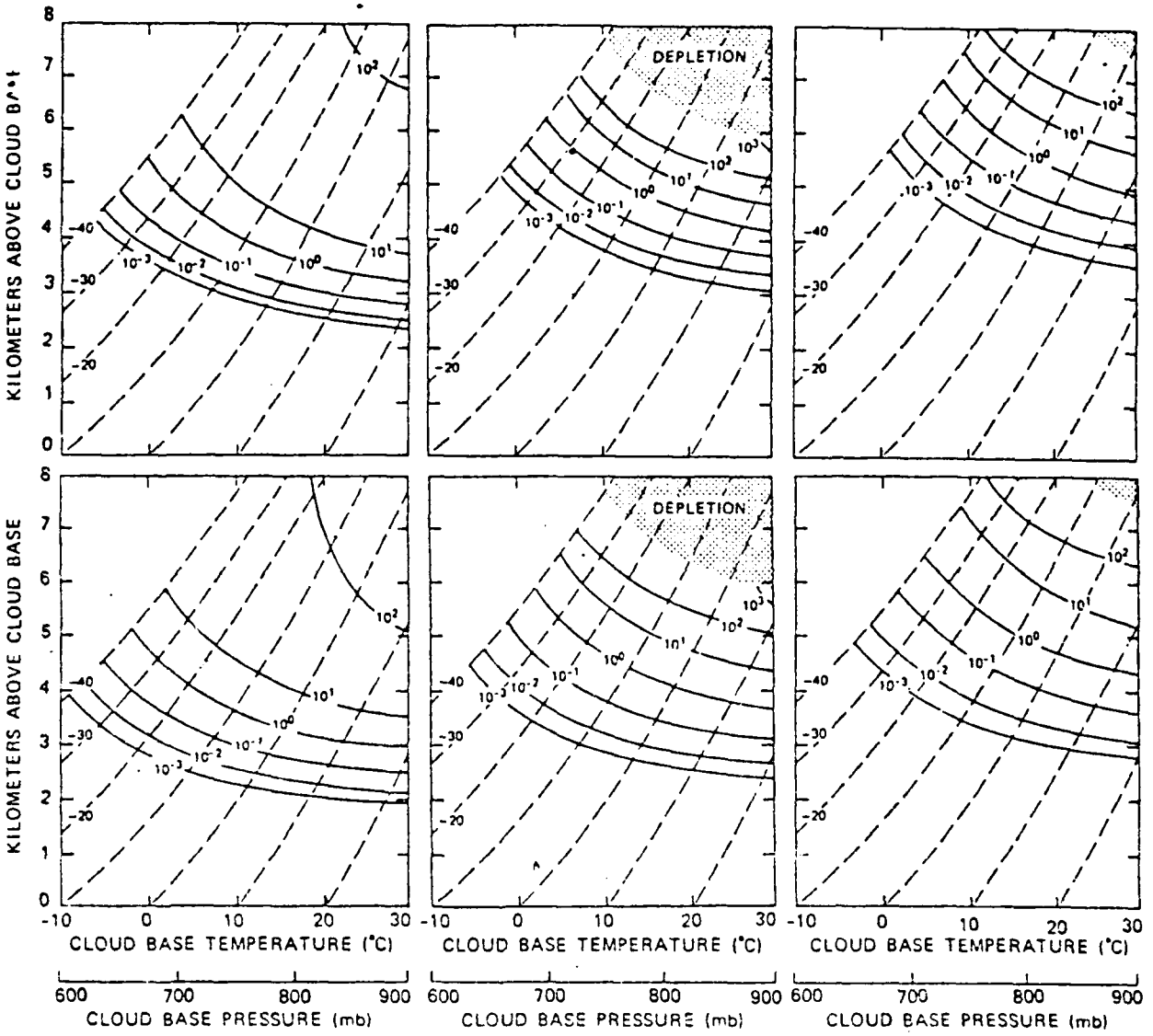

Figure 20. Steady-state concentration of millimeter (top figures) and half millimeter (bottom figures) drops in 10 (left figures), 15 (center), and 20 m/sec (right) updrafts.

ICE-MULTIPLICATION

In some clouds, many more ice crystals are observed at temperatures of -10°C, or warmer, than can be accounted for by measured concentrations of ice nuclei. This has long been interpreted as evidence for some sort of ice multiplication mechanism. In a series of articles, Hallett and Mossop have reported on laboratory experiments supporting a possible "splintering" mechnaism for the production of secondary ice crystals (Hallett and Mossop, 1974; Mossop and Hallett, 1974; Mossop, 1978a; Mossop and Wishart, 1978).

In laboratory studies of ice-multiplication Mossop (1978a) suggested that the rate of production of secondary ice crystals is proportional to $N_\ell N_s^{0.93}$, where N_ℓ is the number of large drops ($D > 24$ μm) swept up each second by a falling graupel particle at -5°C and N_s is the corresponding sweep-out rate of small ($D < 13$ μm) drops. Recently Mossop (personal communication) has suggested that the exponent 0.93 may be unrealistically precise and that a simplier proportionality of $N_\ell N_s$ is probably more appropriate.

In many cases, the cloud droplet distribution can be described accurately by a gamma distribution. Following Berry and Reinhardt (1974), for example, the cloud droplet distribution can be expressed as

$$f<x> = \frac{N^2}{L} G(\nu) S^\nu e^{-(1+\nu)S} \qquad (5)$$

where,

$$S = \frac{Nx}{L}$$

$$G(\nu) = \frac{(1+\nu)^{1+\nu}}{\Gamma(1+\nu)}$$

and where f<x> is the number density of drops of mass x, N is the total number concentration of cloud droplets, L is the liquid water content, and ν is a shape parameter specifying the breadth of the distribution. The relative dispersion ($\sigma_r/\bar{r}$) of droplet distribution is often observed to be near 0.2. This corresponds rather closely to a value of $\nu = 2$. In some observations, however, the relative dispersion appears to increase with height above cloud base (e.g., Warner, 1969). In this case the appropriate value of ν could vary from $\nu = 2$ down to $\nu = 0$ (relative dispersion ≈ 0.4).

Whatever the value of ν, of course, it is always possible to integrate (5) to give the number of drops larger or smaller than any specified size limit. This means that, with an appropriate choice for ν, the total droplet distribution can be expressed in terms two physically meaningful parameters: N and L. The relative number of large and small drops swept out by a falling graupel particle, however, will not necessarily be directly proportional to the relative number concentration of large and small drops since the collection efficiency for capture by the graupel will be different for the large and small size-ranges that are of interest. Examination of the collection efficiencies suggest that the collection efficiencies for small drops ($D < 13$ μm) is typically about 80% of the corresponding collection efficiency for large drops ($D > 24$ μm) over a wide range of possible graupel diameters.

Taking this relative collection efficiency into account, Figures 21, 23, and 25 illustrate the relative effectiveness of the Hallett-Mossop ice-multiplication mechanism as a function of the cloud base temperature and droplet concentration. In all cases the contours of relative efficiency

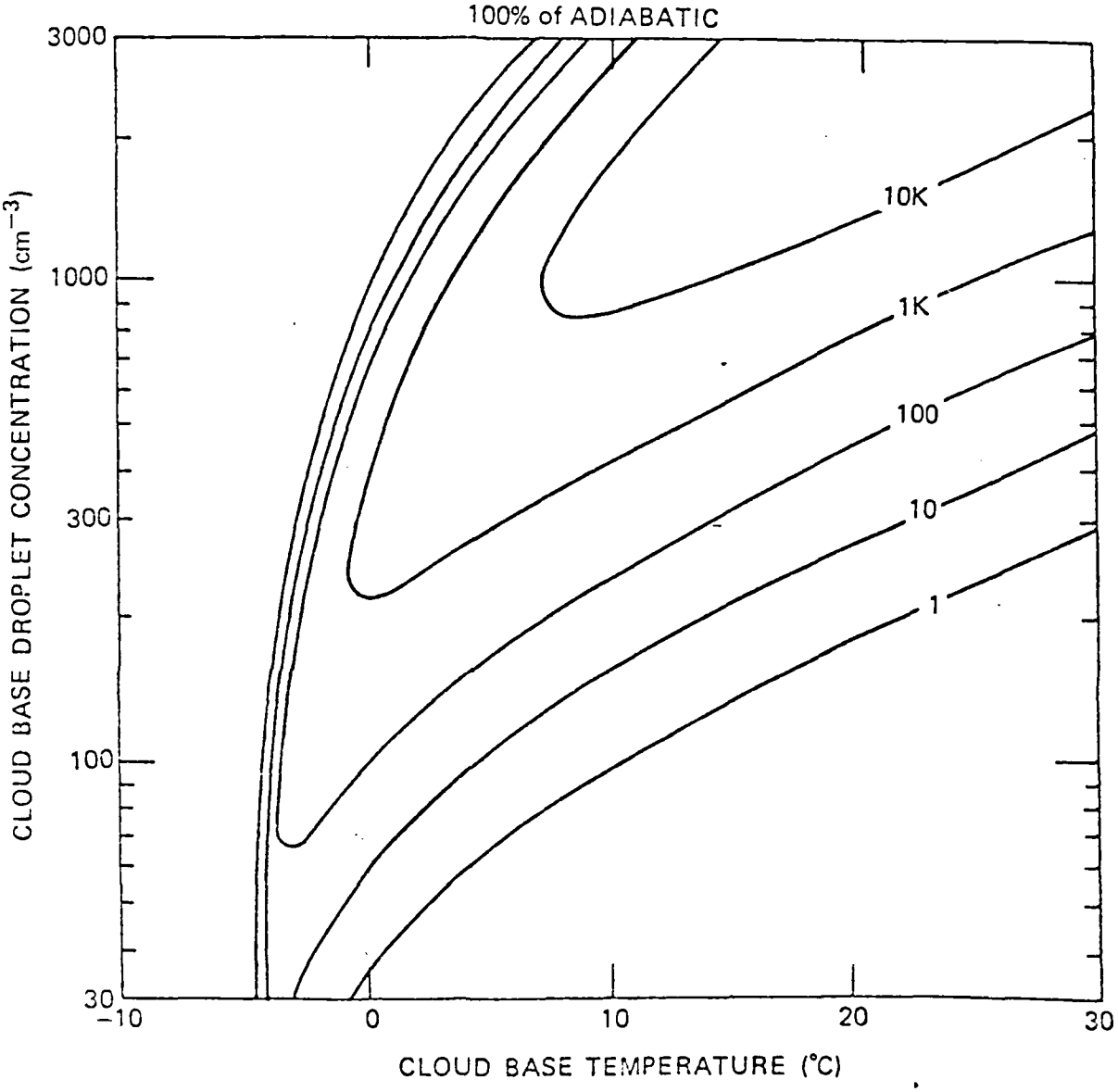

Figure 11. Relative efficiency of the Hallett-Mossop ice-multiplication mechanism for adiabatic water contents.

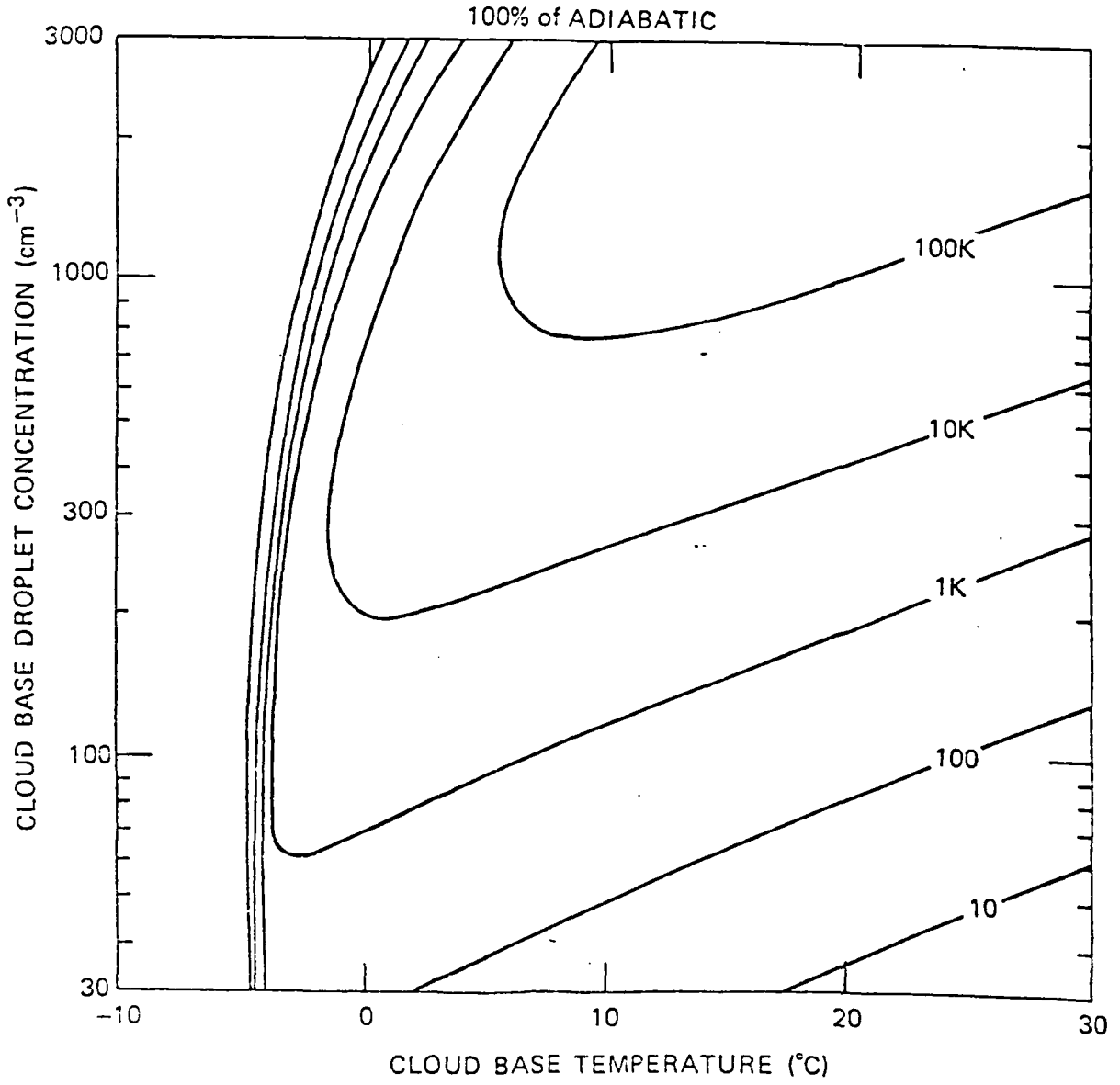

Figure 22. Relative efficiency of the Hallett-Mossop ice-multiplication mechanism for adiabatic water contents.

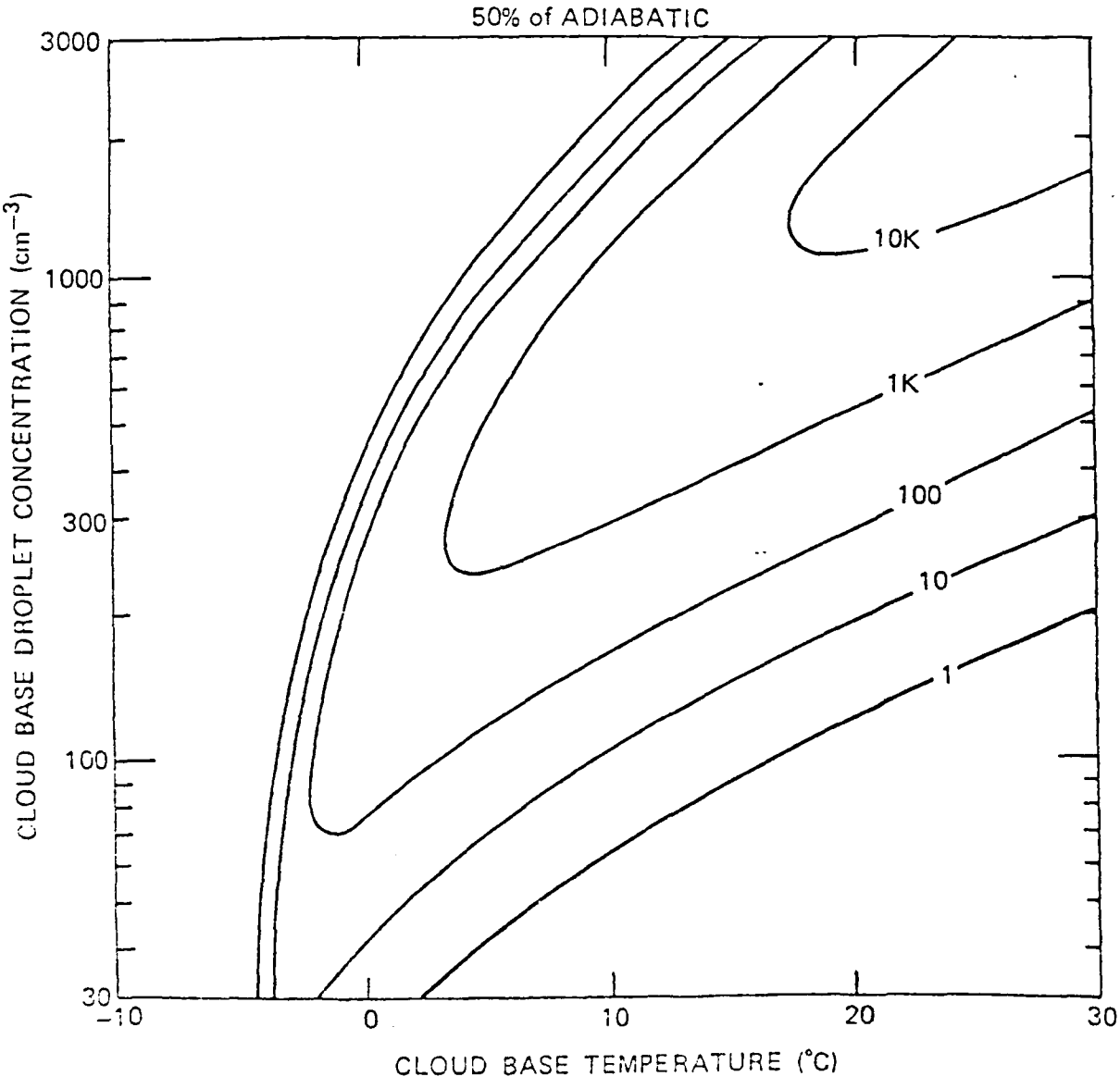

Figure 11. Relative efficiency of the Hallett-Mossop ice-multiplication mechanism for water contents that are 50% of adiabatic.

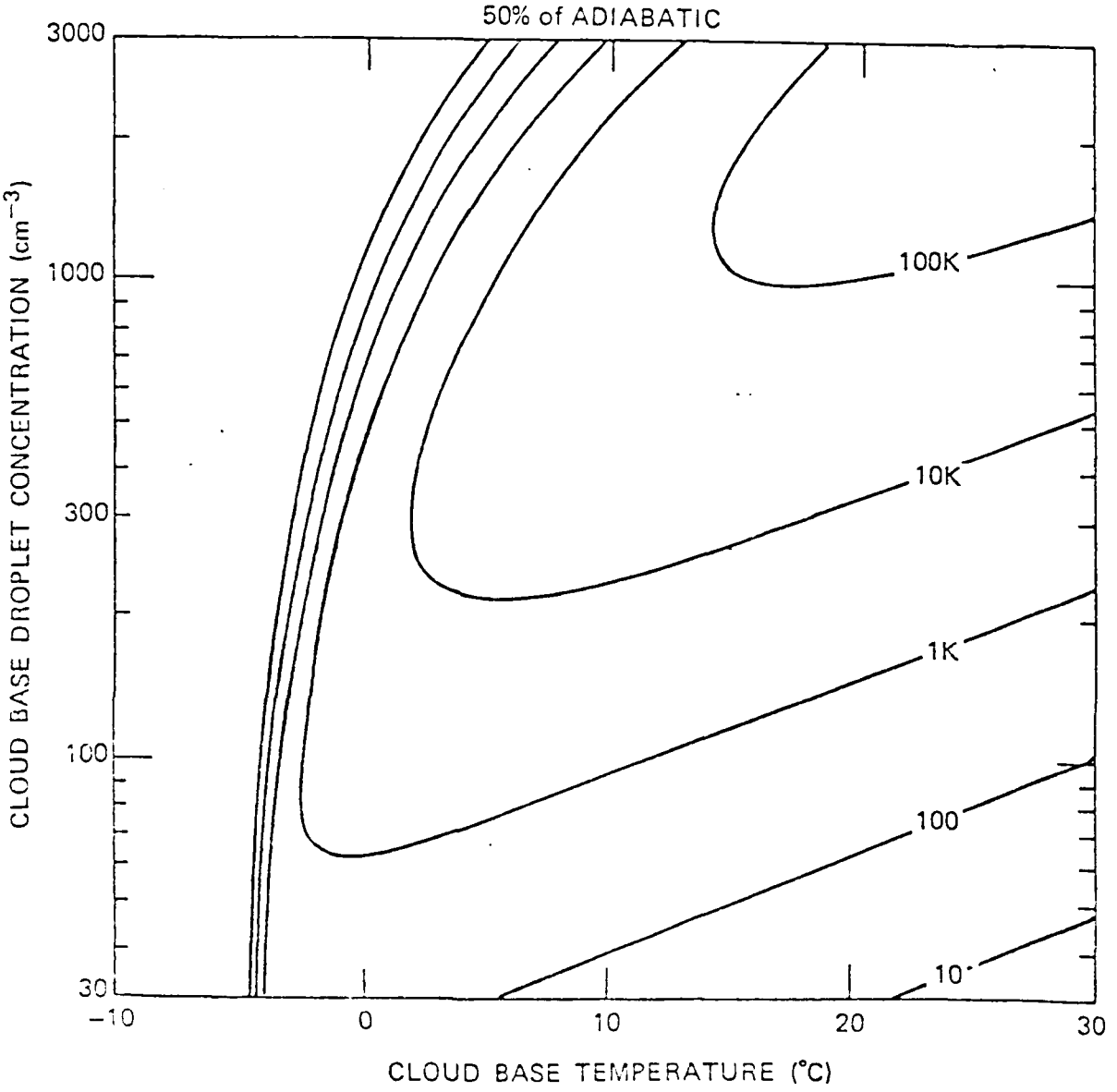

Figure 24. Relative efficiency of the Hallett-Mossop ice-multiplication mechanism for water contents that are 50% of adiabatic.

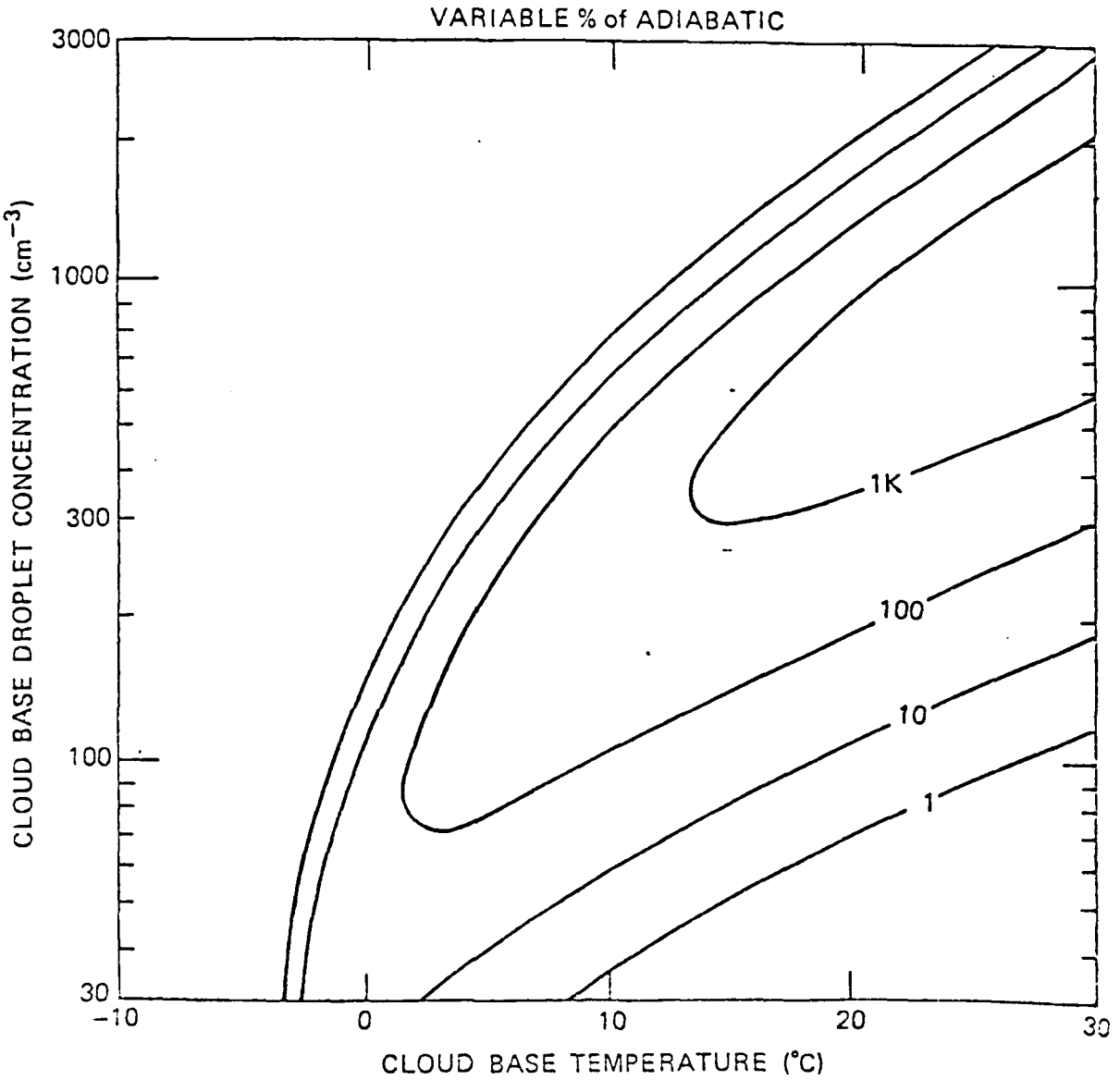

Figure 25. Relative efficiency of the Hallett-Mossop ice-multiplication mechanism for mean water contents (see Figure 2).

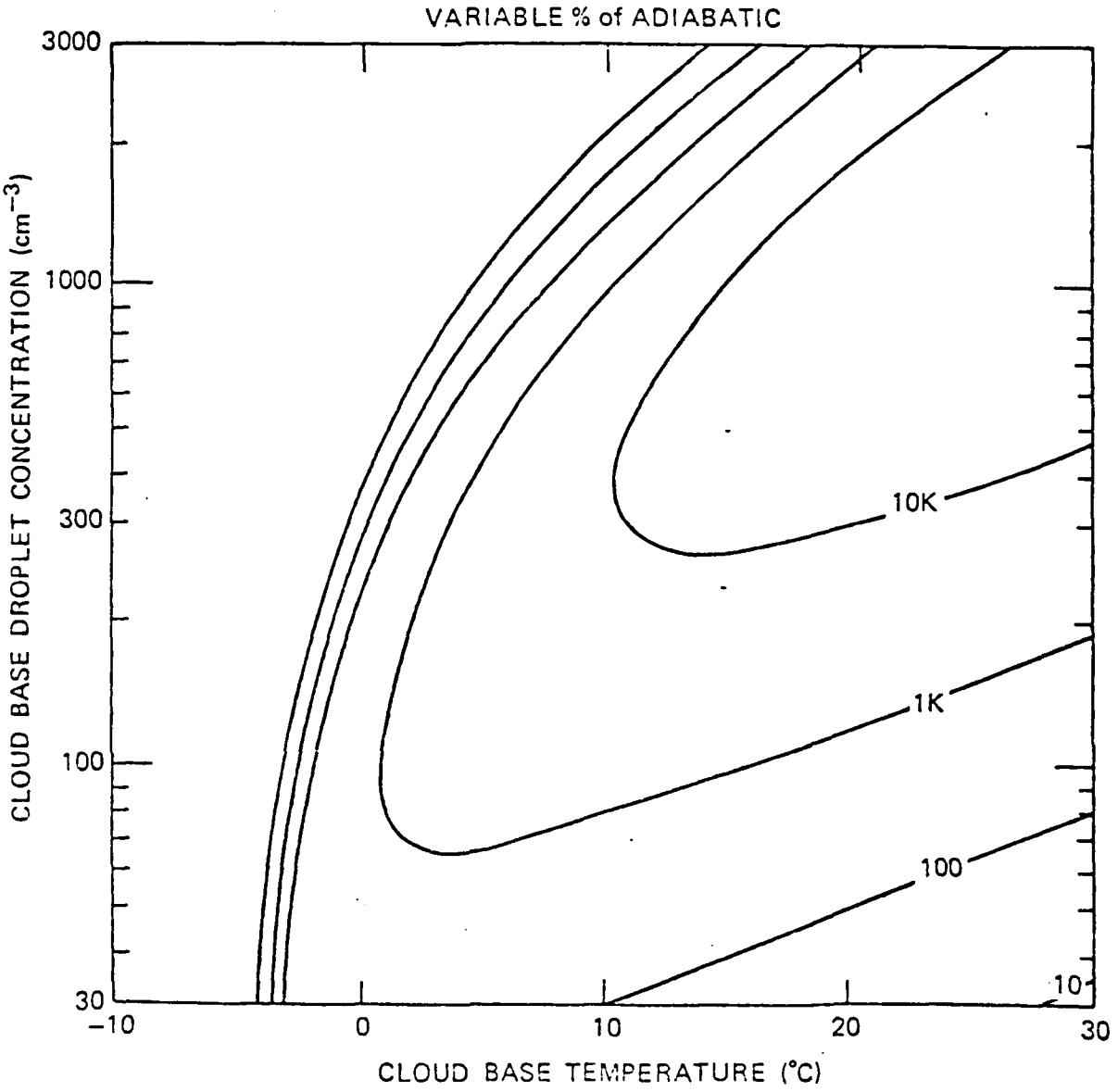

Figure 26. Relative efficiency of the Hallett-Mossop ice-multiplication mechanism for mean water contents (see Figure 2).

are labeled in relative units only. Figure 21 is based on adiabatic water contents, while Figure 23 is appropriate for water contents that are half adiabatic and Figure 25 corresponds to the mean observed water contents shown in Figure 2. In each of these cases, the shape parameter ν was assumed to be constant (=2). Figures 22, 24, and 26 repeat the same sort of estimates of ice-multiplication effectiveness, but in this case invoke a variable ν which ranges from 2 (at cloud base) to 1 (at 750 m above cloud base) and ultimately to 0 (at 2 km altitude and above). These plots agree rather well with the empirical "boundary" suggested by Mossop (1978b) separating conditions conducive for ice multiplication from those not conducive, but goes well beyond the boundary concept.

SNOWFLAKE AGGREGATION

In most detailed microphysical modeling efforts, snowflake aggregation is simply ignored. In recent years, however, aggregation has increasingly been spotlighted as an important physical process that needs to be better understood. While in principle, aggregation of snowflakes into larger and larger units seems to be a rather straightforward problem, the wide variety of particle shapes, bulk densities, and fall behavior as well as the potential interactions between nearby particles have presented formidable obstacles to anything more than a qualitative understanding of the problem. As recently as 1971, Mason said,

> "The growth of these aggregates is governed by the collision and aggregation efficiencies of the crystals and by their relative motions which, because of the aerodynamic problems posed by the complexity and variability of the ice-crystal geometry, are not amenable to quantitative computation."

Passarelli (1978a), has developed an analytical approach to modeling the evolution of the snowflake size distribution by vapor deposition and aggregation of flakes that bypasses many of the difficulties mentioned by Mason. This approach involves assuming an exponential form for the snowflake size distribution,

$$n(D) = N_o e^{-\lambda D} \qquad (4)$$

where $n(D)dD$ is the number of snowflakes (cm^{-3}) in the diameter range from $(D-\frac{1}{2}dD)$ to $(D+\frac{1}{2}dD)$, and then solving the moment conservation equations for the total mass and radar reflectivity in terms of the distributional parameters N_o and λ. The end result is to produce expressions for these parameters as functions of time. Although this approach ignores many of the complexities that can complicate the analysis (e.g. Passarelli and Srivastava, 1979), Passarelli

has had considerable success in applying this analytical approach to observational data (e.g. Passarelli, 1978b; Lo and Passarelli, 1982)

If the snowflake size distribution is truely exponential, then the distributional parameters N_o and λ can be related to other more physically meaningful properties of the distribution such as the total number (n_t) or mass (m_t) of snowflakes per unit volume,

$$n_t = \frac{N_o}{\lambda} \tag{7}$$

$$m_t = \frac{\pi \rho_i N_o}{\lambda^4} \tag{8}$$

where ρ_i is the snowflake bulk density. Alternately, the number or mass of snowflakes larger than a given diameter, D_o, can be expressed as :

$$n(D>D_o) = n_t e^{-\lambda D_o} \tag{9}$$

$$m(D>D_o) = m_t e^{-\lambda D_o} \left[1 + D_o \lambda + \frac{D_o^2 \lambda^2}{2} + \frac{D_o^3 \lambda^3}{6} \right] \tag{10}$$

In many cases, these last two parameters are of more interest than (7) and (8). In terms of precipitation formation, the parameter of interest is the rate of increase of the mass of large flakes which can be expressed as

$$\frac{dm(D>D_o)}{dt} = -\frac{m_t}{6} D_o^4 \lambda^3 e^{-\lambda D_o} \frac{d\lambda}{dt} \tag{11}$$

The critical term in (11) is $d\lambda/dt$, which can be obtained from Passarelli (1978a). For the case of aggregation alone,

$$\frac{d\lambda}{dt} = \frac{C_2 m_t}{(b-1)} \lambda^{-(b-2)} \tag{12}$$

where b is the exponent in a particle fallspeed relation of the form

$$v_t = a\ D^b \tag{13}$$

The constant C_2 in (12) is defined as

$$C_2 = \frac{(1-b)\ a\ E\ I(b)}{2880\ \rho_i} \tag{14}$$

where a and b are defined by the fallspeed relation (13), E is a mean collection efficiency, and ρ_i is the snowflake bulk density. Both E and ρ_i are assumed to be independent of particle size. The term I(b) is defined by a rather intimidating relation:

$$I(b) = \Gamma(p)\ 2^{1-p} \sum_{i=1}^{3} C_i \left[\frac{F(1,p;8-i;\frac{1}{2})}{7-i} - \frac{F(1,p;4+b+i;\frac{1}{2})}{3+b+i} \right] \tag{15}$$

where $p=10+b$, $C_1=C_3=1$, $C_2=2$, Γ represents the gamma function, and F represents Gauss' hypergeometric function. For these arguments, the series solution for F can be expressed as

$$F(1,b;c;\tfrac{1}{2}) = \frac{\Gamma(c)}{\Gamma(b)} \sum_{n=0}^{\infty} \frac{\Gamma(b+n)}{\Gamma(c+n)} \left(\tfrac{1}{2}\right)^n \tag{16}$$

While (15) and (16) can be readily evaluated on modern computers, the constant I(b) itself is rather well behaved over the range of interest (see Figure 27) and can also be estimated using a simple polynomial expression:

$$I(b) = a_1\ b + a_2\ b^2 + a_3\ b^3 \tag{17}$$

where $a_1 = 1.57 \times 10^3$, $a_2 = 1.86 \times 10^3$, and $a_3 = 2.87 \times 10^3$.

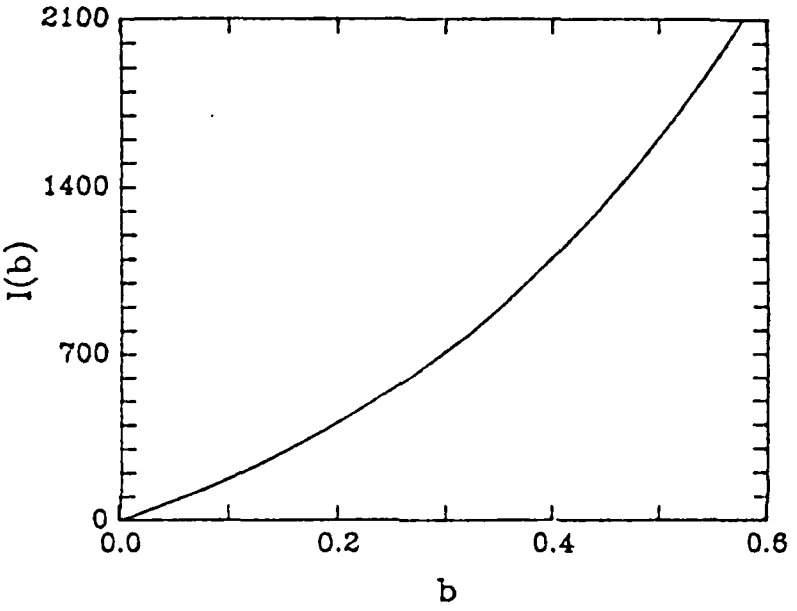

Figure 27.

Figure 28 shows an example of a series of observations of snowflake size distributions that were obtained in a advecting spiral descent (Lo and Passarelli, 1982), plotted as functions of the individual slope, λ, and intercept, N_o, parameters. The general trend of the observations during the descent is from the upper right (highest observations) to lower left (the lowest heights observed). Figure 29 shows, as functions of the same distributional parameters, the rate of increase of large snowflake mass (g cm^{-3} sec^{-1}) for the case E = 1.4, a = 150 (cgs), b = 0.31, D_o = 0.3 cm, and ρ_i = 0.05 g cm^{-3}. For the same case, Figure 30 shows the proportional rate of increase of snowflake mass in large flakes

$$\frac{1}{m(D>D_o)} \quad \frac{dm(D>D_o)}{dt}$$

defined by (10) and (11), which is often a more useful way of expressing the transfer of mass to large particles and was extensively used in the warm rain initiation aspects of this study.

An interesting way to cast figures of this sort in a new light is to convert them to a new coordinate system that moves away from the slope and intercept parameters in favor or more physically meaningful properties such as number or mass concentrations of crystals. Figures 31 and 32, for example, illustrate the same relationships as were shown in figures 29 and 30, but in terms of number and mass rather than abstract "parameters." In this case, the number and mass were defined using 9 and 10 (D_o= 0.03 cm), which is a convenient threshold for data sets obtained from airborne particle probes. Most interestingly, this conversion suggests that it may be possible to parameterize the growth of large aggregates as a relatively simple function of the total ice particle mass-- the same concept used in Kessler-style parameterizations of warm-cloud microphysics. Alternately,

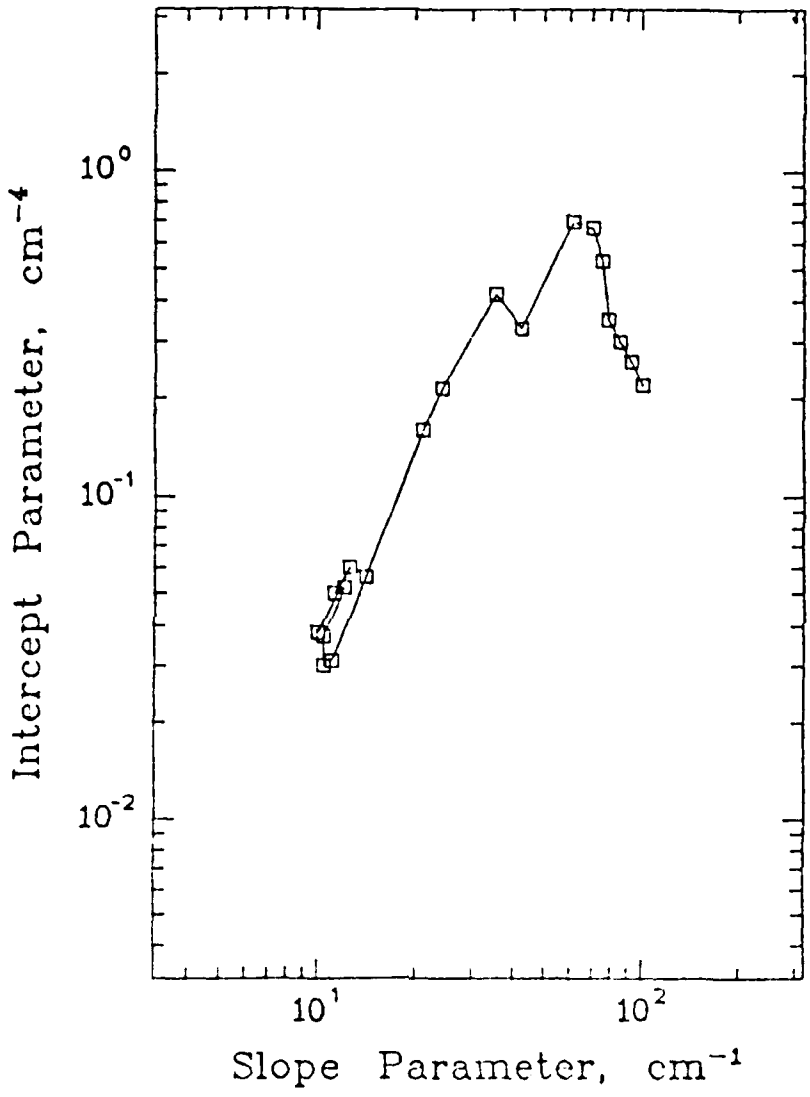

Figure 28. Observational data illustrating snowflake aggregation.

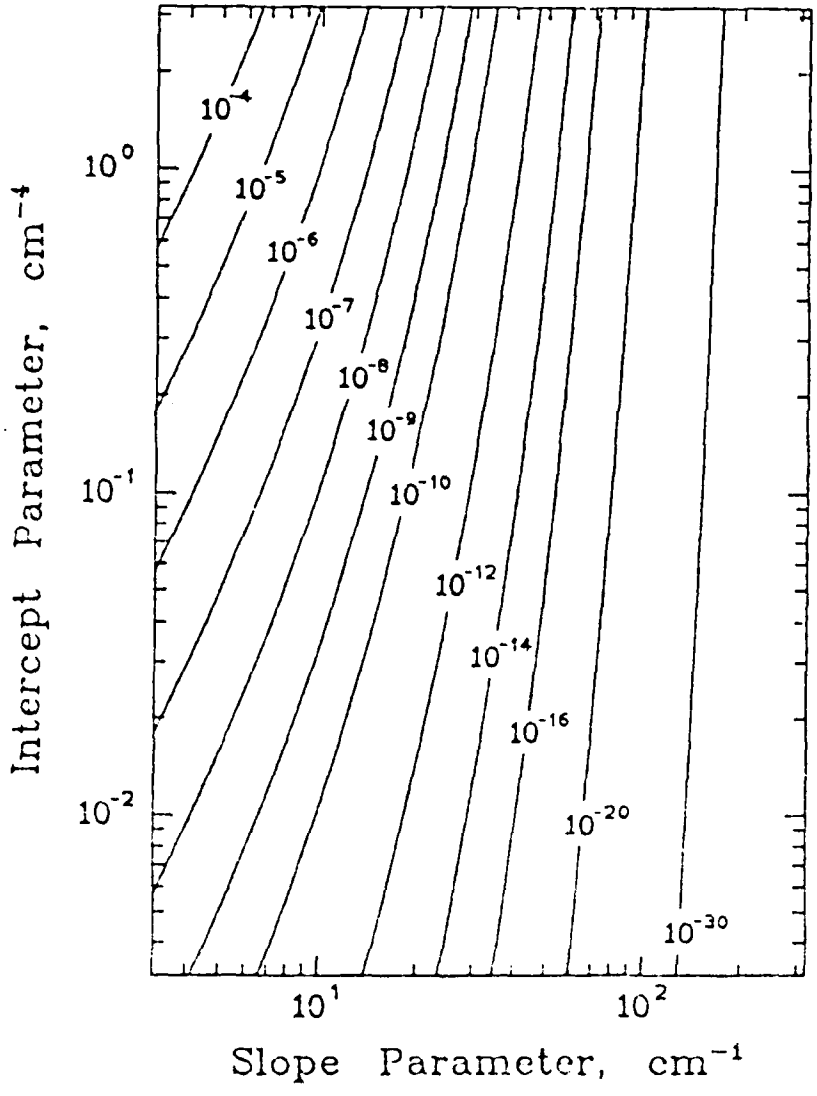

Figure 29. Rate of increase of large snowflake mass (g cm^{-3} sec^{-1}).

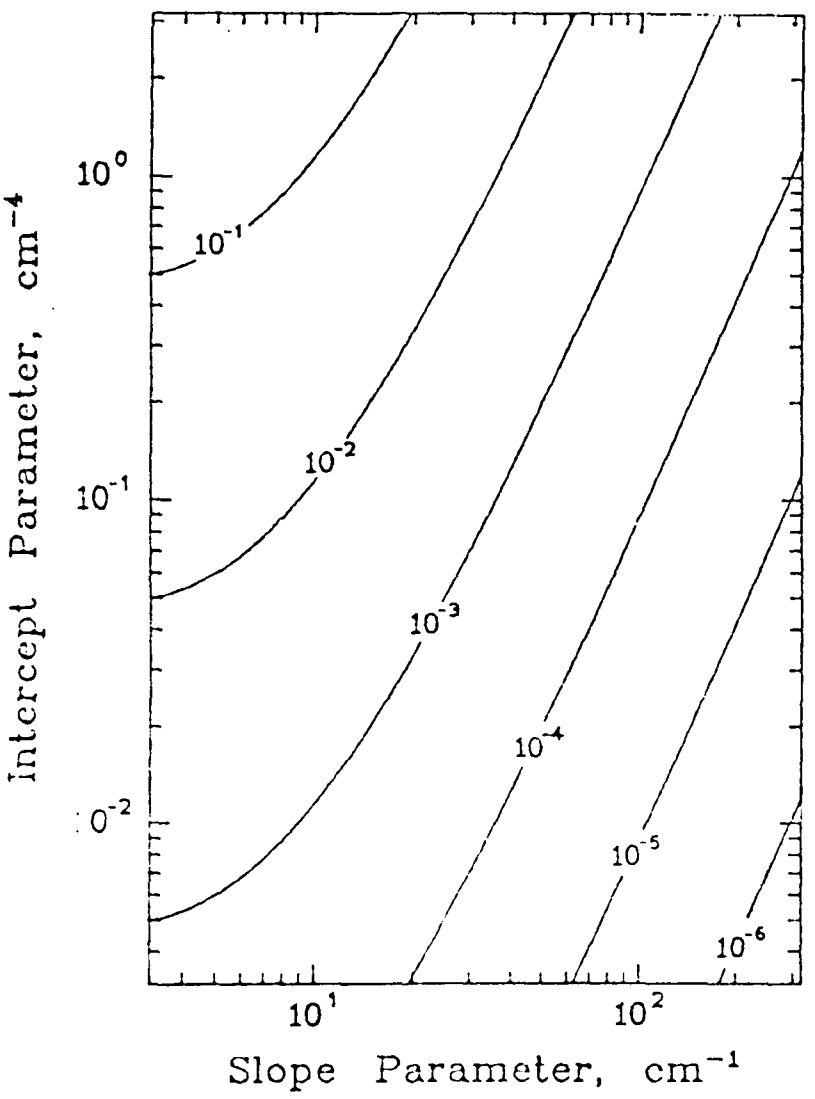

Figure 30. Proportional rate of increase of large snowflake mass (sec^{-1}).

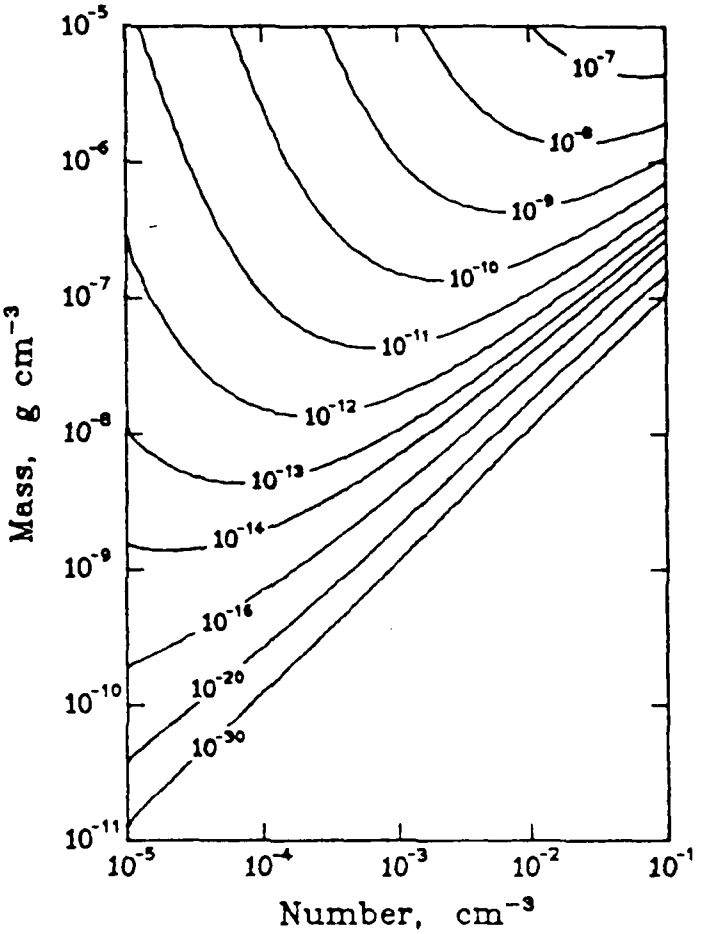

Figure 31. Rate of increase of large snowflake mass (g cm^{-3} sec^{-1}).

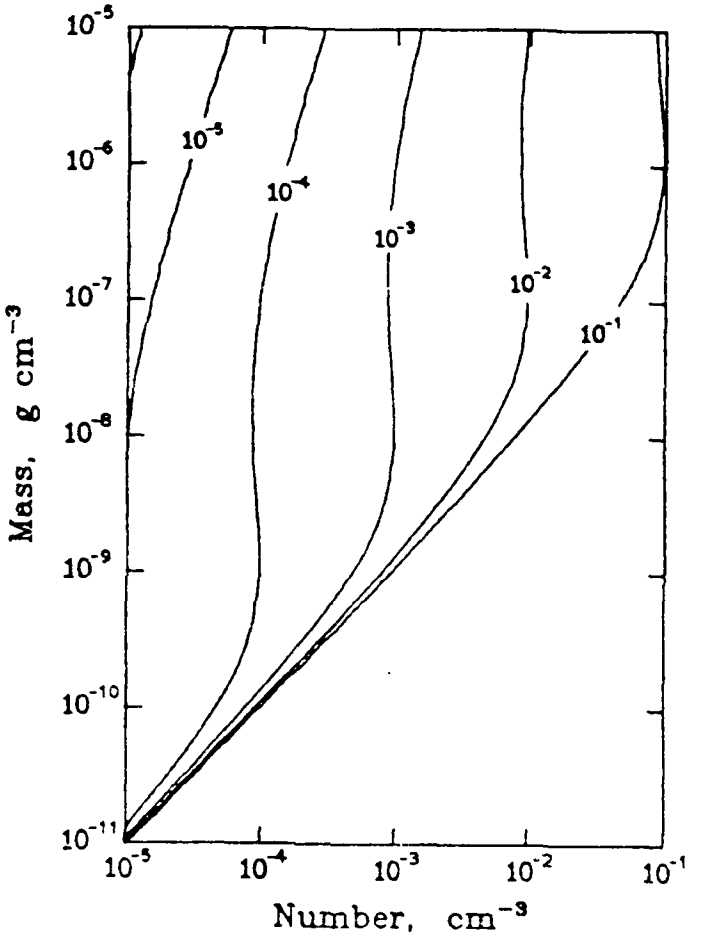

Figure 32. Proportional rate of increase of large ice mixing ratio (sec^{-1}).

this sort of analysis can also play a role in examining observational data, providing a theoretical framework that can give a direct indication of the stability of the particle distribution with respect to aggregation. In Figure 33 this is done by combining the previous figures into a "background" on which the observational spectra shown in Figure 28 is overlaid.

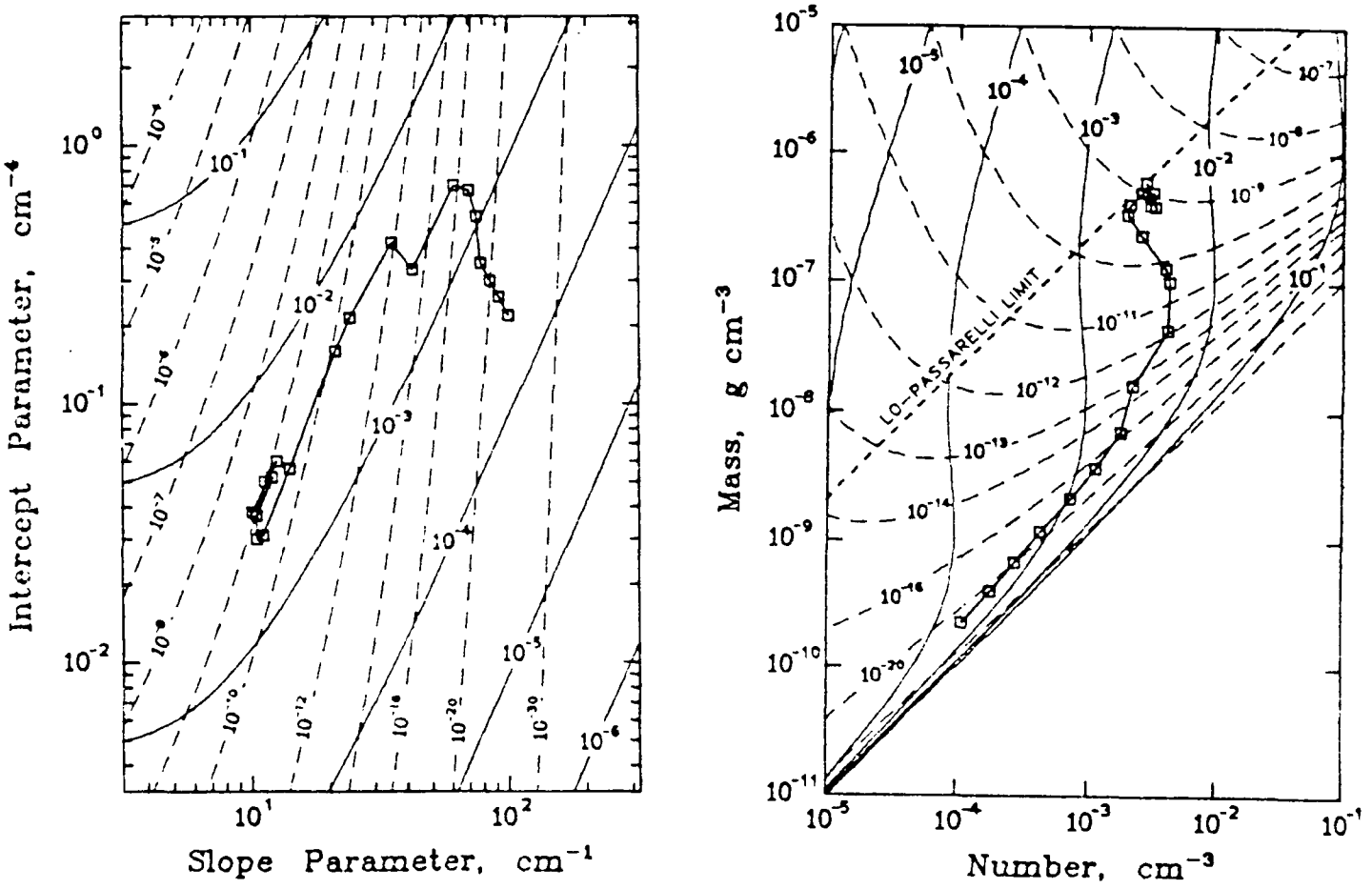

Figure 33. Observational data illustrated in Figure 28 replotted on a background indicating the stability of the spectrum with respect to large aggregate production (see Table 3-3).

REFERENCES

Battan, L. J., 1953: Observations on the formation and spread of precipitation in convective clouds. J. Meteor., 10, 311-324.

Berry, E. X, and R. L. Reinhardt, 1974: An analysis of cloud drop growth by collection: Part I. Double distributions. J. Atmos. Sci., 31, 1814-1824.

Hallett, J., and S. C. Mossop, 1974: Production of secondary ice particles during the riming process. Nature, 249, 26-28.

Johnson, D. B., 1978: Giant nuclei and warm rain initiation. Preprints, Conf. on Cloud Physics and Atmospheric Electricity, American Meteorological Society, Issaquah, 31-34.

_____, 1980: Geographical and climatological variability in the microphysical mechanisms of precipitation development. Proceedings, VIII International Conference on Cloud Physics, Clermont-Ferrand, 401-404.

_____, 1982: The role of giant and ultragiant aerosol particles in warm rain initiation. J. Atmos. Sci., 39, 448-460.

Lo, K. K., and R. E. Passarelli, 1982: The growth of snow in winter storms: An airborne observational study. J. Atmos. Sci., 39, 697-706.

Mason, B. J., 1971: The Physics of Clouds. Clarendon Press, Oxford, 671 pp.

Mossop, S. C., 1978a: The influence of drop size distribution on the production of secondary ice particles during graupel growth. Quart. J. Roy. Meteor. Soc., 104, 323-330.

_____, 1978b: Some factors governing ice particle multiplication in cumulus clouds. J. Atmos. Sci., 35, 2033-2037.

_____, 1979: Reply to comments by Isaac and Schemenauer. J. Atmos. Sci., 36, 2273-2275.

_____, and J. Hallett, 1974: Ice crystal concentration in cumulus clouds: Influence of the drop spectrum. Science, 186, 632-634.

____, and E. R. Wishart, 1978: The mechanism of splintering during rime growth. Geophysical Res. Letters, 5, 1083-1085.

Passarelli, R. E., 1978a: An approximate analytical model of vapor deposition and aggregation growth of snowflakes. J. Atmos. Sci., 35, 118-124.

_____ , 1978b: Theoretical and observational study of snow-size spectra and snowflake aggregation efficiencies. J. Atmos. Sci., 35, 882-889.

_____ , and R. C. Srivastava, 1979: A new aspect of snowflake aggregation theory. J. Atmos. Sci., 36, 484-493.

Warner, J., 1969: The microstructure of cumulus cloud. Part I. General features of the droplet spectrum. J. Atmos. Sci., 26, 1049-1059.

_____, 1970: On steady-state one-dimensional models of cumulus convection. J. Atmos. Sci., 27, 1035-1040.

Are Cold Clouds Microphysically More Efficient Than Warm Clouds?

David B. Johnson

Division of Atmospheric Resources Research
Bureau of Reclamation, Code D-1210
Denver, Colorado 80225

For Submission to Journal of the Atmospheric Sciences

September 1985

Abstract

Riming growth rates for graupel and frozen raindrops are compared with those of unfrozen drops growing by coalescence. The results indicate that graupel can have a considerable advantage over unfrozen raindrops in regions where the cloud droplets are large. On the other hand, if the cloud droplets are small the situation can reverse itself with water drops being favored over graupel. In addition, the results suggest that low density graupel or aggregates may be particularly effective growth centers for accretion, and that particles entering a wet growth regime may experience a sudden jump in growth associated with a change in the particle's surface roughness.

1. Introduction

More than 20 years ago, Braham's (1964) observations of precipitation development in Missouri clouds led him to conclude that snow pellets (graupel) grew faster by riming than unfrozen drops grew through coalescence. This conclusion suggested that the freezing of supercooled drizzle drops increased the precipitation efficiency of summertime convective clouds in the Central United States (Braham, 1964; 1968). At the time that these ideas were introduced, however, quantitative testing of the hypothesis was a long way off. Only recently, in fact, has our knowledge of coalescence and riming progressed to the point that treatment of the problem could be attempted. This paper performs such an evaluation, examining differences in particle growth by riming and coalescence, and seeing whether these differences would be maintained in different geographical or climatological regimes.

The starting point for the current discussion is the familiar growth equation for a particle of mass M, and terminal velocity V, growing by gravitational sweepout of a monodisperse cloud of water droplets of mass m and terminal velocity v:

$$\frac{dM}{dt} = \mathcal{A}\,(V-v)\,E\,\varepsilon\,\chi_c\,\rho_a\,m \qquad , \qquad (1)$$

where $\mathcal{A}$ is the cross-sectional area of the particle normal to the direction of fall, χ_c is the cloud droplet mixing ratio, ρ_a is the air density, E is an appropriately defined collision efficiency, and ε is the fraction of collisions that result in a coalescence. If we restrict

ourselves to oblate spheroidal shapes, the cross-sectional area $\mathcal{A}$ can be expressed as

$$\mathcal{A} = \frac{\pi}{4}\left(\frac{6M}{\pi \rho_i \phi}\right)^{2/3} \quad ,$$

where in addition to the terms already defined, ρ_i is the bulk density of the collecting particle and ϕ is the axis ratio of the oblate spheroid.[1]

The major goal of this study is to examine the expected growth rates of graupel or frozen drops as compared to those of liquid drops of the same mass. This can be done most easily by normalizing the riming growth rates predicted by (1) with the corresponding coalescence growth rate for an unfrozen drop of identical mass. This results in a quantitative estimate of the relative growth rate, to be represented by the symbol $\mathcal{Y}$, such that

$$\mathcal{Y} = \frac{dM\ (\text{graupel})}{dt} \Big/ \frac{dM\ (\text{liquid})}{dt} \quad , \qquad (2)$$

where the numerator and denominator are both evaluated using (1). The relative growth rate defined by (2), is the primary quantity that will be used in the subsequent discussions. No consideration will be made of other modes of growth, such as condensation or aggregation. In many cases, convective precipitation development can be thought of as a two-stage process involving production of embryos that are large enough to

---

[1] If the diameters of three principal axes of the spheroid are D_1, D_2, and D_3 such that $D_1 = D_2$ and $D_3 < D_1$, then $\phi \equiv D_3/D_1$.

begin to grow effectively by riming or coalescence and the subsequent growth of these embryos to precipitable sizes. This study focuses on the second stage of that process.

2. Formulation

It is readily apparent that there are three critical parameters in (1) that need to be evaluated: the terminal velocity, the collision efficiency, and the coalescence efficiency. Historically, each of these parameters has been subject to considerable uncertainty. In each case, however, recent work permits us to make more quantatitive estimates of the parameter values than previously possible.

a. Terminal Velocities

Terminal velocities for water drops are relatively easy to estimate. Beard (1976), for example, gives appropriate expressions as functions of drop size, ambient temperature, and pressure. Ice particle terminal velocities, on the other hand, are less well known and considerably more complicated. For these particles, the terminal velocity will depend on the particle's size, shape, bulk density, and surface roughness as well as the environmental temperature and pressure.

The starting point for the graupel terminal velocity estimates will be an expression for the fall velocity of a smooth spherical particle of bulk density ρ_i falling in air with dynamic viscosity η and density ρ_a :

$$V_S = \frac{C_1 \eta}{\rho_a D} \left[2 + C_2 \underset{\sim}{X} - 2 \left(1 + C_2 \underset{\sim}{X}\right)^{0.5} \right] ,$$

where

$$\underset{\sim}{X} = \left[\frac{8Mg\,\rho_a}{\pi\,\eta^2}\left(\frac{\rho_i - \rho_a}{\rho_i}\right)\right]^{0.5} \quad ,$$

M and D are the particle mass and diameter, g is the acceleration of gravity, and C_1 and C_2 are constants equal to 20.52 and 0.0901, respectively. The dynamic viscosity of the air, η, is exclusively a function of temperature, while air density, ρ_a, depends on both temperature and pressure. The dimensionless variable $\underset{\sim}{X}^2$ is often termed the Best number. Equation (3) is ultimately based on Abraham's (1970) expression for the drag coefficient of a sphere as a function of Reynolds number, as discussed by Beard (1980). The actual terminal velocity of the ice particles can be obtained by multiplying V_S by correction factors for shape or roughness:

$$V = f\,V_S \quad . \qquad (4)$$

Since a particle's drag coefficient is inversely proportional to the square of its terminal velocity, the appropriate correction factor will be of the form

$$f = (C_{DS}/C_D)^{0.5} \quad , \qquad (5)$$

where C_D is the drag coefficient for the nonspherical or rough-surfaced particle while C_{DS} is the drag coefficient of a smooth spherical particle. By limiting consideration to oblate spheroids, shape effects can be described as an additive factor of the form $C_D = C_{DS} + \xi$, where ξ is a simple function of the axis ratio of the spheroid (Beard, 1976). In

this case, $\xi = 0.8\ (1-\lambda)$. Roughness effects are less well known, but may be evaluated by comparing graupel drag coefficient estimates based on fall velocity and mass measurements (e.g., Heymsfield, 1978) with the corresponding coefficients for smooth spheres. Even though this sort of data typically includes <u>both</u> roughness and shape effects, there is a strong suggestion that roughness effects may be expressed as a multiplicative factor of the form $C_D = \zeta C_{DS}$. For dry graupel particles having Reynolds numbers > 100, typical surface roughnesses seem to correspond to a value of $\zeta = 2$. For Reynolds numbers < 100, roughness seems to be progressingly less important and ζ can be assumed to drop linearly with the logarithm of the Reynolds number from 2.0 at Reynolds number 100 to 1.0 at a Reynolds number of 1.0. If surface roughness doubles the drag coefficient, the terminal velocity will be reduced to about 0.7 that of a water drop of similar mass, which is exactly the reduction in fall speed measured by Braham (1964).

It may be interesting to note that the "golf ball" effect, in which added roughness in the form of dimpling on the surface of the ball <u>reduces</u> drag, is not applicable to frozen raindrops or graupel. In the case of the golf ball, the dimpling serves to help induce turbulence in the boundary layer of the projectile sooner than it would occur if the ball were smooth. This turbulence delays the separation of the boundary layer, with a corresponding reduction in drag. This phenomenon, however,

is only observed at very high Reynolds numbers (approximately 10^5). Therefore, if it is applicable to all atmospheric particles, it is only of concern for large hail (Mason, 1971).[2]

b. Collision efficiencies

A cloud droplet being overtaken by a larger particle will tend to follow the airflow as it diverts around the particle. This means that a large particle will actually collide with only a fraction of the cloud droplets in its direct path of fall. This fraction is termed the collision efficiency, E. In general, collision efficiencies between falling particles need to be known as functions of the size shape, bulk density, and surface properties of the interacting particles, and as functions of the ambient air temperature and pressure as well. To date, most studies of collision efficiencies have been concerned with collisions between liquid drops with very little work being done on rime growth. The major exceptions to this generalization are the wind tunnel study of Pflaum and Pruppacher (1979) and the suggestion by Hall (1980) that Beard and Grover's (1974) algorithm for estimating efficiencies with which small raindrops collide with cloud droplets or large aerosol particles could be extended to include either liquid or solid collectors. In their study, Beard and Grover followed Langumir's (1948) approach in developing quantitative expressions for the collision efficiencies in terms of two dimensionless parameters: the Stokes impaction parameter and the Reynolds number of the collecting particle. This means that it is easy

---

[2]A letter in June 1979 issue of Scientific American has an interesting example of an inappropriate application of the golf ball analogy to small particles.

to obtain collision efficiency estimates for almost any type of collector or set of environmental conditions by merely making appropriate modifications to these two parameters. If we limit our consideration to collectors that have oblate spheroidal shapes, the Reynolds number, $\underset{\sim}{R}$, and Stokes impaction parameter, $\underset{\sim}{K}$, can be expressed as

$$\underset{\sim}{R} = \frac{V \rho_a}{\eta} \left(\frac{6M}{\pi \rho_i \ell} \right)^{1/3}$$

$$\underset{\sim}{K} = \frac{C_{SC} \underset{\sim}{R} d^2 \rho_\ell}{9 \rho_a} \left(\frac{6M}{\pi \rho_i \ell} \right)^{-2/3} ,$$

where in addition to terms already defined, C_{SC} is the Cunningham factor (see Beard and Grover, 1974), d is the cloud droplet diameter, and ρ_ℓ is the density of liquid water.

This approach, however, is based on flow around smooth spheres and does not account for perturbations in the flow filed caused by surface roughness or flow through the particle. Of course, surface roughness still plays an important role in determining the collision efficiency through its inclusion in the terminal velocity estimates, even if there is no attempt to consider specific disturbances to the fluid flow introduced by the rough surface. In particular, increased surface roughness will slow the fall of the graupel, reducing its characteristic Reynolds number and this in turn lowers the collision efficiency.

Heymsfield and Pflaum (1985) recently reexamined Pflaum and Pruppacher's original data on the riming of frozen drops and concluded

that the collision efficiency estimates obtained with the formulas of Beard and Grover generally agreed quite well with the wind tunnel estimates of mean collision efficiencies during graupel growth. While the available data only covered a portion of the domain of interest, this study confirms that the Beard and Grover formulation will often provide a useful first approximation for the collision efficiencies of growing graupel. Ultimately, however, it is likely that a correction term will be needed to adjust these calculated efficiencies for factors such as the shape, bulk density, and surface roughness of the graupel.

For simplicity, collision efficiencies for both raindrops and graupel will be calculated using the equations of Beard and Grover (1974). While other sources are available to estimate collision efficiencies for liquid collectors, the Beard and Grover formulation tends to be as good as any of the alternatives for most sizes of interest, and is virtually unique in permitting extrapolation of the collision efficiencies to different environmental conditions. In addition, it is clearly advangageous to use the same basic formulation for both liquid and solid hydrometeors to avoid any bias in the relative growth rates that might result from inconsistencies in the collision efficiency calculations.

In calculating graupel growth rates, it is necessary to extend the calculations beyond Reynolds number 400, which represents the upper limit explicitly considered by Beard and Grover. Beard and Grover did suggest an equation for larger particles, but this equation was merely intended to provide a rough estimate for large collectors using poten-

tial flow approximations. If this equation is arbitrarily introduced for all $\underset{\sim}{R} > 400$, there will be a sharp discontinuity in the growth estimates at $\underset{\sim}{R} = 400$ since the potential flow calculations result in significantly increased collision efficiencies. In the upcoming calculations, the transition to the potential flow solution is smoothed by simply interpolating between the two formulations over the Reynolds number range of 400 to 2400.

c. Coalescence efficiencies

The coalescence efficiency, ε, represents the fraction of collisions that actually result in coalescence. Failure to coalesce may be due to the drops bouncing apart before the air film trapped between them can drain, or by the rapid breakup of a large drop created by temporary coalescence of the interacting drops. In the present context, the first mechanism is the one of primary interest.

While it has long been known that colliding drops will not always coalesce, it has been difficult to develop quantitative expressions for ε that have general applicability. Perhaps the best available expressions are the empirical formulas of Beard and Ochs (1984). In using these equations, however, Ochs and Beard (1985) suggest that the calculated efficiencies be constrained to stay in the range of 50 to 100 percent.

In analyzing their laboratory data, Beard and Ochs (1984) made use of a modified Weber number. This dimensionless parameter involves a

characteristic radius of deformation and a representative impact speed (Schotland, 1960; Foote, 1975). In Ochs and Beard (1984) the relevant deformation radius was interpreted as the small droplet radius while the characteristic impact speed was associated with the terminal velocity of the large drop. In this case the Weber number becomes

$$\underset{\sim}{W} = \frac{\rho_\ell \, d \, V^2}{2 \, \sigma} \quad ,$$

where ρ_ℓ is the density of liquid water, d is the diameter of the small droplet, V is the terminal velocity of the collector drop, and σ is the surface tension of liquid water. When the Weber number is small, the large drop does not deform significantly and the coalescence efficiency is near unity. As the Weber number increases, the possible deformation of the large drop should increase, with an associated reduction in the coalescence efficiency (Ochs and Beard, 1984; Beard and Ochs, 1984). This analysis supports the intuitive conclusion that graupel or frozen drops, which do not deform, should always collect the supercooled cloud drops they strike.

In their laboratory experiments, Ochs and Beard have taken considerable care to minimize the charge on the interacting drops and to restrict the strength of any electric fields that might be present. Their results are thus applicable to small clouds in the initial stages of precipitation growth before charge separation mechanisms have had a chance to operate. Once electrical forces are operating, the coalescence efficiencies are likely to change. While different investigators have exa-

mined a variety of scenarios involving charged drops and imposed electrical fields, there is no generally accepted treatment of the problem. As a result, the magnitude, and even the direction, of possible electrical effects remains unresolved. In spite of these uncertainties, there is usually a tendency to assume that electrical effects may be expected to enhance coalescence.

3. Results

In examining the relative growth rates of graupel particles, the range of parameters considered will be extended well beyond the conditions Braham observed in Missouri clouds. The critical variables involved include the size, shape, bulk density, and surface roughness of the graupel particle as well as the diameter of the cloud droplets.

Figures 1, 2, and 3 illustrate many of the key results of this study, showing the relative growth rates of spherical graupel particles of two different bulk densities as functions of the particle's spherical melted diameter, D_0, where

$$D_0 = \left(\frac{6M}{\pi \rho_i}\right)^{1/3}$$

The actual diameter of the graupel particles, of course, would be simply $D_0(\rho_i/\rho_i)^{1/3}$. In each case, the curves labeled "smooth" used terminal velocities for the collecting particle based on drag coefficients for smooth spheres while the curves labeled "rough" used the surface roughness algorithm for dry graupel discussed in section 2a. Figure 1 was

calculated for a cloud droplet diameter of 12 μm, while the figures 2 and 3 are based on cloud droplet diameters of 16 and 20 μm, respectively. A cloud droplet diameter of 12 μm may be appropriate for the cold-based continental clouds of the High Plains (e.g., Cooper and Lawson, 1984), while the larger cloud droplets would be more appropriate for warmer clouds or clouds with lower droplet concentrations.

All in all, these results support Braham's conclusion that the freezing of large supercooled drops in warm-based clouds may significantly accelerate precipitation development (e.g., Fig. 3). When a supercooled drizzle drop freezes, there should be an immediate jump in the accretional growth rate associated with an increase in coalescence efficiency to $\varepsilon = 1.0$. Like liquid drops, newly frozen drops would be expected to have smooth surfaces. So long as the surface remains smooth, the growth rate of the particle will remain high. As the particle rimes, however, the surface will quickly roughen (e.g., Heymsfield and Pflaum, 1985), with corresponding reductions in the terminal velocities, efficiencies, and growth rates to more modest values. In this case, drop freezing would be accompanied by a sudden, but short, spurt in accretional growth. Even after this spurt has ended, the rime growth rates may still be significantly larger than for water drops of the same mass. While the associated growth from the vapor (sublimation) would also be greater than for a comparable unfrozen drop, these growth rates are usually small for particles of this size, as compared to growth rates for coalescence or riming, and may be neglected.

This pattern of a sudden spurt in growth following freezing would also be expected in clouds composed of smaller droplets (e.g., figs. 1 and 2). The main difference would be that the magnitude of the growth spurt will be smaller, and the subsequent growth rates may often slow to less than that of a liquid drop of comparable mass.

One of the interesting features of this analysis is the relative insensitivity of the relative growth rates to changes in the bulk density of the graupel. This result is examined in more detail in figure 4, illustrating the relative growth rates as functions of the graupel bulk density. In each plot, separate curves are drawn for D_0 = 0.5 mm and D_0 = 2.0 mm. In these examples, only the surface roughness algorithm for dry graupel was used.

For a cloud droplet diameter of 12 μm, the growth curves are relatively flat with a hint of a maximum in the bulk density range of 0.5 to 0.6 g cm^{-3} before dropping off rather sharply as the bulk density falls below 0.1. For slightly larger cloud droplets (d = 16 μm), the relative growth rates are larger for all bulk densities, with maximum values associated with bulk densities in the range of 0.2 to 0.3 g cm^{-3}. For d = 20 μm, the relative growth rates increase still further with the maximum values corresponding to bulk densities near 0.1 g cm^{-3}. In the present model, the treatment of very low bulk density particles (< 0.1 g cm^{-3}) is suspect since no airflow through the particle is permitted. While it is not necessarily clear what the net effect of such flows would be, it seems that at the very least this would tend to increase the particle terminal velocities and result in increased collision efficiencies and accretional growth rates.

Up to this point, only spherical graupel particles have been considered. Figure 5 extends the calculations to oblate spherioidal shapes with axis ratios down to 0.3. As in figure 4, these examples all use the surface roughness algorithm for dry graupel. And again, as in figure 4, separate curves are drawn for D_o = 0.5 mm and D_o = 2.0 mm. In this case the maximum graupel diameter would be simply $D_o [\rho_\ell/(\phi \rho_i)]^{1/3}$. All the plots in this figure were based on a cloud droplet diameter of 16 μm, with separate panels corresponding to bulk densities of 0.1, 0.3, and 0.7 g cm^{-3}. While there is an interesting crossover in the curves in each panel, the principal result is that the relative growth rates do not show great variation with shape. For the warm-based clouds, however, there is a distinct tendency for increased growth rates as the axis ratio gets smaller.

Since the collision efficiency estimates are based on spherical collectors, the predicted collision efficiencies are likely to be underestimated for low axis ratio oblate spheroids. Hall (1980) has developed an alternative set of equations to estimate collision efficiencies for "plate-like" particles which can be used to illustrate the range of uncertainty present in calculated growth rates for $\phi \ll 1$. Hall's collision efficiency formulation parallels that of Beard and Grover (1974), but is based on the results of Pitter and Pruppacher (1974) and Pitter (1977) for oblate spheroids of axis ratio 0.05. As in the work of Beard and Grover, the collecting particles are assumed to have smooth surfaces that are impermeable to airflow. Relative growth rates using Hall's collision efficiencies are plotted as dashed lines in figure 5.

As should be expected, the relative growth rates are significantly larger using Hall's collision efficiencies. In addition, these results do not evidence the low bulk density drop off in growth rates predicted for spherical collectors (e.g., Fig. 4). Although the current model is not well suited to evaluate the riming of snowflakes and aggregates, the results suggest that these low density particles, which often have axis ratios in the range of 0.3 to 0.5, may be quite effective growth centers for accretion.[3]

4. Discussion

This analysis of the relative growth rates of graupel and supercooled raindrops tends to confirm Braham's conclusion that graupel particles in warm-based clouds may be expected to grow faster by riming than unfrozen drops of the same mass grow through coalescence. The Missouri clouds that Braham was studying, however, seem particularly favorable to graupel growth and his conclusions should not be generalized to clouds in other geographical areas, such as the High Plains. In fact, if the supercooled cloud droplets are small enough, graupel particles can often grow significantly slower than waterdrops of comparable mass. These microphysical growth rates, of course, are only one aspect of precipitation efficiency. Since the changes in accretional growth rates associated with phase changes can be rather dramatic, however, it seems

---

[3]Recent studies by Rasmussen and Lew (1985) also suggest that aggregates may rime more effectively than previously thought.

likely that this could well influence the probability that a cloud develops precipitation or the amount of precipitation produced.

In examining the relative growth rates defined by (1) and (2), it is apparent that graupel particles are increasingly favored over liquid drops as the collecting particles get larger. Increasing the cloud droplet diameter, d, can also produce significant increases in the relative growth rates and is probably the critical factor in controlling the geographical variability of the present results. In general, warm cloud bases and low droplet concentrations promote large cloud droplets while cold cloud bases and high droplet concentrations tend to reduce the mean droplet diameter. The sensitivity to droplet size is linked to the coalescence efficiency, which is one of the two critical terms that determine the difference between the growth of liquid and solid collectors. The importance of this term to the overall result also suggests that the charged particles and electric fields of a mature thunderstorm may often affect the microphysical efficiency of precipitation development. For example, if the charged environment in a thunderstorm were found to increase coalescence efficiencies to values near 1.0, raindrop coalescence growth might be enhanced by as much as a factor of two.

It is important to note that the increased growth expected for a newly frozen raindrop as $\varepsilon \rightarrow 1$ is seldom realized for very long. In general, this increase will progressively be offset by the increasing surface roughness as the particle rimes, slowing its fall and lowering the collision efficiency. The end result is thus a balance between the effects of different coalescence efficiencies and surface roughness fac-

tors for liquid drops and graupel. Other factors, such as particle shape and bulk density, also play a role in the microphysical growth rates, but are generally less important.

The insensitivity to changes in particle bulk densities is particularly interesting to examine. From (3), it is apparent that for spherical particles of the same mass and roughness, the fall velocity is essentially proportional to the inverse of the particle diameter. The area swept out, on the other hand, is directly proportional to the square of the diameter. Decreasing the bulk density thus increases the volume swept out by the graupel particle, in an amount proportional to the particle's increase in diameter. The lower fall velocity, however, reduces the collision efficiency and almost totally offsets the increased sweep-out volume. This balance between increasing the sweep-out volume and decreasing the collision efficiency is also the key factor in explaining the lack of sensitivity to changes in shape.

The most direct application of this study is to compare particle growth before and after a change of phase. This could involve the freezing of a supercooled drizzle drop or melting of a falling graupel particle before it is recycled into another updraft. In addition, these analyses can be applied to wet growth, where a graupel particle collects supercooled water so quickly that the latent heat released cannot be dissipated rapidly enough to freeze all the water that is accreted. In most cases, wet growth should generate a smooth surface on the growing graupel with an associated jump in growth rate. Examination of figures

1 to 3, in fact, suggests that the onset of wet growth may often mean a doubling in the growth rate. This means that the transition back to dry growth will often take place at substantially lower water contents than required to initiate wet growth in the first place. Since such transitions depend on the prior history of the particle, they represent a good example of a hysteresis loop. At some point, as the water coat becomes thicker, the surface of the wet graupel should start to deform during collisions with the result that the coalescence efficiency may begin to approach that of an unfrozen waterdrop.

This study can also be used to compare the relative growth rates of different kinds of precipitation embryos. It is necessary to keep in mind, of course, that all types of embryos are not equally likely to be found in any given cloud and thus the comparisons are largely academic. In addition, it is not imperative that relative growth estimates of this sort be made on the basis of particles of the same mass. Heymsfield (1982), for example, has performed a similar comparison for particles of the same diameter. The growth rate is so dependent on the particle mass, however, that the results of such comparisons simply show that particles of high bulk density grow faster than comparable diameter particles of low bulk density. The interesting feature of the present analysis is that the bulk density dependence is reduced to a second order effect when the growth rate comparisons are made on the basis of particles of the same mass. In fact, the lower bulk density graupel forms were often found to be slightly more effective as precipitation embryos than higher bulk density graupel or frozen drops.

While the overall pattern of the results should be fairly accurate, it is important to remember that both of the critical parameters that control the magnitude of the relative growth rates are still subject to considerable uncertainty. Our quantitative knowledge of coalescence efficiencies, for example, is still in its infancy and almost no quantitative work has been done on the effects of surface roughness. If anything, however, these lingering uncertainties only highlight Braham's insight in his pioneering analysis of Missouri clouds.

Acknowledgments

This study was performed at the University of Illinois with support from the Air Force Office of Scientific Research under grant 82-0179. In the course of this work, I had a number of helpful discussions with Professor Roscoe Braham of the University of Chicago; Bob Czys, Harry Ochs, and Ken Beard from the University of Illinois; and Art Jameson at Applied Research Corporation, Landover, Maryland. I am also indebted to John Pflaum for sending me a preprint copy of his upcoming article with Andy Heymsfield.

REFERENCES

Abraham, F. F., 1970: Functional dependence of drag coefficient of a sphere on Reynolds number. Phys. Fluids, 13, 2194-2195.

Beard, K. V., 1976: Terminal velocity and shape of cloud and precipitation drops aloft. J. Atmos. Sci., 33, 851-864.

Beard, K. V., 1980: The effects of altitude and electrical force on the terminal velocity of hydrometeors. J. Atmos. Sci., 37, 1363-1374.

Beard K. V., and S. N. Grover, 1974: Numerical collision efficiencies for small raindrops colliding with micron size particles. J. Atmos. Sci., 31, 543-550.

Beard, D. V., H. T. Ochs, 1984: Collection and coalescence efficiencies for accretion. J. Geophys. Res., 89, 7165-7169.

Braham, R. R., Jr., 1964: What is the role of ice in summer rain-showers? J. Atmos. Sci., 21, 640-645.

Braham, R. R., Jr., 1968: Meteorological bases for precipitation development. Bull. Amer. Meteor. Soc., 49, 343-353.

Cooper, W. A., and R. P. Lawson, 1984: Physical interpretation of results from the HIPLEX-1 experiment. J. Climate Appl. Meteor., 23, 823-840.

Foote, G. B., 1975: The water drop rebound problem: Dynamics of collision. J. Atmos. Sci., 32, 390-402.

Hall, W. D., 1980: A detailed microphysical model within a two-dimensional dynamic framework: Model description and preliminary results. J. Atmos. Sci., 37, 2486-2507.

Heymsfield, A. J., 1978: The characteristics of graupel particles in northeastern Colorado cumulus congestus clouds. J. Atmos. Sci., 35, 284-295.

Heymsfield, A. J., 1982: A comparative study of the rates of development of potential graupel and hail embryos in high plains storms. J. Atmos.Sci., 39, 2867-2897.

Heymsfield, A. J., and J. C. Pflaum, 1985: A quantitative assessment of the accuracy of techniques for calculating graupel growth. Submitted to J. Atmos. Sci.

Langmuir, I., 1948: The production of rain by a chain-reaction in cumulus clouds at temperatures above freezing. J. Meteor., 5, 175-192.

Mason, B. J., 1971: The Physics of Clouds, Clarendon Press, 671 pp.

Ochs, H. T., and K. V. Beard, 1984: Laboratory measurements of collection efficiencies for accretion. J. Atmos. Sci., 41, 863-867.

Ochs, H. T., and K. V. Beard, 1985: Effects of coalescence efficiencies on the formation of precipitation. J. Atmos. Sci., 42, 1451-1454.

Pflaum, J. C., and H. R. Pruppacher, 1979: A wind tunnel investigation of the growth of graupel initiated from frozen drops. J. Atmos. Sci., 36, 680-689.

Pitter, R. L., 1977: A re-examination of riming on thin ice plates. J. Atmos. Sci., 34, 684-685.

Pitter, R. L., and H. R. Prupacher, 1974: A numerical investigation of collision efficiencies of simple ice plates colliding with supercooled water drops. J. Atmos. Sci., 31, 551-559.

Rasmussen, R. M., and J. K. Lew, 1985: A wind tunnel study on the accretional growth of snowflakes: Implications for precipitation enhancement. Fourth WMO Scientific Conference on Weather Modification, WMO/TD-No. 53, World Meteorological Organization, Geneva, pp. 55-60.

Schotland, R. M., 1960: Experimental results relating to the coalescence of water drops with water surfaces. Disc. Faraday Soc., 30, 72-77.

Figure Captions

Figure 1. Relative growth rates of graupel particles with bulk densities of 0.3 and 0.7 g cm^{-3} as functions of melted drop diameter (D_o). In this case, the results are based on a cloud droplet diameter of 12 μm.

Figure 2. Relative growth rates of graupel particles with bulk densities of 0.3 and 0.7 g cm^{-3} as functions of melted drop diameter (D_o). In this case, the results are based on a cloud droplet diameter or 16 μm.

Figure 3. Relative growth rates of graupel particles with bulk densities of 0.3 and 0.7 g cm^{-3} as functions of melted drop diameter (D_o). In this case, the results are based on a cloud droplet diameter of 20 μm.

Figure 4. Relative growth rates of rough surface graupel particles of melted diameters 0.5 and 2.0 mm as functions of particle bulk density. Separate plots are shown for cloud droplet diameters of 12, 16, and 20 μm.

Figure 5. Relative growth rates of rough surfaced oblate spheroidal graupel particles of melted diameters 0.5 and 2.0 mm as functions the axis ratio of the particle. The dashed lines at the left of each panel are based on collision efficiencies for plate-like particles (see text for discussion). Separate plots are shown for bulk densities of 0.1, 0.3, and 0.7 g cm^{-3}. In each case, the results are based on a cloud droplet diameter of 16 μm.

AD-A170 317 A THEORETICAL FRAMEWORK FOR EXAMINING GEOGRAPHICAL 2/2
VARIABILITY IN THE MIC.. (U) ILLINOIS STATE WATER SURVEY
DIV URBANA D B JOHNSON JUN 86 AFOSR-TR-86-0484
UNCLASSIFIED AFOSR-82-0079 F/G 4/2 NL

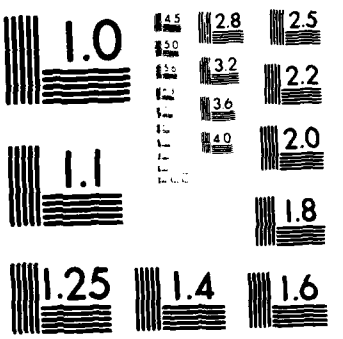

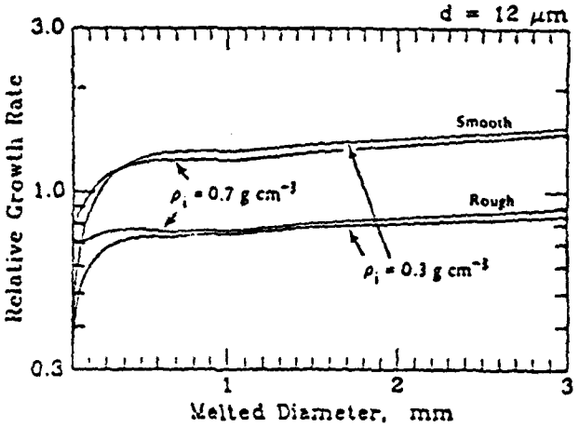

Figure 1. Relative growth rates of graupel particles with bulk densities of 0.3 and 0.7 g cm^{-3} as functions of melted drop diameter (D_o). In this case, the results are based on a cloud droplet diameter of 12 μm.

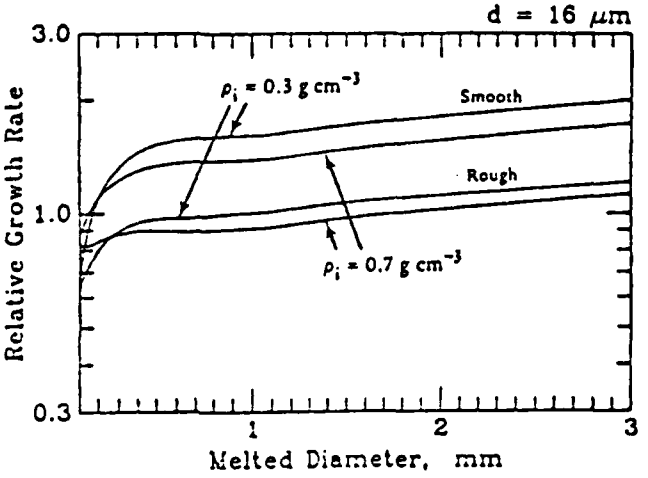

Figure 2. Relative growth rates of graupel particles with bulk densities of 0.3 and 0.7 g cm^{-3} as functions of melted drop diameter (D_o). In this case, the results are based on a cloud droplet diameter or 16 μm.

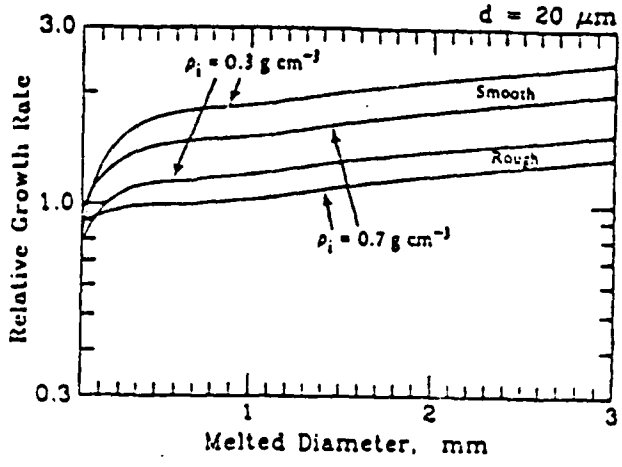

Figure 3. Relative growth rates of graupel particles with bulk densities of 0.3 and 0.7 g cm^{-3} as functions of melted drop diameter (D_o). In this case, the results are based on a cloud droplet diameter of 20 μm.

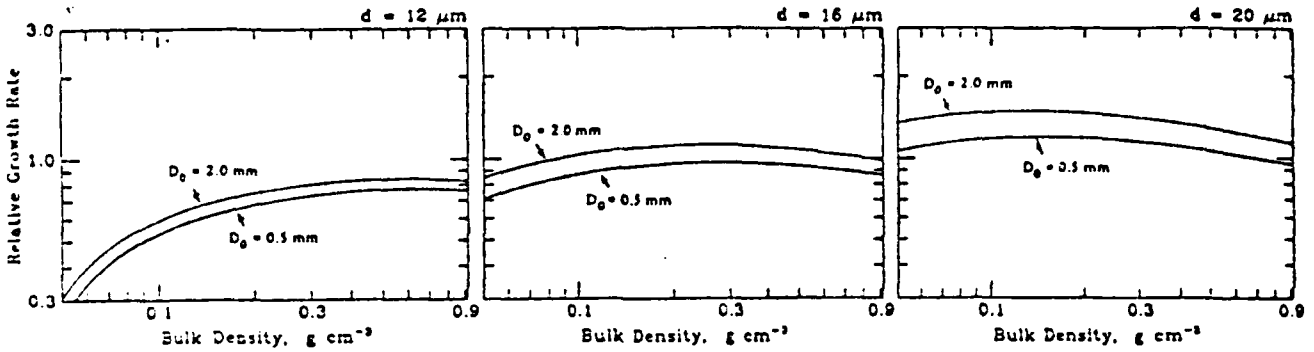

Figure 4. Relative growth rates of rough surface graupel particles of melted diameters 0.5 and 2.0 mm as functions of particle bulk density. Separate plots are shown for cloud droplet diameters of 12, 16, and 20 μm.

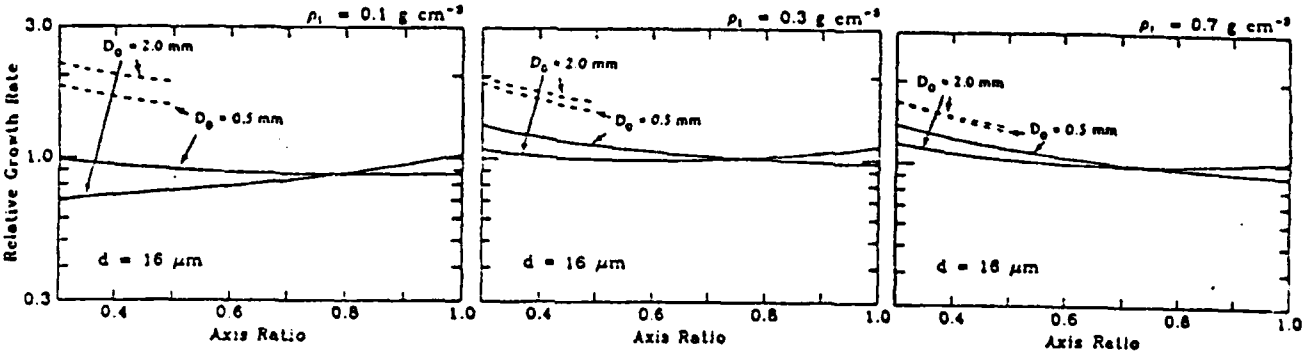

Figure 5. Relative growth rates of rough surfaced oblate spheroidal graupel particles of melted diameters 0.5 and 2.0 mm as functions the axis ratio of the particle. The dashed lines at the left of each panel are based on collision efficiencies for plate-like particles (see text for discussion). Separate plots are shown for bulk densities of 0.1, 0.3, and 0.7 g cm^{-3}. In each case, the results are based on a cloud droplet diameter of 16 μm.

END

DTIC

9-86